(2)

SGI-R-90-143

ESTIMATION OF EXPLOSION MOMENTS AT MURUROA AND TECTONIC RELEASE ORIENTATIONS AT NOVAYA ZEMLYA

W.C. TUCKER
G.R. MELLMAN
M. HENRY

SIERRA GEOPHYSICS, INC.
11255 KIRKLAND WAY
KIRKLAND, WASHINGTON 98033

MAY 1990

FINAL REPORT
JULY 1988 - JULY 1989

SPONSORED BY DEFENSE ADVANCED RESEARCH PROJECT AGENCY (DoD)
1400 WILSON BOULEVARD
ARLINGTON, VIRGINIA 22209
ARPA ORDER NO. 4511, AMENDMENT 13

MONITORED BY AIR FORCE TECHNICAL APPLICATIONS CENTER/TTR
HEADQUARTERS UNITED STATES AIR FORCE
PATRICK AIR FORCE BASE, FLORIDA 32925

UNCLASSIFIED

SECURITY CLASSIFICATION OF THIS PAGE

REPORT DOCUMENTATION PAGE

1a. REPORT SECURITY CLASSIFICATION SECRET	1b. RESTRICTIVE MARKINGS
2a. SECURITY CLASSIFICATION AUTHORITY DD254 dated 23 September 1986	3. DISTRIBUTION/AVAILABILITY OF REPORT Unlimited
2b. DECLASSIFICATION/DOWNGRADING SCHEDULE OADR	
4. PERFORMING ORGANIZATION REPORT NUMBER(S) SGI-R-90-143	5. MONITORING ORGANIZATION REPORT NUMBER(S)
6a. NAME OF PERFORMING ORGANIZATION Sierra Geophysics, Inc.	6b. OFFICE SYMBOL (If applicable) 4R088
6c. ADDRESS (City, State and ZIP Code) 11255 Kirkland Way Kirkland, WA 98033	7a. NAME OF MONITORING ORGANIZATION Air Force Technical Applications Ctr/TTR
	7b. ADDRESS (City, State and ZIP Code) Headquarters United States Air Force Patrick Air Force Base, FL 32925
8a. NAME OF FUNDING/SPONSORING ORGANIZATION Defense Advanced Research Projects Agency	8b. OFFICE SYMBOL (If applicable) NMRO
8c. ADDRESS (City, State and ZIP Code) 1400 Wilson Boulevard Arlington, VA 22209	9. PROCUREMENT INSTRUMENT IDENTIFICATION NUMBER F08606-87-C-0021
11. TITLE (Include Security Classification) See Section 16	10. SOURCE OF FUNDING NOS. PROGRAM ELEMENT NO. / PROJECT NO. DT7122 / TASK NO. / WORK UNIT NO.
12. PERSONAL AUTHOR(S) W.C. Tucker, G.R. Mellman, M. Henry	
13a. TYPE OF REPORT Final	13b. TIME COVERED FROM Jul '88 TO Jul '89
14. DATE OF REPORT (Yr., Mo., Day) 1990 MAY	15. PAGE COUNT 87
16. SUPPLEMENTARY NOTATION Estimation of Explosion Moments at Mururoa and Tectonic Release Orientations at Novaya Zemlya	

17. COSATI CODES		
FIELD	GROUP	SUB. GR.
8	11	

18. SUBJECT TERMS (Continue on reverse if necessary and identify by block number)

Mururoa, Novaya Zemlya, Explosions, Tectonic Release, Moment Tensor, Yield

19. ABSTRACT (Continue on reverse if necessary and identify by block number)

We applied a least-squares moment tensor inversion technique to 10 presumed nuclear explosions from the French Polynesian test site at Mururoa. Our results indicate that tectonic release typically is quite low (with F#'s ranging from .09 to .46) and makes little contribution to event moment. Assuming an oblique thrust orientation for the tectonic release mechanism, we find that the Δm_b between Mururoa and NTS is roughly .2 to .25 magnitude units. Finally, we compared yield estimates generated from three different magnitude-yield relations and found that they were reasonably close to one another and to the one known yield value.

We next used a search technique to jointly invert multiple types of data for six Northern Novaya Zemlya presumed nuclear explosions to find the average tectonic release orientation (strike, slip, and dip). P waveform, SH polarity, and surface wave data were used in the inversion, but SV amplitude data had too much scatter to be included. We found that the available data was insufficient to distinguish between a thrust and an oblique normal orientation. We suggest that an

20. DISTRIBUTION/AVAILABILITY OF ABSTRACT UNCLASSIFIED/UNLIMITED ☐ SAME AS RPT. ☒ OTIC USERS ☐	21. ABSTRACT SECURITY CLASSIFICATION Unclassified
22a. NAME OF RESPONSIBLE INDIVIDUAL Dr. Nazieh Yacoub	22b. TELEPHONE NUMBER (Include Area Code) (407) 494-5263
	22c. OFFICE SYMBOL AFTAC/TTR

DD FORM 1473, 83 APR EDITION OF 1 JAN 73 IS OBSOLETE.

UNCLASSIFIED

SECURITY CLASSIFICATION OF THIS PAGE

improved distribution of stations recording SH polarities, more accurate SV data, and/or geologic knowledge of the source region could provide enough additional information to determine the orientation. The presence of multiple, substantially different orientations that fit waveform, surface wave, and polarity data suggests that more effort needs to be made to systematically search the model space for alternative solutions in studies involving both isotropic and double couple sources. (JHD)

TABLE OF CONTENTS

		PAGE
	LIST OF FIGURES	iv
	LIST OF TABLES	vii
1.0	ABSTRACT	1
2.0	INTRODUCTION	2
3.0	SURFACE WAVE MOMENT DETERMINATIONS FOR THE MURUROA TEST SITE	3
	3.1 INTRODUCTION	3
	3.2 MURUROA DATA	6
	3.3 STATION CORRECTION AND SOURCE PARAMETER RESULTS	11
	3.4 YIELD ESTIMATES	27
	3.5 CONCLUSIONS	33
4.0	JOINT INVERSION OF SURFACE WAVE AND BODY WAVE DATA	37
	4.1 INTRODUCTION	37
	4.2 DATA	38
	4.2.1 SURFACE WAVES	38
	4.2.2 SH POLARITY	38
	4.2.3 RELATIVE P AMPLITUDES	40
	4.2.4 SV WAVES	40
	4.2.4.1 SV/P RATIO	41
	4.2.4.2 STATION CORRECTIONS	45
	4.2.4.3 STATISTICAL FIT CRITERION	49
	4.3 JOINT INVERSION RESULTS	52
	4.4 CONCLUSIONS	71
5.0	REFERENCES	73

LIST OF FIGURES

		PAGE
FIGURE 1	Azimuthal map showing the location of the Mururoa test site and the great circle paths from it to the 7 SRO stations used in this study.	4
FIGURE 2	Long period vertical seismograms from stations ANMO, MAJO, and TATO showing the effects of interference.	7
FIGURE 3	Rayleigh wave data for station ANMO for event 7/19/80.	9
FIGURE 4	Transverse seismogram for station ANMO for event 7/19/80.	10
FIGURE 5	Log station correction values for Rayleigh waves plotted as a function of azimuth.	14
FIGURE 6a	Radiation pattern plots for the Mururoa event of 7/25/79.	16
FIGURE 6b	Same as Figure 6a except for event 3/23/80.	17
FIGURE 6c	Same as Figure 6a except for event 6/16/80.	18
FIGURE 6d	Same as Figure 6a except for event 7/19/80.	19
FIGURE 6e	Same as Figure 6a except for event 12/3/80.	20
FIGURE 6f	Same as Figure 6a except for event 4/19/83.	21
FIGURE 6g	Same as Figure 6a except for event 5/25/83.	22
FIGURE 6h	Same as Figure 6a except for event 5/12/84.	23
FIGURE 6i	Same as Figure 6a except for event 11/2/84.	24
FIGURE 6j	Same as Figure 6a except for event 12/6/84.	25

LIST OF FIGURES
(Continued)

		PAGE
FIGURE 7	Offset (.9log(M_I)-m_b) vs F# at Mururoa assuming four different tectonic release orientations.	26
FIGURE 8	log(M_I) vs m_b for Mururoa events.	29
FIGURE 9	Normalized offset (.9log(M_I)-m_b) as a function of period for Mururoa events.	30
FIGURE 10	Average offset as a function of period for various test sites.	31
FIGURE 11a	Original body wave amplitudes for five Novaya Zemlya events plotted in polar coordinates.	42
FIGURE 11b	Same as Figure 11a except plotted in rectangular coordinates.	43
FIGURE 12	SV to P amplitude ratios for five Novaya Zemlya events plotted in both polar and rectangular coordinates.	44
FIGURE 13	Log station corrections plotted as a function of azimuth.	46
FIGURE 14a	Body wave amplitudes with station corrections applied for five Novaya Zemlya events plotted in polar coordinates.	47
FIGURE 14b	Same as Figure 14a except plotted in rectangular coordinates.	48
FIGURE 15	Various fits to the SV amplitudes of event 9/12/73.	51
FIGURE 16a	Joint SH and surface wave inversion of NNZ event of 9/12/73. 2 allowable SH inconsistencies and F# = .25.	53
FIGURE 16b	Same as Figure 16a except with F# = .35.	54

LIST OF FIGURES
(Continued)

		PAGE
FIGURE 16c	Same as Figure 16a except with F# = .45.	55
FIGURE 16d	Same as Figure 16a except with F# = .55.	56
FIGURE 16e	Same as Figure 16a except with F# = .65.	57
FIGURE 16f	Same as Figure 16a except with F# = .75.	58
FIGURE 17a	Joint SH and surface wave inversion of NNZ event of 9/12/73. 0 allowable SH inconsistencies with F# = .25.	60
FIGURE 17b	Same as Figure 17a except with F# = .30.	61
FIGURE 18a	Joint P wave, SH polarity, and surface wave inversion of NNZ event of 9/12/73. 2 allowable SH inconsistencies with F# = .25.	62
FIGURE 18b	Same as Figure 18a except with F# = .30.	63
FIGURE 18c	Same as Figure 18a except with F# = .35.	64
FIGURE 18d	Same as Figure 18a except with F# = .40.	65
FIGURE 18e	Same as Figure 18a except with F# = .45.	66
FIGURE 19a	Joint P wave, SH polarity, and surface wave inversion of NNZ event of 9/12/73. 0 allowable SH inconsistencies and F# = .25.	67
FIGURE 19b	Same as Figure 19a except with F# = .30.	68

LIST OF TABLES

		PAGE
TABLE 1	List of Mururoa events used in this study	5
TABLE 2	List of possibly interfering events	8
TABLE 3	Data use matrix	12
TABLE 4	Rayleigh station corrections	13
TABLE 5	Source parameter results	15
TABLE 6	Moment, offset, and F# results	28
TABLE 7	M_I-m_b relations and m_b site bias	32
TABLE 8	Magnitude-yield relations	34
TABLE 9	Mururoa yield estimates	35
TABLE 10	Novaya Zemlya events and their source parameters	39
TABLE 11	List of SV amplitudes used for fitting event 9/12/73	50
TABLE 12	Constraints on δ log (M_I) for 9/12/73 event	69
TABLE 13	Solutions using surface, P, and SH waves (no inconsistencies)	70
TABLE 14	Constraints on δ log (M_I) using surface, P, and SH waves (1 inconsistency)	72

1.0 ABSTRACT

We applied a least-squares moment tensor inversion technique to 10 presumed nuclear explosions from the French Polynesian test site at Mururoa. Our results indicate that tectonic release typically is quite low (with F#'s ranging from .09 to .46) and makes little contribution to event moment. Assuming an oblique thrust orientation for the tectonic release mechanism, we find that the δm_b between Mururoa and NTS is roughly .2 to .25 magnitude units. Finally, we compared yield estimates generated from three different magnitude-yield relations and found that they were reasonably close to one another and to the one known yield value.

We next used a search technique to jointly invert multiple types of data for six Northern Novaya Zemlya presumed nuclear explosions to find the average tectonic release orientation (strike, slip, and dip). P waveform, SH polarity, and surface wave data were used in the inversion, but SV amplitude data had too much scatter to be included. We found that the available data was insufficient to distinguish between a thrust and an oblique normal orientation. We suggest that an improved distribution of stations recording SH polarities, more accurate SV data, and/or geologic knowledge of the source region could provide enough additional information to determine the orientation. The presence of multiple, substantially different orientations that fit waveform, surface wave, and polarity data suggests that more effort needs to be made to systematically search the model space for alternative solutions in studies involving both isotropic and double couple sources.

2.0 INTRODUCTION

In previous reports, we explored the use of long period surface wave moment tensor solutions to correct explosion yield estimates for the effects of tectonic release. We examined long period moment tensor results for the Nevada Test Site (NTS) and Shagan River test areas (Given and Mellman, 1986 and 1986S) and used these results to derive M_I-m_b and M_I-yield relationships. More recently we applied this method to events from the Novaya Zemlya test area and examined the frequency dependence of moment tensor solutions for NTS, Shagan River, and Novaya Zemlya (Tucker et al., 1989). In the current report, we apply the long period surface wave method to the French test site, Mururoa. This provides another test of the portability of M_I-yield relationships, as well as the applicability of path correction procedures.

Earlier work on NTS, Shagan River, and Novaya Zemlya has suffered from the presence of large outlier events, where the surface waves were either far too large or far too small for the observed m_b. It has been suggested that these outliers represent events whose tectonic release orientations differ from those of the "average" events. In the second part of this report, we use an error tolerant search method to determine the orientation of tectonic release based on P waveform, SH polarity, SV amplitude, and surface wave joint inversion. Our goals in this inversion are to unambiguously determine an "average" tectonic release orientation, and to examine variations in tectonic release orientation from event to event. We applied this joint inversion method to six Northern Novaya Zemlya events previously studied by Burger et al. (1986) and Tucker et al. (1989).

3.0 SURFACE WAVE MOMENT DETERMINATIONS FOR THE MURUROA TEST SITE

3.1 Introduction

One of the challenges in explosion seismology is determining the yield of underground nuclear explosions using seismic information. Since yield can not be measured directly from the seismograms, the usual procedure is to develop a relationship between yield and magnitude based on a set of reference events. Magnitudes for additional events can be measured and used in the relation to estimate yields. Commonly used magnitudes include m_b and M_s. One difficulty with the surface wave magnitude M_s is that it may be biased by the presence of tectonic release which adds double couple energy to the isotropic energy of the explosion. Moment tensor inversion is designed to reduce this bias by allowing the double couple component to be isolated and removed.

The equations and procedures used in performing moment tensor inversion were described in detail by Given and Mellman (1986). Briefly, this technique involves determining an amplitude and polarity value for each long period seismogram after correcting for path propagation effects such as attenuation, dispersion, and geometric spreading. The signed amplitude values for many stations for many events are then inverted in an iterative, least squares fashion to simultaneously determine a correction factor for each station and three source parameters for each event. These source parameters, defined as combinations of the moment tensor elements, can be combined with a tectonic release orientation to determine the isotropic moment, M_I. Using this technique, Given and Mellman (1986 and 1986S) studied events at Shagan River and NTS, while Tucker et al. (1989) studied events at Novaya Z mlya. In the current report, we use moment tensor inversion to study events at Mururoa, the French Polynesian test site in the Tuamotu Archipelago region (see Figure 1). This study focuses on 10 events that occurred between 1979 and 1984, were recorded by SRO stations, and range in Lilwall magnitude from 5.2 to 5.7 (see Table 1). These same events were also studied by Stevens and McLaughlin (1989), although they neglected tectonic release when computing moment (M_0). They found that the relation $m_b = .9 \log(M_0) - 8.62$ was appropriate for Mururoa and suggested an m_b bias of .2 with respect to NTS. As the current study finds that tectonic release is a relatively minor factor at this site, it is not surprising that similar M_I-m_b and m_b bias results were obtained.

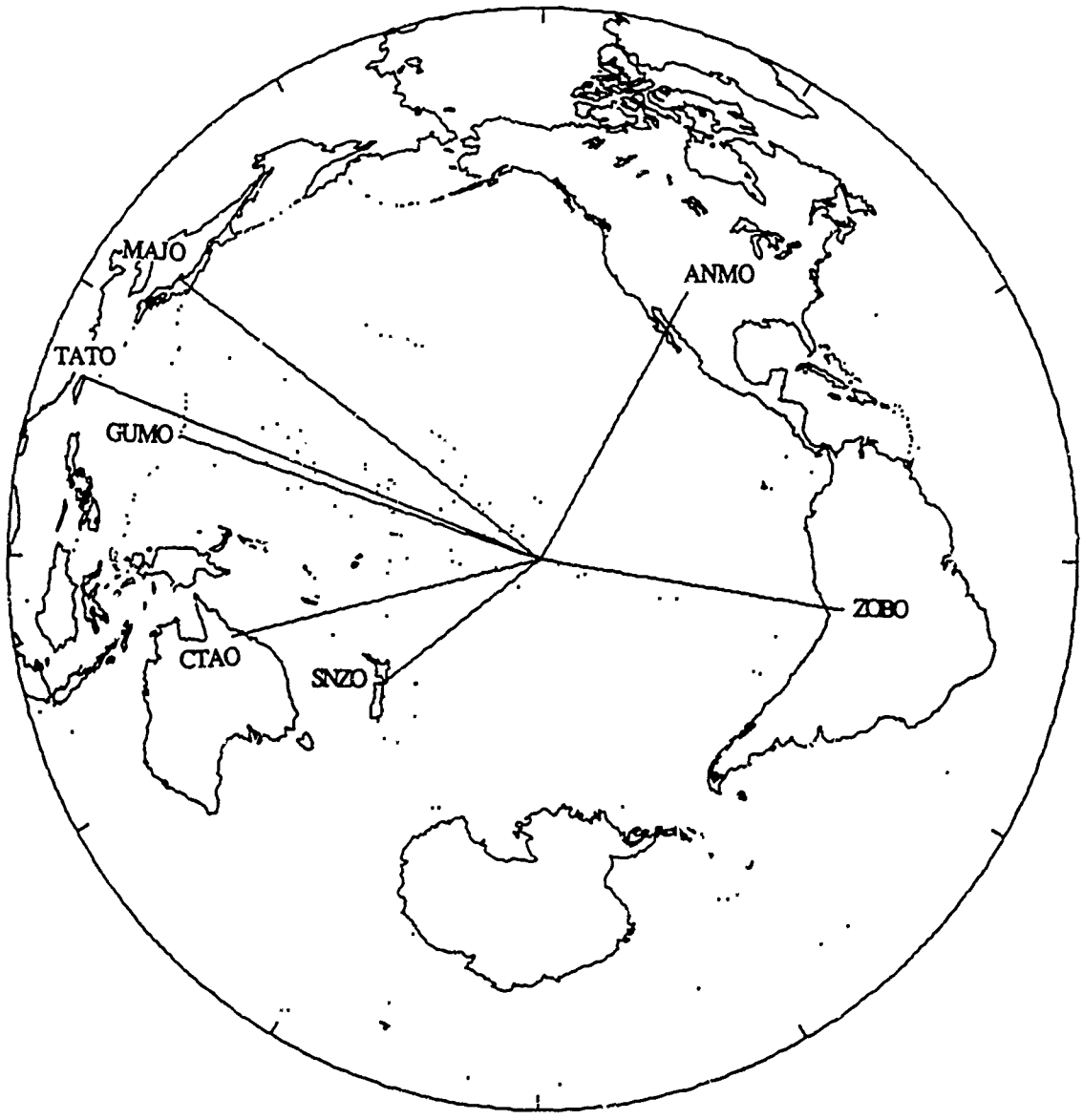

FIGURE 1: Azimuthal map showing the location of the Mururoa test site and the great circle paths from it to the seven SRO stations used in this study.

DATE	TIME	LILWALL m_b
07/25/79	17:56:59	5.74
03/23/80	19:36:59	5.49
06/16/80	18:26:59	5.20
07/19/80	23:46:59	5.54
12/03/80	17:32:59	5.39
04/19/83	18:52:58	5.49
05/25/83	17:30:58	5.68
05/12/84	17:30:58	5.41
11/02/84	20:44:59	5.42
12/06/84	17:28:59	5.43

TABLE 1: List of Mururoa events used in this study.

3.2 Mururoa Data

As clearly shown in Figure 1, the distance between Mururoa and the SRO stations is typically greater than 65^0 so that it takes between 1/2 and 1 hour for the explosion signals to arrive at the stations. This long travel time leaves ample time for the arrival of interfering signals from earthquakes which have occurred later, but closer, than the explosion. This situation occurs, for example, at stations ANMO, MAJO, and TATO for the Mururoa event of 4/19/83 which was followed less than 20 minutes later by a magnitude 5.1 earthquake near central Alaska. The distance between ANMO and the Mururoa event is 7155 km, while the distance between ANMO and the Alaskan event is only 4335 km. Assuming a velocity of 3.5 km/s, the signal from the earthquake is expected to arrive less than six minutes after the signal from the explosion. Although the ANMO data may be salvaged by windowing and filtering, it is clear that the data at station TATO can not be recovered as the two signals are expected to arrive within two minutes of each other (see Figure 2). A list of potentially interfering events is given in Table 2.

For unobstructed data, the first step in attempting to recover the size and orientation of the tectonic release from the observed surface wave seismograms is to correct the radiation pattern back to the source by removing path and propagation effects. Although the geometric spreading and instrument corrections are quite straight forward to apply, the remaining corrections for phase velocity, attenuation, and transmission differences between the source and receiver regions are extremely sensitive to the path being traveled and must be defined for every source-receiver pair. Stevens and McLaughlin (1989) have generated a number of these path corrections for a variety of test sites and stations. Although path correction information for Mururoa to 13 stations was provided by S-Cubed, data from only seven stations were used for moment tensor analysis in the current study. Data from the remaining stations were discarded as they did not appear to correct consistently enough to provide reliable amplitude measurements. Once the data have been corrected for path effects, the amplitude and phase spectra can be computed (see Figure 3). The scalar amplitude used in the inversion is a weighted average of the spectral amplitude values and its sign (polarity) is determined by the trend of the phase spectra. A trend towards π or $-\pi$ indicates normal (negative) polarity, that expected from a pure explosion uncontaminated by tectonic release, while a trend towards 0 indicates reversed (positive) polarity. None of the Mururoa data show any reversed Rayleigh waves. In addition, no Love waves could be identified with certainty (see Figure 4). These two observations suggest that the typical amount of tectonic release at Mururoa is low.

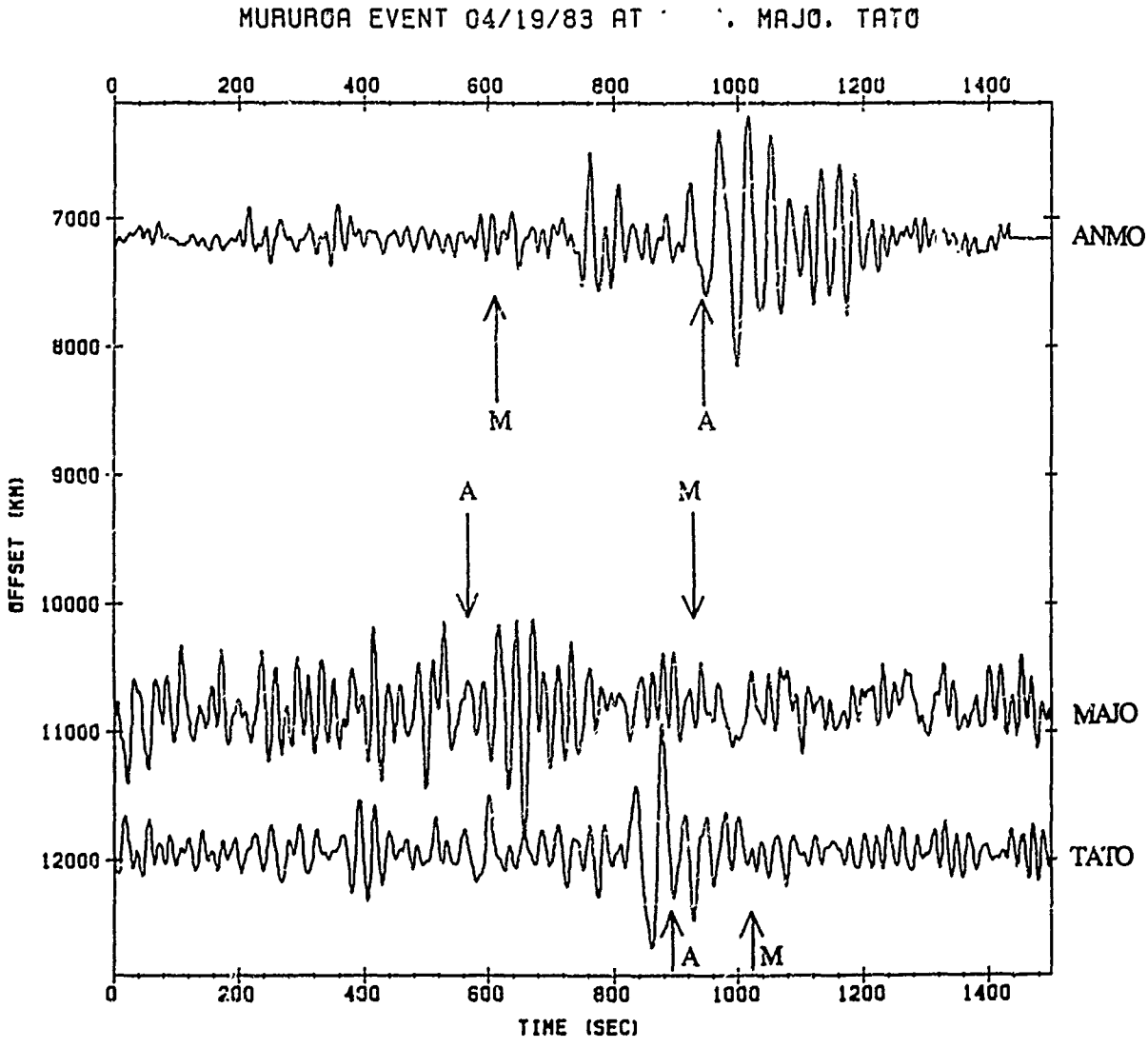

FIGURE 2: Long period vertical seismograms from stations ANMO, MAJO, and TATO showing the effects of interference. A magnitude 5.1 earthquake occurred near central Alaska roughly 20 minutes after the Mururoa event of 4/19/83. The expected arrival times of the signals from these two events was computed assuming a velocity of 3.5 km/s. The Mururoa signal is marked with an "M", while the Alaskan signal is marked with an "A".

DATE	TIME	m_b	LOCATION
07/25/79	17:45:10	XX	Central Chile
03/23/80	19:27:56	4.9	Santa Cruz
03/23/80	20:09:03	4.7	Afghanistan-USSR
06/16/80	19:02:34	4.2	Mindanao
07/19/80	23:31:55	4.8	Celebes
07/20/80	00:23:32	4.9	Mexico-Guatemala
07/20/80	00:24:05	5.5	Mexico-Guatemala
04/19/83	19:12:49	5.1	Central Alaska

TABLE 2: List of possibly interfering events.

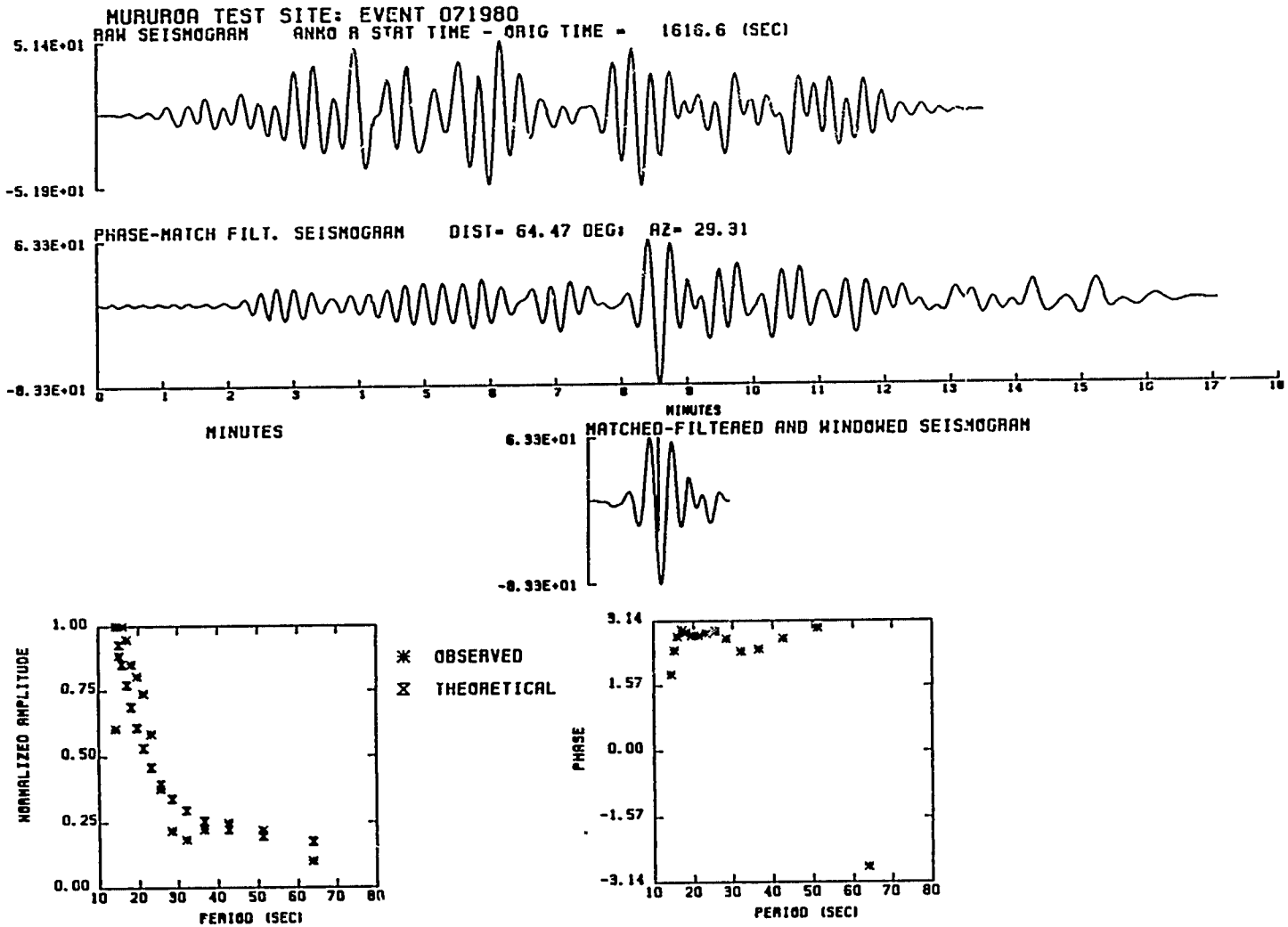

FIGURE 3: Rayleigh wave data for station ANMO for event 7/19/80. The top seismogram shows the raw data, while the next shows the data after it has been corrected for propagation effects such as dispersion, attenuation, and geometric spreading. The amplitude and phase spectra are displayed on the bottom. Note that the phase spectra trends towards π. This indicates that the data has normal polarity and shows no evidence of contamination by tectonic release.

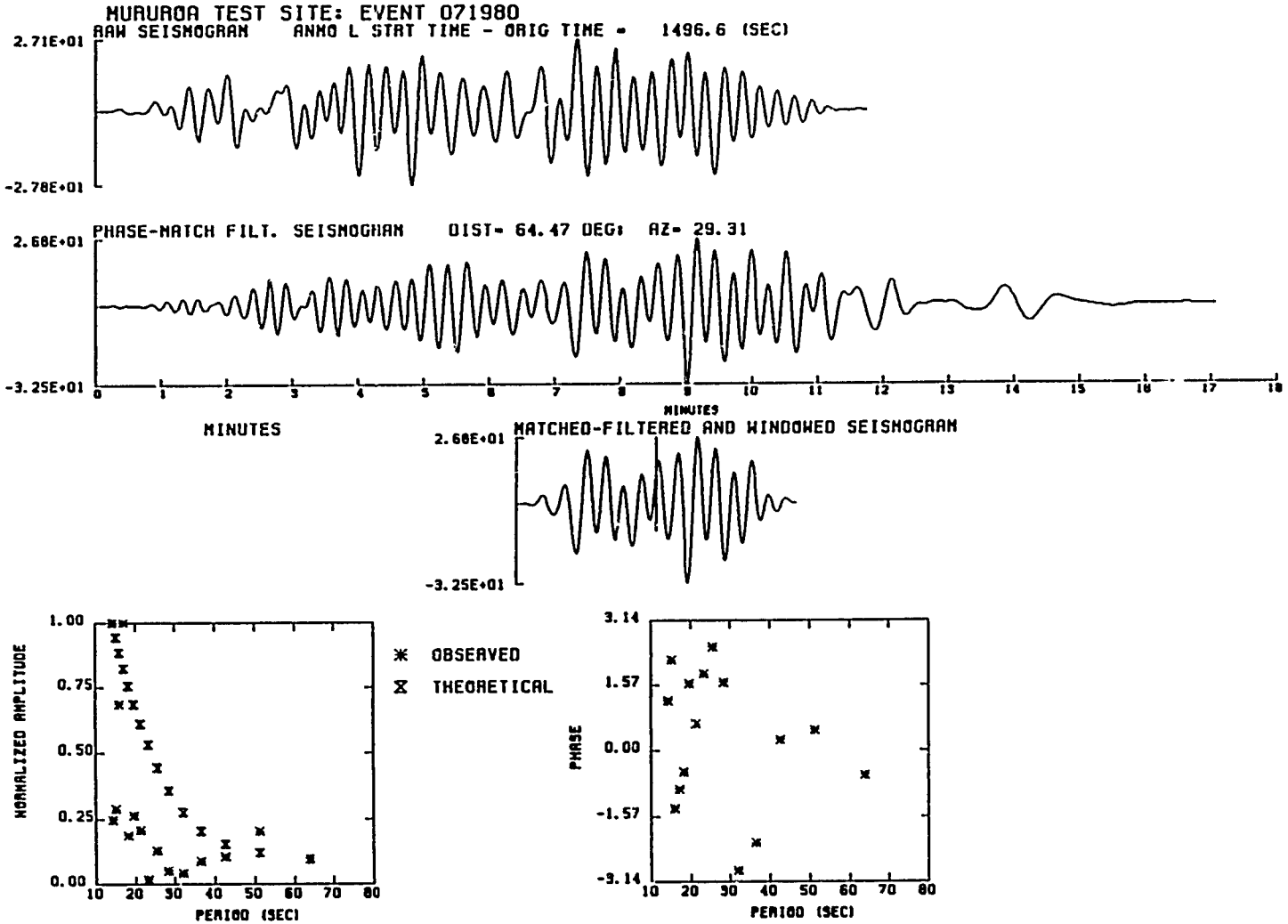

FIGURE 4: Transverse seismogram for station ANMO for event 7/19/80. Because this event experienced little contamination by tectonic release, the Love wave signal is too small to identify.

The combination of relatively small event size, low tectonic release, and large event-station distances severely limits both the quantity and quality of data that can be used in this study. Table 3 lists the Rayleigh wave data actually used. Note that no Love wave information is included.

3.3 Station Correction and Source Parameter Results

The signed amplitudes for many stations for many events are inverted in an iterative, linearized, damped least-squares fashion to give values for both a correction factor, a_i, for each station and three source parameters, S_k, for each event. The station correction factors are designed to compensate for magnitude variations between individual stations which are typically attributed to site specific effects due to the geology under a station and to any uncorrected propagation effects. Table 4 lists and Figure 5 shows the resulting station corrections.

The resulting source parameters, listed in Table 5, were used to generate the theoretical radiation pattern curves shown in Figure 6. Clearly, the fit between the observed and the theoretical amplitudes is quite good. Most of the events show fairly low amounts of tectonic release with the 5/12/84 event having the least and the 7/25/79 event having the most. Also, the strike of the tectonic release appears to be roughly 205^0 (assuming an oblique thrust mechanism) for almost all of the events. The noticeably different orientations of events 5/12/84, 11/02/84, and 4/19/83 can be explained by the quality of the solutions for those events. The 5/12/84 event contains so little tectonic release energy that the preferred strike has no meaning, the 11/02/84 event solution is poorly constrained as it was determined from only three pieces of data, and the 4/19/83 event solution is probably biased by energy from the interfering Alaskan earthquake (see Figure 2) which was not completely removed from the ANMO seismogram. The isotropic moment, M_I, depends on the source parameters, S_k, the elastic structure near the source, and the mechanism (dip and slip) of the accompanying tectonic release. The source parameters (shown in Table 5) were determined by inversion and the elastic structure (α = 3.0 km/s and β = 1.7 km/s) was taken from Stevens and McLaughlin (1989). If independent geological information was available for Mururoa, it could be used to select the tectonic release orientation. Lacking this, the slip and dip can be treated as regression coefficients and varied until $\log(M_I)$ scales with explosion size independent of the amount of tectonic release. The body wave magnitude, m_b, is assumed to provide a stable measure of explosion size as it appears to be unaffected by tectonic release and F#, defined as the double couple to isotropic moment ratio, is a measure of the amount of tectonic release. Thus, the preferred orientation is that which produces the least trend on a plot of "offset" $(.9*\log(M_I)-m_b)$ vs F#. Although Figure 7 clearly indicates that the preferred tectonic release

RALEIGH STATION	EVENT DATE									
	072579	032380	061680	071980	120380	041983	052583	051284	110284	120684
ANMO	-1	-1	-1	-1	-1	-1	-1	-1	-1	-1
CTAO	-1	-1	0	0	0	-1	-1	-1	0	-1
GUMO	0	-1	-1	-1	-1	-1	0	-1	-1	-1
MAJO	-1	-1	-1	-1	-1	0	0	-1	-1	-1
SNZO	-1	-1	-1	-1	-1	-1	-1	0	0	-1
TATO	0	0	0	0	-1	0	-1	-1	0	-1
ZOBO	-1	0	-1	-1	-1	-1	-1	0	0	0

TABLE 3: Data use matrix.

STATION	AZIMUTH	MULTIPLICATIVE CORRECTION	LOG CORRECTION
ANMO	29.34	1.361	0.134
CTAO	255.91	1.353	0.131
GUMO	287.71	0.805	-0.094
MAJO	306.36	0.692	-0.160
SNZO	232.46	0.571	-0.243
TATO	290.45	1.067	0.028
ZOBO	98.97	1.601	0.204

TABLE 4: Rayleigh station corrections.

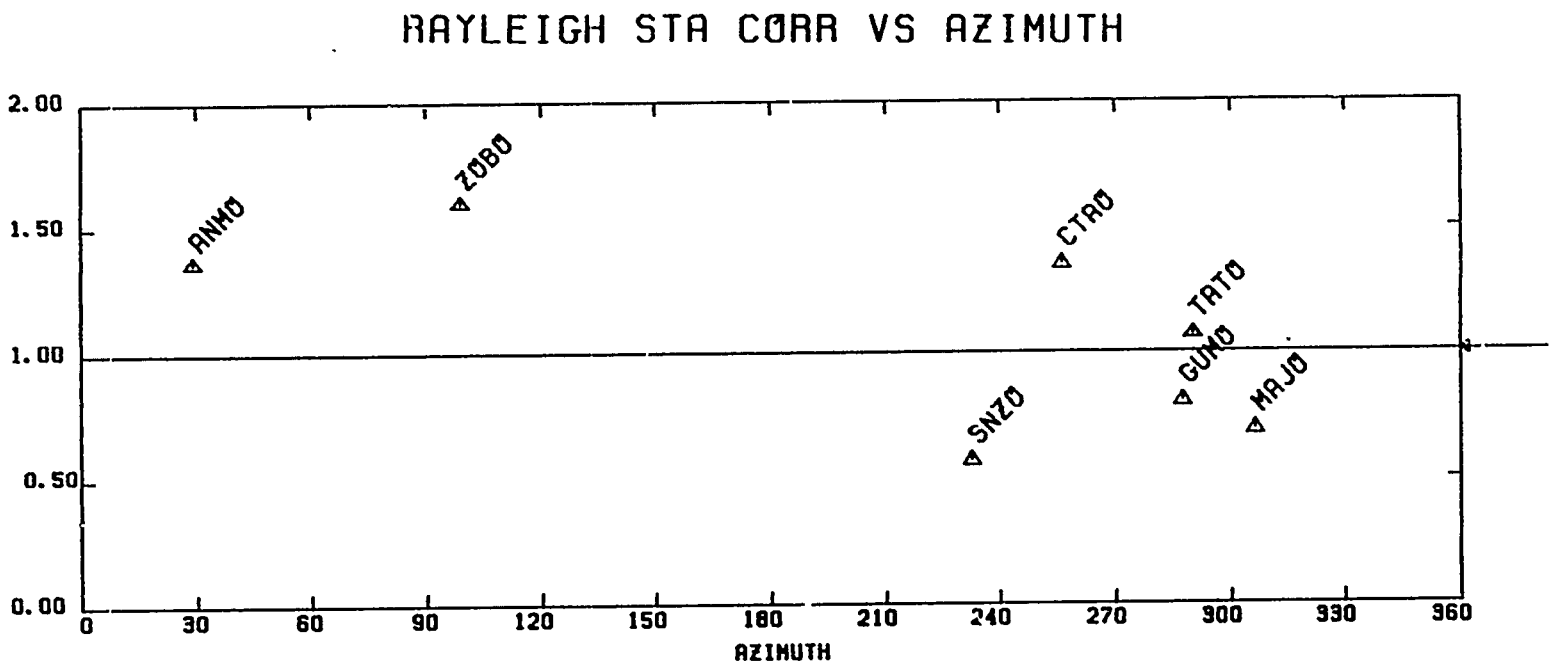

FIGURE 5: Log station correction values for Rayleigh waves plotted as a function of azimuth. Given an observed amplitude, A, and a log station correction, c, the corrected amplitude, B, is computed as follows: $B = A * 10^{C}$.

DATE	S0	S1	S2
07/25/79	5.470	2.620	-2.750
03/23/80	1.560	0.093	-0.374
06/16/80	1.170	0.108	-0.496
07/19/80	2.800	0.814	-1.140
12/03/80	2.040	0.463	-0.457
04/19/83	2.480	-0.687	-0.108
05/25/83	3.300	0.977	-0.872
05/12/84	2.540	-0.219	-0.098
11/02/84	2.130	0.281	0.000
12/06/84	2.750	-0.209	-0.872

TABLE 5: Source Parameter Results

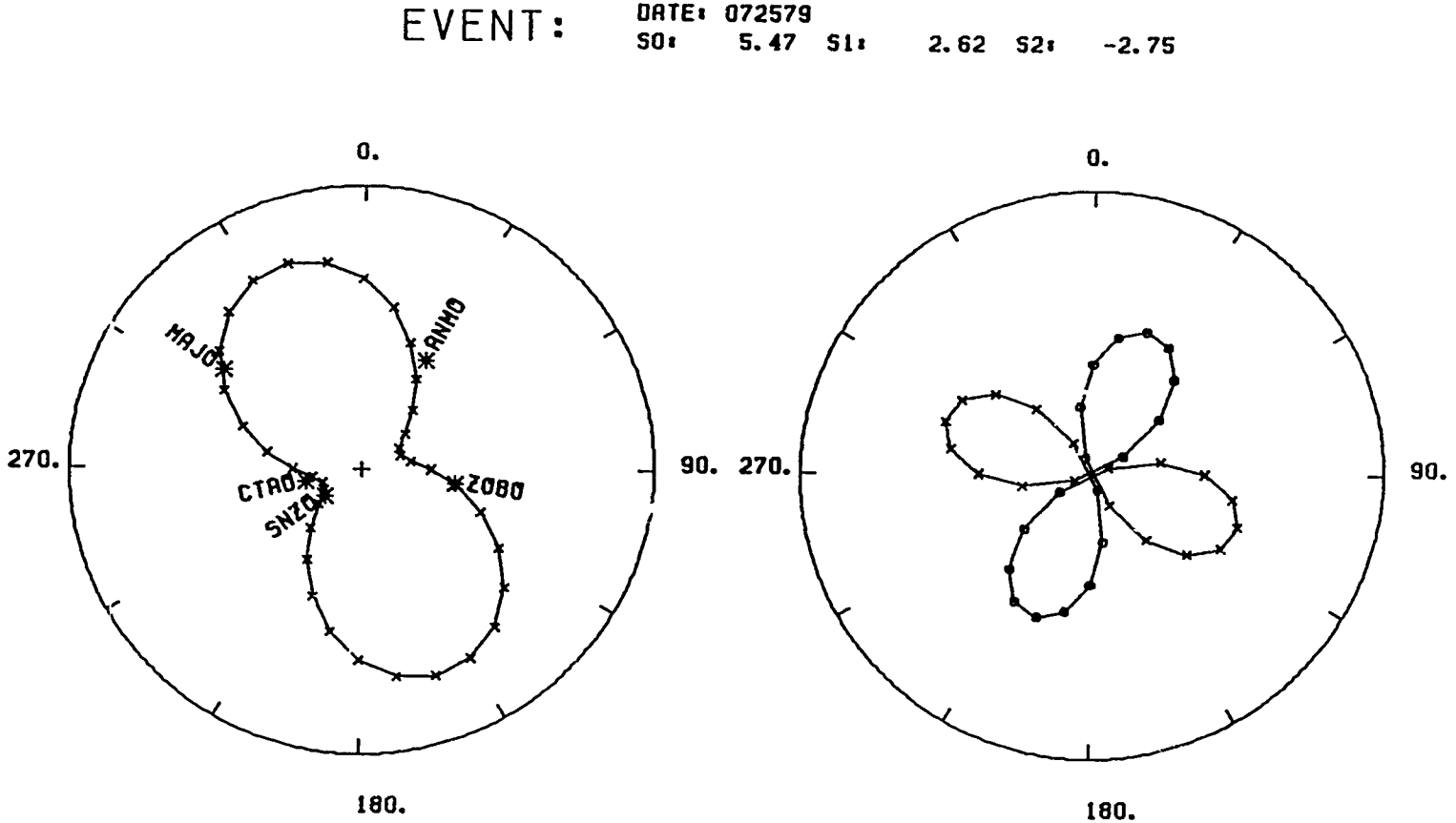

FIGURE 6a: Radiation pattern plots for the Mururoa event of 7/25/79. The plots show amplitude, proportional to distance from the center, as a function of azimuth, measured clockwise from North at the top. The observed values are plotted as discreet points with asterisks indicating normal polarity and open stars indicating reversed polarity. The theoretical values are plotted as a continuous line with crosses indicating normal polarity and open circles indicating reversed polarity. The circle on the left shows Rayleigh wave results and that on the right shows Love wave results.

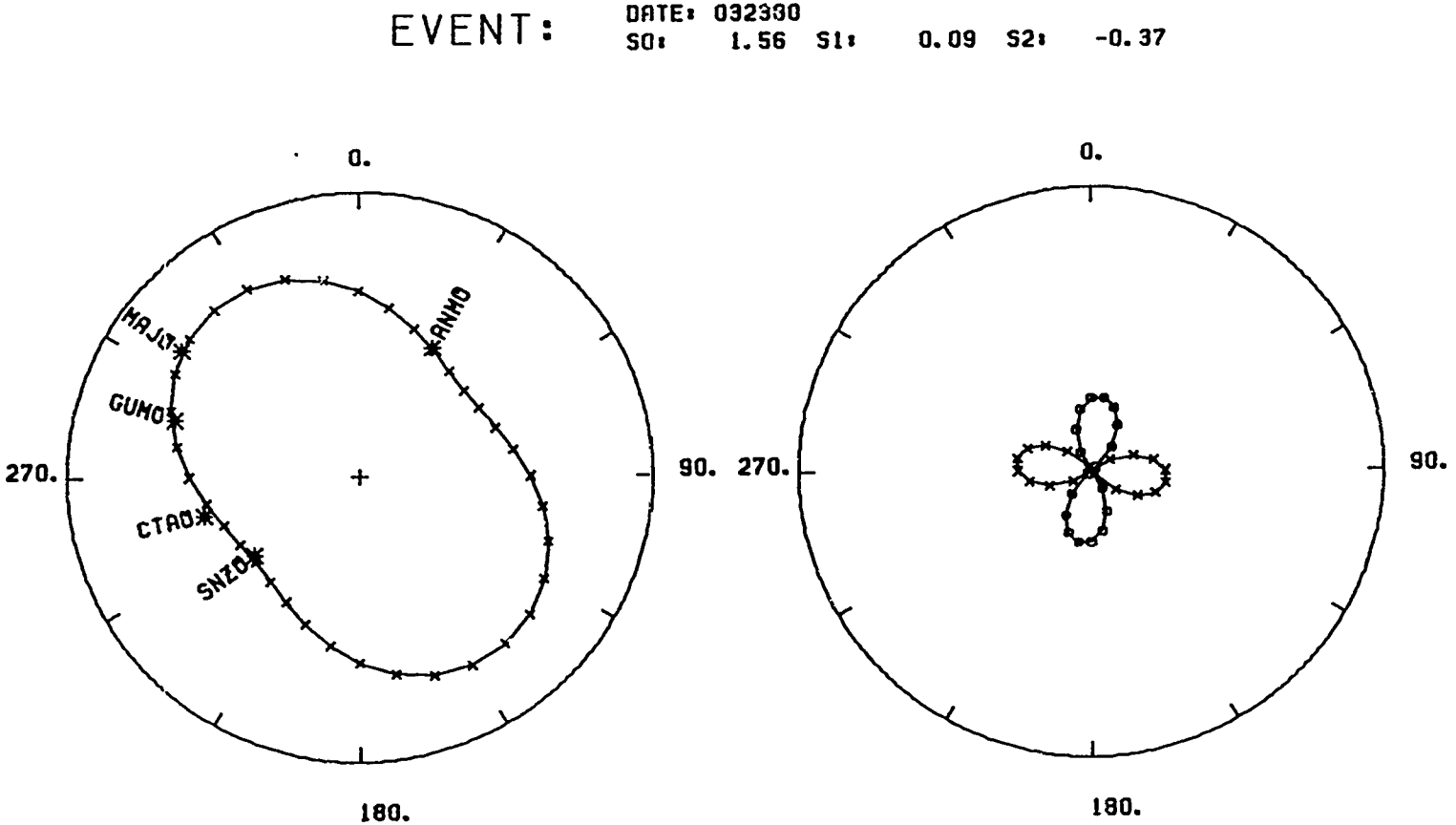

FIGURE 6b: Same as Figure 6a except for event 3/23/80.

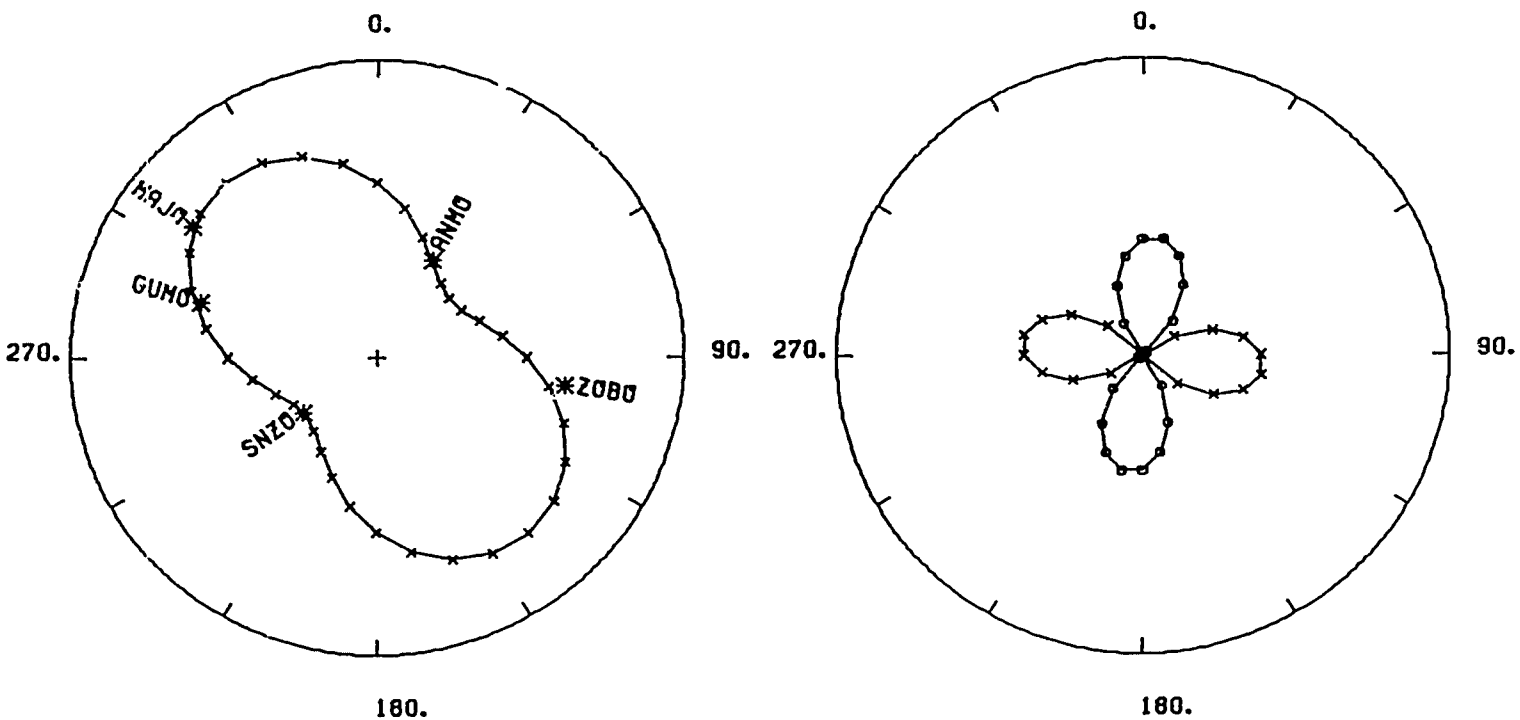

FIGURE 6c: Same as Figure 6a except for event 6/16/80.

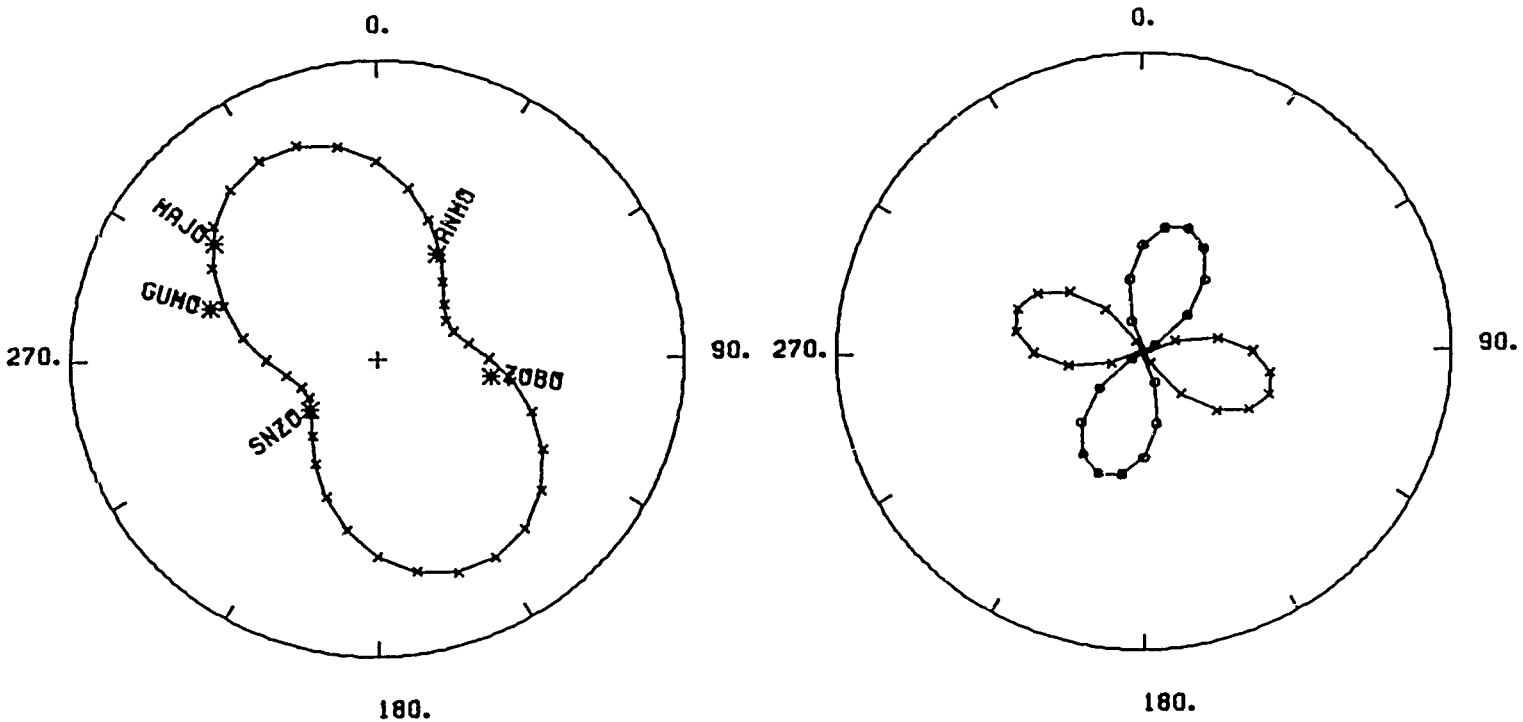

FIGURE 6d: Same as Figure 6a except for event 7/19/80.

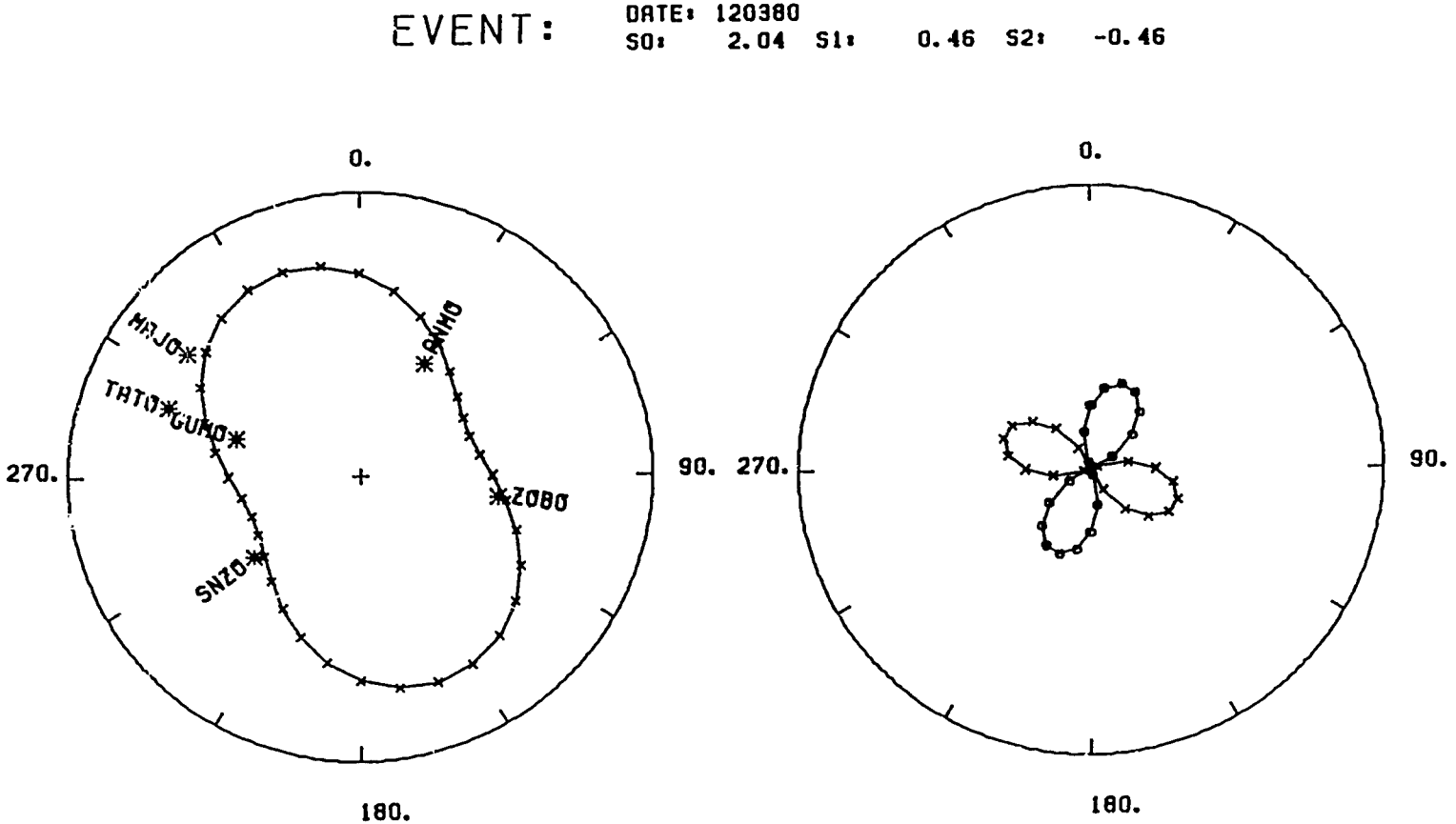

FIGURE 6c: Same as Figure 6a except for event 12/3/80.

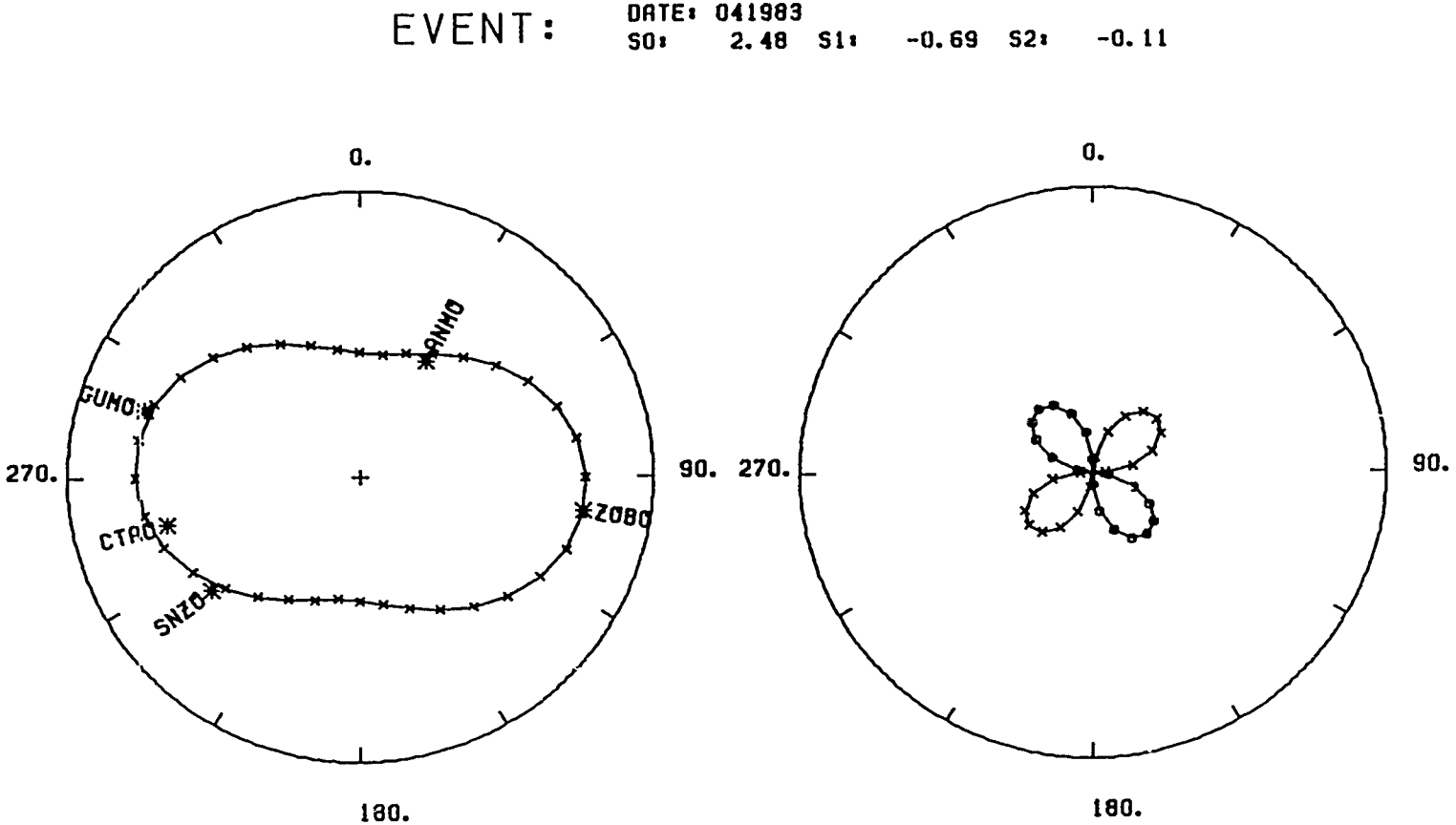

FIGURE 6f: Same as Figure 6a except for event 4/19/83.

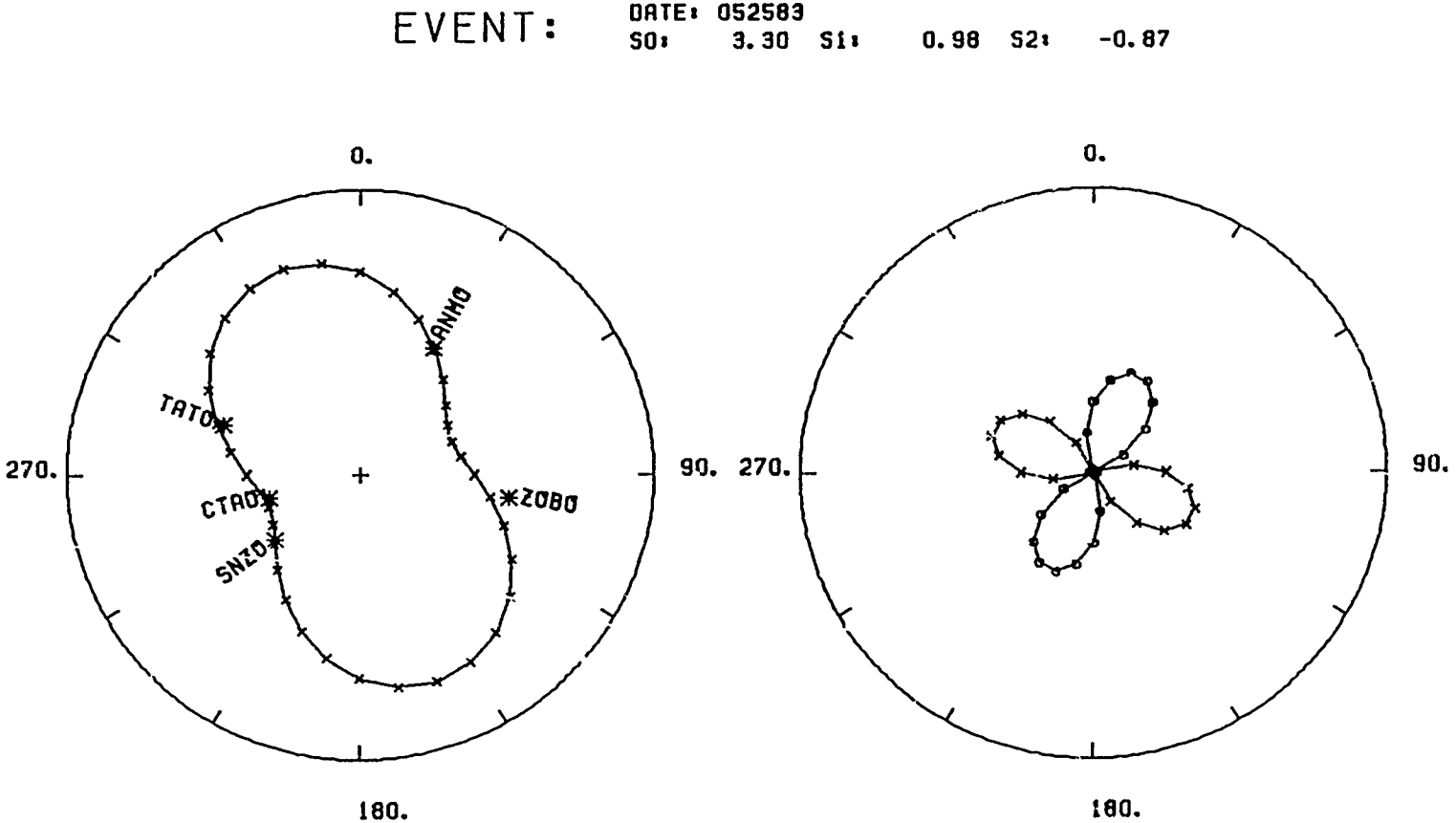

FIGURE 6g: Same as Figure 6a except for event 5/25/83.

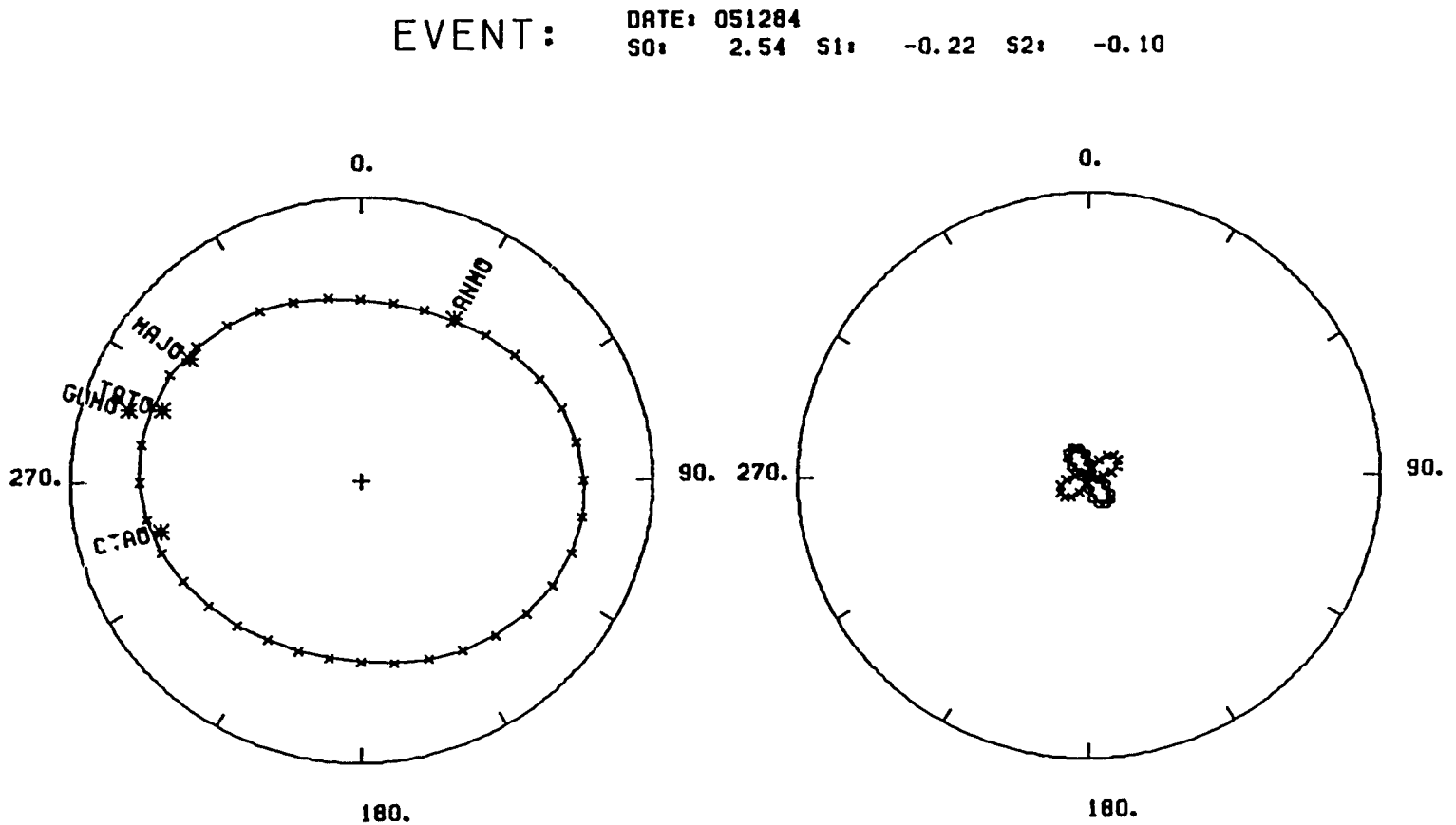

FIGURE 6h: Same as Figure 6a except for event 5/12/84.

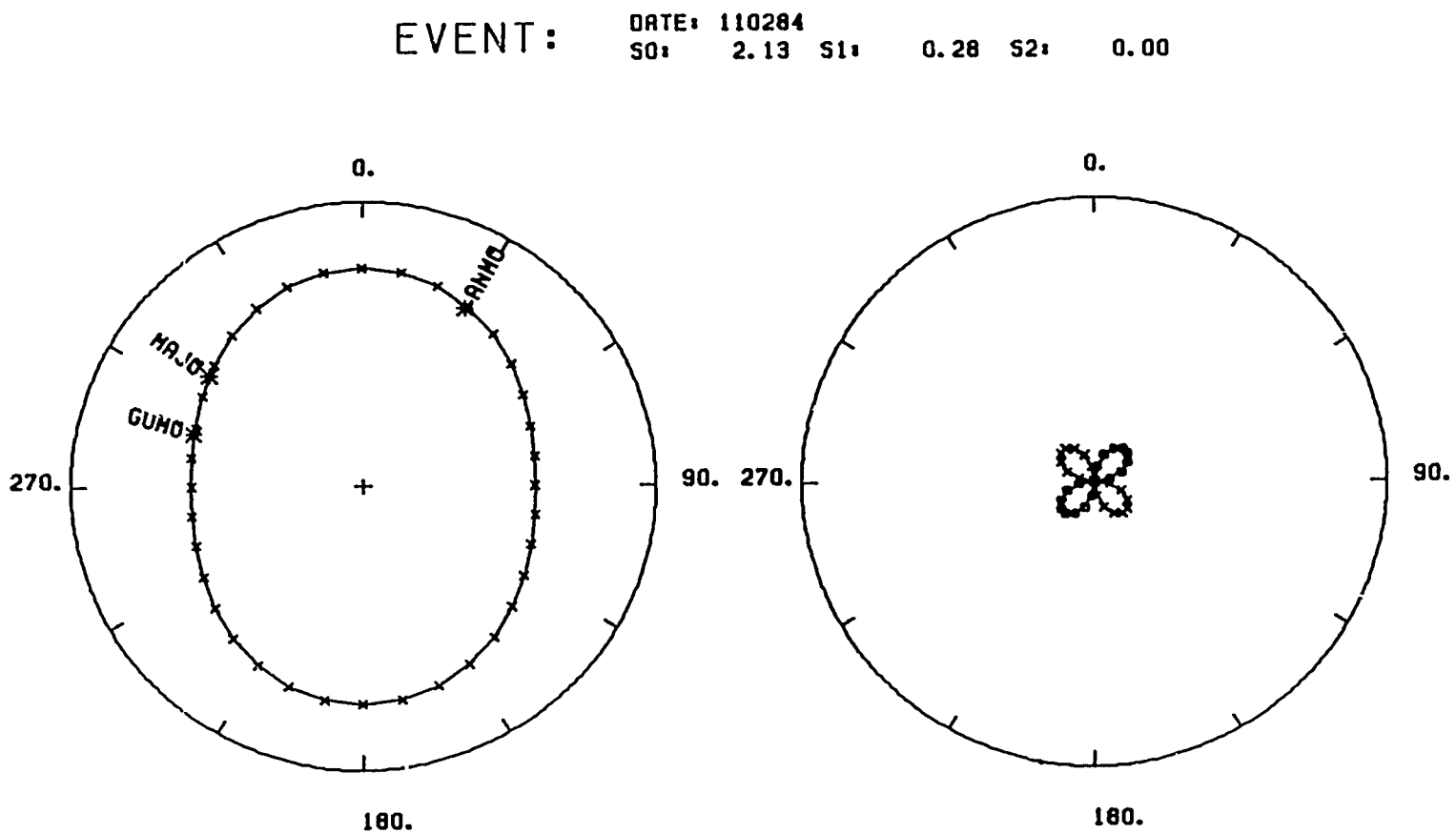

FIGURE 6i: Same as Figure 6a except for event 11/2/84.

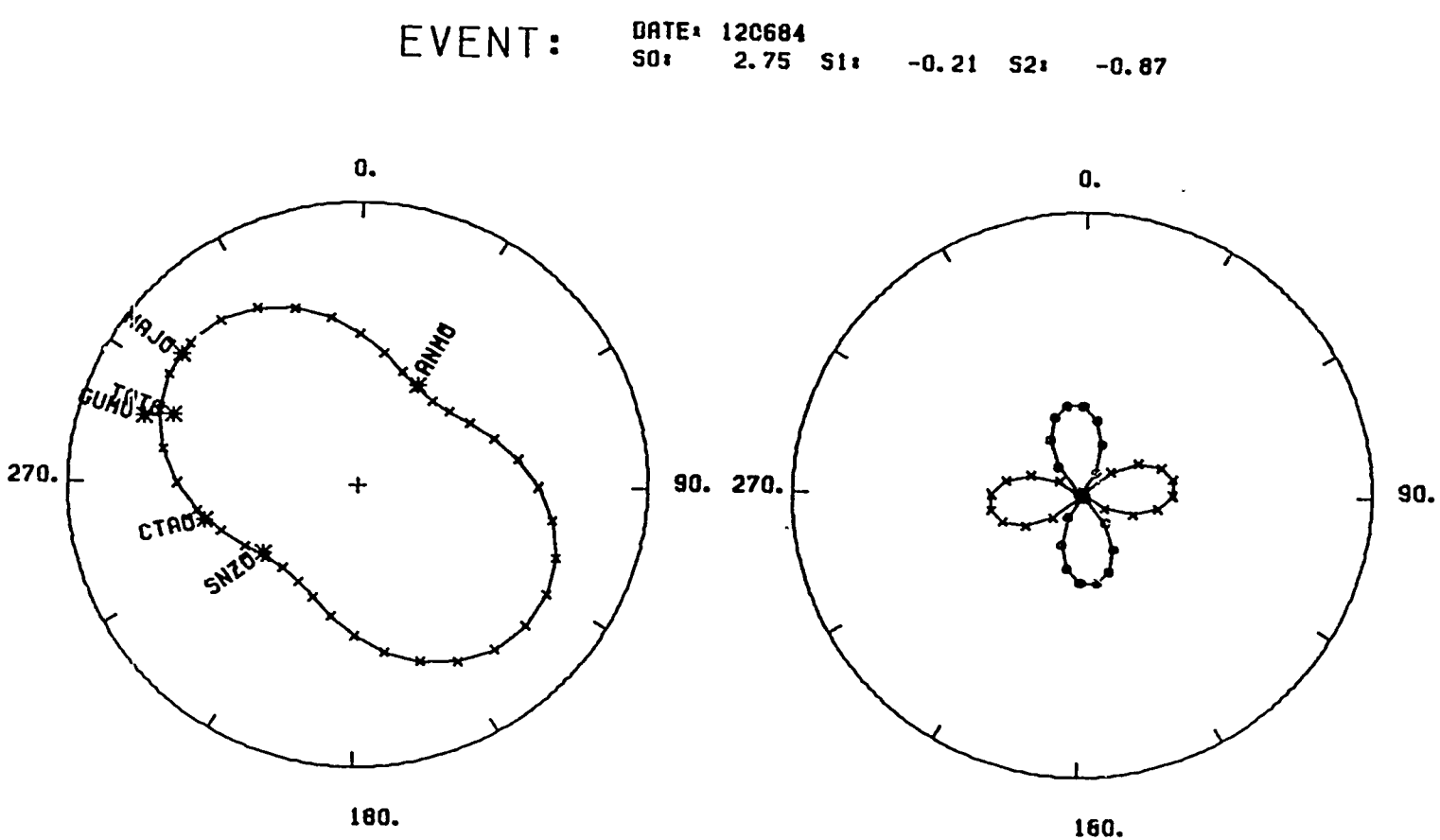

FIGURE 6j: Same as Figure 6a except for event 12/6/84.

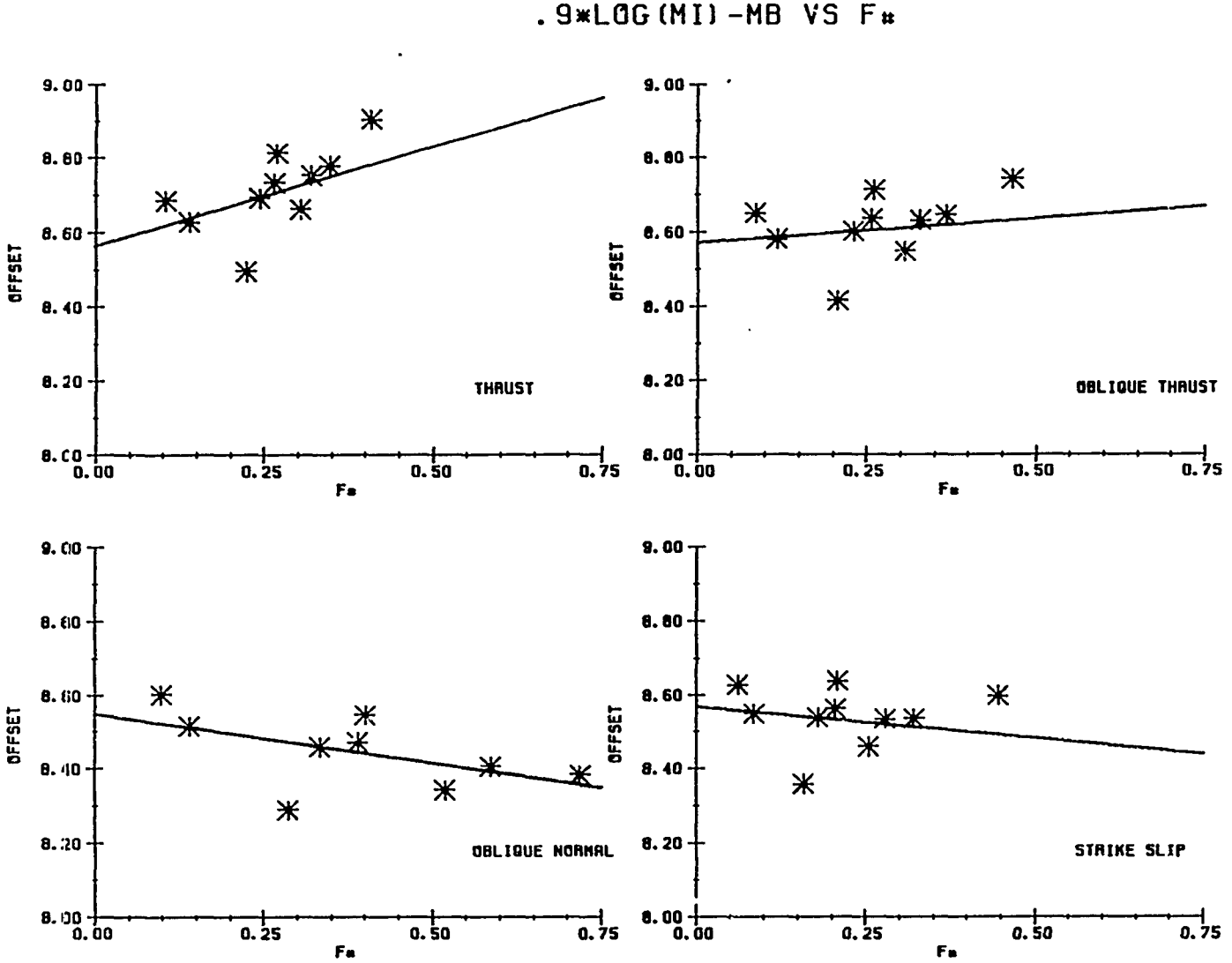

FIGURE 7: Offset (.9log(M_x)-m_b) vs F# at Mururoa assuming four different tectonic release orientations. The orientation which results in the flattest slope is preferred because it appears to properly remove the tectonic release contamination for all events independent of the relative proportion of tectonic release to explosion size.

orientation is somewhere between oblique thrust (slip=30^{o},dip=45^{o}) and strike slip (slip=0^{o},dip=90^{o}), this identification remains tentative because it is based on a very small range of F#'s. The F#'s and isotropic moments, computed for both the oblique thrust and strike slip mechanisms, are listed in Table 6. The correspondence between log(M_I) and Lilwall m_b can be seen directly in Figure 8, where M_I has been computed assuming an oblique thrust orientation. Although the fit line drawn on that plot was constrained to have a slope of .9 for consistency with previous Shagan River and NTS results (Given and Mellman, 1986), the slope of the best fitting unconstrained line was .86. The scatter in log(M_I) with respect to m_b is roughly .1. In previous work, Tucker et al. (1989) added another dimension to the moment tensor inversion process by applying weighting functions with narrow frequency bands at 15 center frequencies to determine the scalar amplitudes used in solving for the source parameters. After removing an average frequency behavior, they found that at Shagan River and at NTS there was no appreciable frequency difference with respect to "offset" (.9log(M_I)-m_b) between events. The Novaya Zemlya events, however, show large frequency differences, with substantial scatter at long periods. Examined in this manner, the Mururoa events appear quite homogeneous and show no appreciable frequency differences between events (see Figure 9). When the average frequency behaviors at each test site are compared, the Mururoa events show a decrease in offset at higher periods, similar to Novaya Zemlya and NTS (see Figure 10). The significance of these trends is unclear at the present time.

3.4 Yield Estimates

For test sites where the yields of some underground nuclear explosions are known, estimating the yields of other events may be accomplished by establishing magnitude-yield relationships based on the known yields. Where no yield information is available, yield estimates are made by "transporting" magnitude-yield relations from other test sites, with corrections for source and path differences where appropriate. It is generally believed that M_s- (and therefore M_I-) yield relations show less variation from site to site than m_b-yield relations. Thus, a constant "site bias" term (δm_b), developed using M_s or M_I as calibration for m_b may be introduced when an m_b-yield relation is transported to another area.

Table 7 lists M_I-m_b relationships for various test sites. Those for NTS and Shagan River were developed by Given and Mellman (1986) while those for Mururoa are from this study. Since all the listed relations have the same .9 slope, δm_b depends solely on the constant. Taking NTS as a reference, the δm_b at Mururoa ranges from .19 to .27 depending on the tectonic release orientation assumed. These bias values are almost identical to the .2-.3 range determined by Stevens and McLaughlin (1989). Since there is little tectonic release at Mururoa

	STRIKE SLIP			OBLIQUE THRUST		
DATE	Log(M_I)	OFFSET	F#	Log(M_I)	OFFSET	F#
07/25/79	15.930	8.597	0.446	16.092	8.743	0.465
03/23/80	15.385	8.357	0.159	15.450	8.415	0.207
06/16/80	15.261	8.534	0.279	15.368	8.631	0.329
07/19/80	15.639	8.536	0.321	15.761	8.645	0.367
12/03/80	15.502	8.562	0.205	15.584	8.635	0.257
04/19/83	15.587	8.538	0.180	15.659	8.603	0.230
05/25/83	15.711	8.460	0.255	15.810	8.549	0.306
05/12/84	15.597	8.627	0.061	15.623	8.651	0.086
11/02/84	15.521	8.549	0.085	15.556	8.581	0.118
12/06/84	15.632	8.638	0.209	15.715	8.713	0.261

TABLE 6: Moment, Offset, and F# Results.

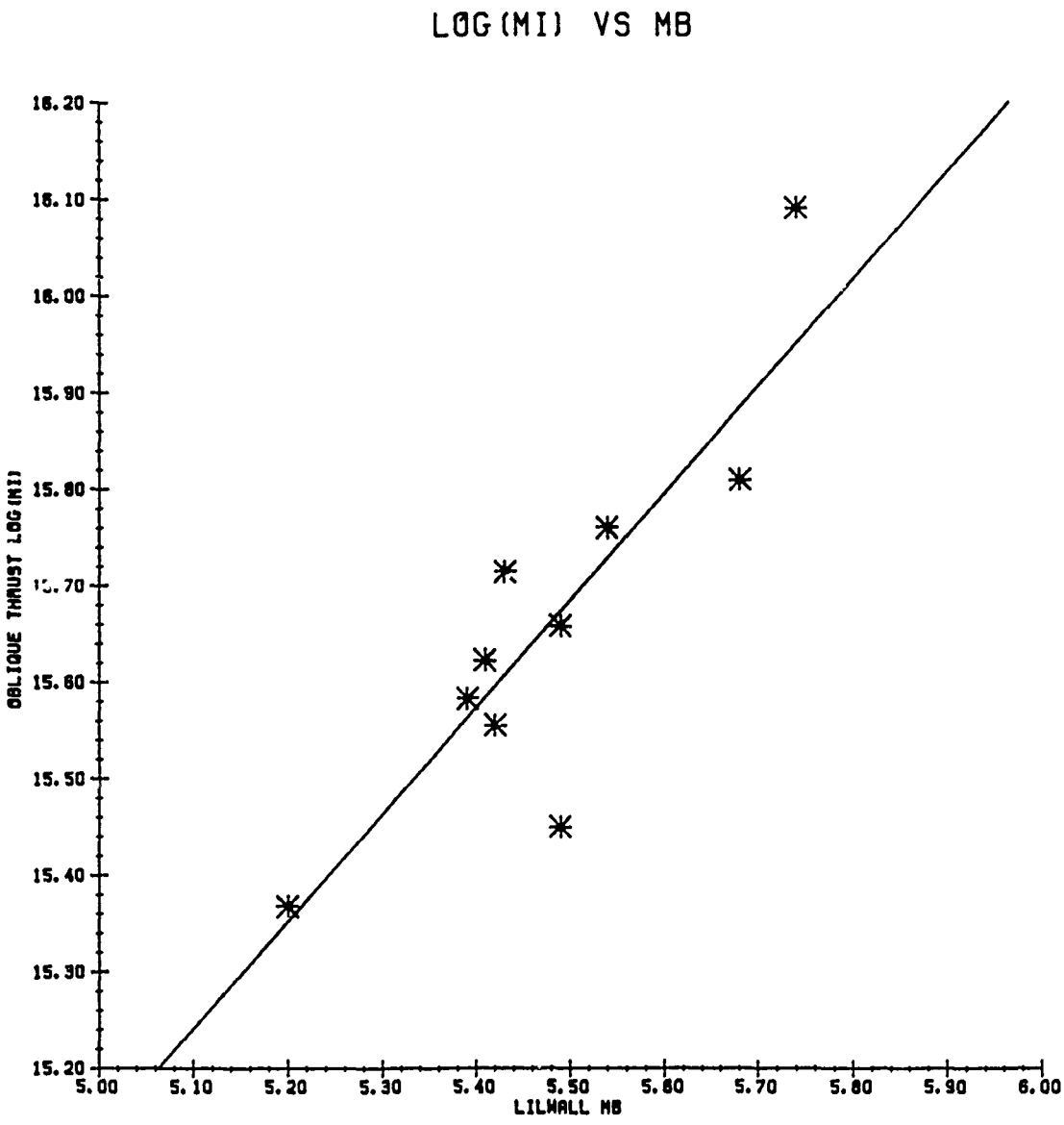

FIGURE 8: $\log(M_I)$ vs m_b for Mururoa events was computed assuming that the tectonic release orientation was an oblique thrust (dip=45^o, slip=30^o). The equation of the fit line is $m_b = .9 \log(M_I) - 8.62$. The scatter is about 0.1.

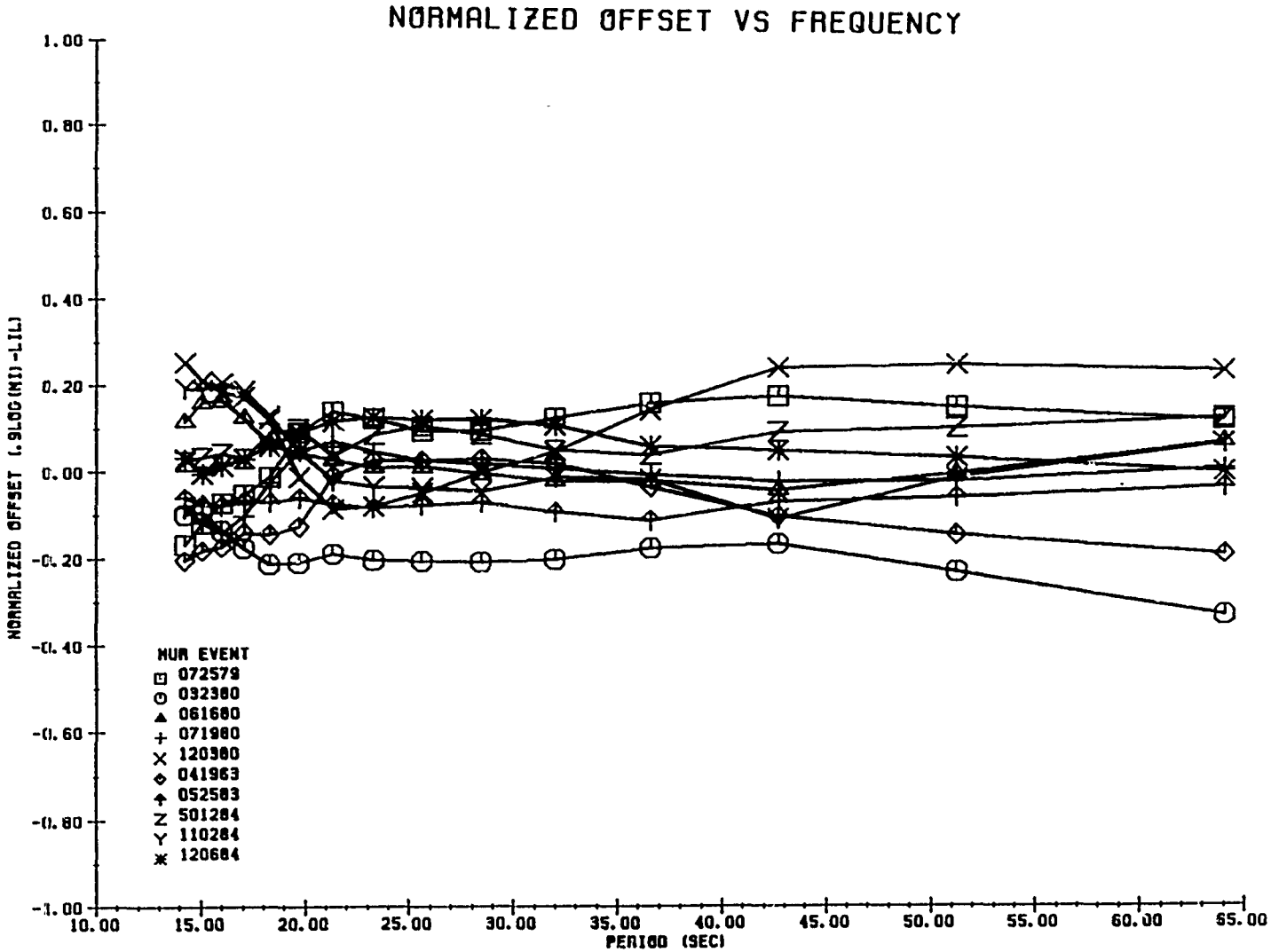

FIGURE 9: Normalized offset ($.9\log(M_I)-m_b$) as a function of period for Mururoa events. Narrow weighting windows with various center frequencies were applied to the observed data and the inversion results were recomputed. The offset vs frequency data was normalized by removing the average at each period. Note that the resulting curves are extremely consistent from event to event.

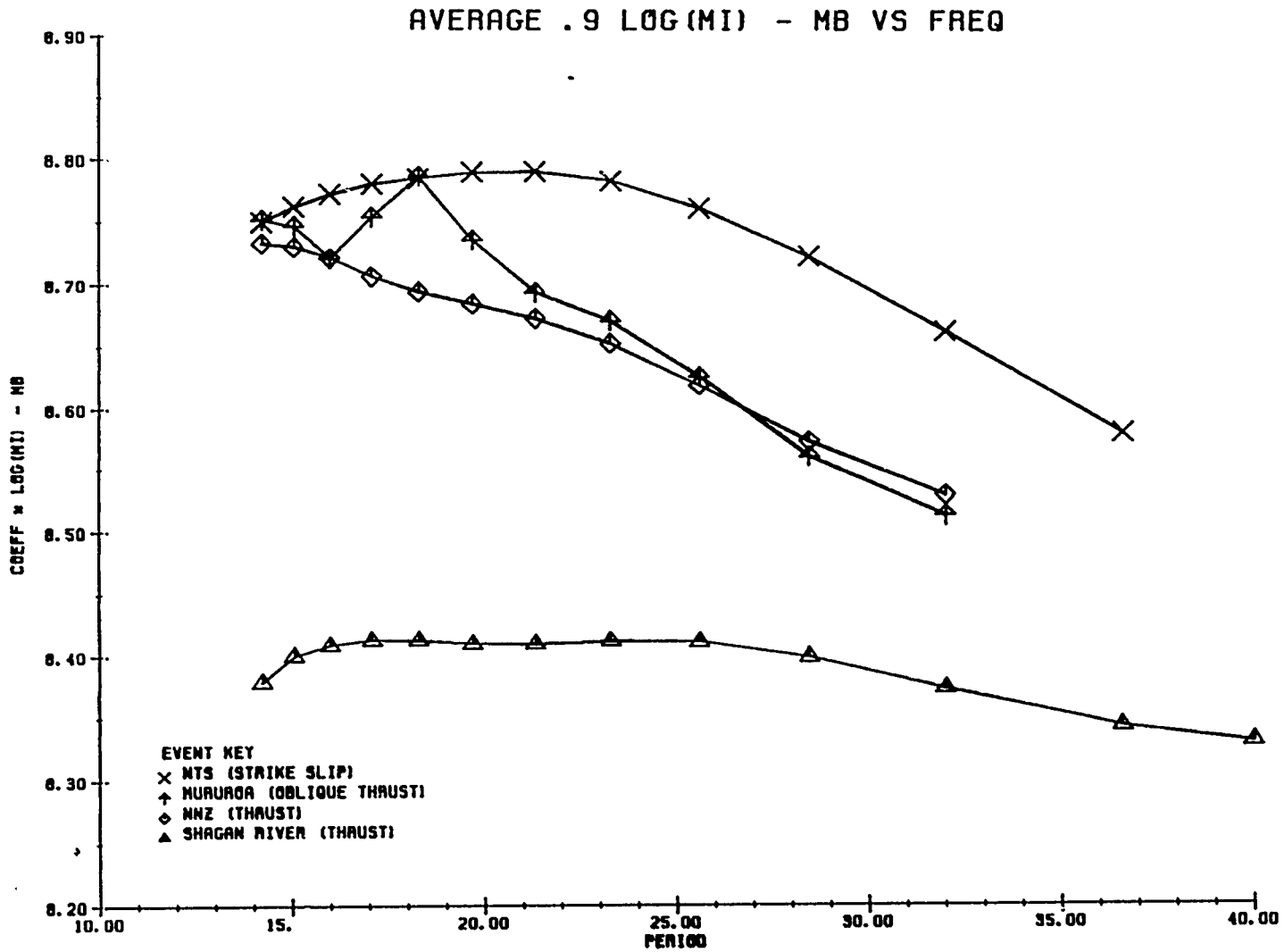

FIGURE 10: Average offset as a function of period for various test sites. Note that the Shagan River data appear to show the least variation with frequency. The data from the other test sites are shifted from each other, but appear quite similar in their variation with frequency.

SITE	M_I -m_b RELATION	SITE BIAS
Mururoa (ss)	m_b = .9 log(M_I) - 8.54	.27
Mururoa (ot)	m_b = .9 log(M_I) - 3.62	.19
Shagan River	m_b = .9 log(M_I) - 8.48	.33
All NTS	m_b = .9 log(M_I) - 8.81	.00

TABLE 7: M_I-m_b relations and m_b site bias.

and the major difference between the two studies is that M_I explicitly accounts for tectonic release while M_0 does not, it is not surprising that both M_I and M_0 give the same results.

Because a handful of yields are known for events at Mururoa, we can begin to test the accuracy of various magnitude-yield relations (and the validity of transporting them across test sites). Table 8 shows some magnitude-yield relations. The M_I-yield relation was developed by Given and Mellman (1986S) based on data from NTS. One m_b-yield relation was developed by Murphy and O'Donnell (1987S) based on five older Mururoa events for which they had both yield values and m_b values available. Unfortunately, the m_b values they used were those given by Alewine rather than those given by Lilwall. So, we modified their relation by including a constant which represents the average difference between the Alewine and Lilwall m_b's for the four events for which both m_b values were available. Another m_b-yield relation, listed by Given and Mellman (1986S) and based on data from NTS, was "transported" to Mururoa by including the oblique thrust δm_b value of .19. Using the M_I-yield relation, the modified m_b-yield relation, and the transported m_b-yield relation with the appropriate magnitude values, we computed three different sets of yield estimates for the Mururoa events. These estimates are shown in Table 9. Although all three sets of yield estimates are quite similar, the estimates computed from both the M_I and the transported m_b relations are consistently smaller than those computed from the modified m_b relation. The only yield value known for these events falls between the various estimates.

3.5 Conclusions

After being corrected for receiver and propagation effects, the amplitudes and polarities of Rayleigh waves from 10 Mururoa presumed nuclear explosions were inverted for station corrections and source parameters. Before the isotropic moment can be uniquely determined, the orientation of the tectonic release must be assumed. The choice of this orientation was guided by the criterion that the quantity $.9\log(M_I)-m_b$ should be invariant with respect to F#, a measure of the relative amount of tectonic release. Tectonic release for the Mururoa events appears to be between oblique thrust and strike slip. Among the Mururoa events, there appears to be some range in the amount of tectonic release as their F#'s vary from .09 for the event of 5/12/84 to .46 for the event of 7/25/79. The range of F#'s for the Mururoa events is less than a quarter of the range found by Given and Mellman (1986) for events from Shagan River. Although this does not rule out the possibility that tectonic release might be extremely large for some future Mururoa event, it does suggest that typically, tectonic release is not as big a factor at Mururoa as it is at Shagan River. By comparing various M_I-m_b relations, we find that the δm_b site bias between Mururoa and NTS is roughly .2 to .25 magnitude units. This result is similar to that found by Stevens and McLaughlin (1989) with M_0. Finally, we

RELATION	REFERENCE
$Log(Y) = 1.0log(M_I) - 14.07$	Given & Mellman 1986S
$Log(Y) = 1.0\ m_b - 3.88$	Murphy & O'Donnell 1987S
$Log(Y) = 1.0\ m_b - 3.71$	modified for Lilwall m_b
$Log(Y) = 1.11\ m_b - 4.22$	Given & Mellman 1986S (NTS)
$Log(Y) = 1.11\ m_b - 4.43$	transported to Mururoa

TABLE 8: Magnitude-yield relations

DATE	MODIFIED m_b	$\log(M_T)$	TRANSPORTED m_b
07/25/79	2.03	2.02	1.95
03/23/80	1.78	1.38	1.67
06/16/80	1.49	1.30	1.35
07/19/80	1.83	1.69	1.73
12/03/80	1.68	1.51	1.56
04/19/83	1.78	1.59	1.67
05/25/83	1.97	1.74	1.88
05/12/84	1.70	1.55	1.58
11/02/84	1.71	1.49	1.59
12/06/84	1.72	1.65	1.60

TABLE 9: Mururoa yield estimates

generated three sets of yield estimates for the Mururoa events using various magnitude-yield relations. All three sets of estimates were reasonably close to each other.

4.0 JOINT INVERSION OF SURFACE WAVE AND BODY WAVE DATA

4.1 Introduction

Long period surface waves are capable of constraining only three of the six possible degrees of freedom in the seismic moment tensor. The unconstrained degrees of freedom have a significant effect on the corrections for tectonic release that are made to explosion moment. To date, the orientation of the tectonic components has been inferred from either earthquake data, body wave data, or F# vs offset (Given and Mellman, 1986). In order to establish the orientation of tectonic release directly from explosion data, information from multiple data types must be used.

At first glance, moment tensor inversion appears perfectly suited to use multiple data types simultaneously. Problems quickly arise, however, because of the degree to which the solution depends on amplitude normalization of the differing data types. Joint moment tensor inversion of body and surface waves, for example, is critically dependent on absolute attenuation of the body waves and, to a lesser degree, on surface wave path corrections and body wave receiver corrections. Despite much work, there is still considerable uncertainty in all of these corrections, at least in an absolute sense. It is therefore desirable to base an inversion on quantities which are independent of absolute moment and which do not make critical assumptions about body or surface wave Q. These quantities include the relative amplitudes of certain body phases, the polarity of SH waves, the relative radiation patterns between events, and the relative size of surface wave source parameters.

For a general moment tensor solution, there are six degrees of freedom. By working with normalized seismograms, we can reduce this to five degrees of freedom. If we restrict the sources to those consisting of an explosion plus a single double couple, we need only consider a family of solutions containing four model parameters; three specifying fault orientation and one specifying the relative amount of explosion to tectonic release moment (F#). Since only a few (4 or 5) model parameters are unknown, optimal models can be determined by an exhaustive search of the model parameter space, rather than using gradient methods to find a single optimal solution. This search methodology, similar to that used by McLaughlin et al. (1983) in examining constraints on double couple solutions by relative body wave phase amplitude data, allows multiple solutions to be determined easily and allows inequality conditions on the data fit to be incorporated.

In this report, we examine the constraints that may be placed on a tectonic release mechanism by the addition of SH polarity data, relative P, pP, and sP amplitude data, and SV amplitude data to long period surface wave data. We studied the set of six Northern Novaya Zemlya

explosions listed in Table 10. As these events have been studied previously (Burger et al., 1986 and Tucker et al., 1989), some intermediary or processed results were available. We have chosen to use this processed data in our inversion, rather than return to the original seismograms, so that we can concentrate on extending the results of the previous studies rather than merely repeating their efforts. If we had chosen to perform our inversion using the waveforms directly, it would have been necessary to establish the permissible error for normalized waveforms. As always in waveform matching studies, significant uncertainty is introduced by the choices made for t^* and for the time functions used for the explosion and the tectonic release.

4.2 Data

4.2.1 Surface Waves

The surface wave data we used in the moment tensor inversion consist of the three surface wave source parameters S_0, S_1 and S_2 determined for each event by Tucker et al. (1989). In order to remove the effect of absolute moment, we work with a ratio of quadrapole to total surface wave energy for each event. Thus, we define

$$(1) \qquad d_{S1} = \left(\frac{S_1^2 + S_2^2}{S_0^2 + S_1^2 + S_2^2} \right)^{1/2}$$

$$(2) \qquad d_{S2} = \arctan \left(\frac{S_2}{S_1} \right)$$

d_{S1} is a measure somewhat similar to F#, but is independent of tectonic release orientation. d_{S2} is a measure of the orientation of the observed quadrapole radiation. A source model, consisting of an F#/orientation pair, is said to fit the data if the predicted values of d_{S1} and d_{S2} are within some tolerance of the observed values. In general we have used a tolerance of .1 on d_{S1} and 10^0 on d_{S2}. These tolerances are consistent with formal error estimates from the inversion studies of Given and Mellman (1986S).

4.2.2 SH Polarity

The SH polarity data we used has been taken from Burger et al. (1986) who determined it by observing the first break direction and by matching waveforms for a total of 10 stations. A

DATE	MARSHALL m_b	S0	S1	S2
10/14/70	6.77	48.90	-1.24	18.00
09/27/71	6.63	75.20	-3.83	21.30
09/28/72	6.46	43.60	-0.63	8.93
09/12/73	6.96	136.00	1.54	52.20
08/29/74	6.54	48.70	0.21	7.89
08/23/75	6.55	31.50	-2.41	9.40

TABLE 10: Novaya Zemlya events and their source parameters.

model is said to fit the SH polarity data if the number of incorrectly predicted SH polarities is less than n, where we used values of n = 0, 1, 2. SH polarity information is by far the most robust of the auxiliary data types used, and provides the most reliable constraints on the tectonic release mechanism. Note, however, that SH waves are of limited use when non-double couple mechanisms are considered, as neither moment tensor solutions $M_{xx} = M_{yy} = 1$ nor $M_{zz} = 1$ excite SH waves. Tradeoffs between these two solutions provide a major ambiguity.

4.2.3 Relative P Amplitudes

Relative amplitudes of the short period body wave phases P, pP, and sP have been used for some time to constrain double couple mechanisms. Burdick and Mellman (1976) did waveform inversions based on these relative amplitudes. Pearce (1977) used the ratios of these amplitudes to constrain focal mechanisms. McLaughlin et al. (1983) extended Pearce's work to use as constraints the upper bounds on amplitude ratios rather than the ratios themselves. In the present work, we define the observed amplitude ratios for each station:

(3) $d_{p1} = A_{pP} / A_P$

(4) $d_{p2} = A_{sP} / A_P$

These observed ratios are derived from the Burger et al. (1986) body wave solutions which were determined from waveform fitting at five stations. We take the P, pP, and sP amplitudes to represent a combined explosion and tectonic release amplitude, and require that prospective solutions fit all d_{p1} and d_{p2} to within ±.2. These are fairly generous bounds which produce noticeable waveform changes.

As it has often been noted that pP amplitudes for explosions are appreciably smaller than those predicted by linear elasticity, we have experimented in this inversion with pP/P ratios of .5 to .9. While varying this ratio does allow some shift in permissible orientations, it allows relatively little change in the number of permissible solutions given the body wave data constraints.

4.2.4 SV Waves

Although variations in shear wave attenuation and the presence of shear-coupled PL and other near surface conversions make them extremely difficult to use, SV waves are a potentially powerful constraint on tectonic release orientation. For the SV wave information to be useful

in a practical sense, a strong correlation must exist between the theoretical and measured radiation patterns.

The theoretical radiation patterns of the P and SV phases can be written as five term polynomials in trigonometric "powers" of the station azimuth, Θ: $\sin(2\Theta)$, $\cos(2\Theta)$, $\sin(\Theta)$, $\cos(\Theta)$, 1. The coefficient for each term is a complex function of the orientation (strike, slip, and dip) of the double couple source (Aki and Richards, 1980). Although the explosion source itself produces only P waves, a large P to S conversion coefficient allows the explosion to contribute significant amounts of SV energy. Fortunately, the P and SV radiation patterns expected from the explosion are isotropic. Thus, the observed radiation patterns are expected to be generally sinusoidal with an enhanced constant term.

To measure the actual radiation patterns for the Novaya Zemlya events of interest, we started with long period body wave data from roughly 60 World Wide Standard Seismic Network (WWSSN) stations and equalized them to a distance of 50° by applying the geometrical spreading correction described by Kanamori and Stewart (1976). We then measured the peak-to-peak time domain amplitudes for both the P, and SV phases. These are plotted in Figure 11, where it becomes immediately apparent that the expected patterns are completely obscured by the extreme scatter in the observed amplitudes. We must somehow greatly reduce this scatter before we can hope to use the SV phase to constrain the tectonic release orientation.

4.2.4.1 SV/P Ratio

We first tried to reduce the scatter by working with the ratio of the SV to P amplitudes rather than with the individual amplitudes. This ratio process should reduce the influence of some common path and instrument effects. Unfortunately, the improvement may be rather minimal because differences in the P and S attenuation and velocity remain. However, the ratio process also implements a necessary step in determining the tectonic release orientation by removing the explosion contribution. Because explosion sources are much more efficient generators of P wave energy than double couple sources and because the size of the tectonic release at Novaya Zemlya is small compared to the size of the explosions, the double couple contribution to the observed P amplitude can be ignored. So, upon taking the SV to P ratio, the explosion contribution to the isotropic component of the SV amplitude is reduced to a constant (representing the conversion coefficient) that is the same for all events and which can be subtracted, leaving only the double couple component. Figure 12 shows the amplitude ratio results. Again, the data show severe scatter and no apparent sinusoidal pattern.

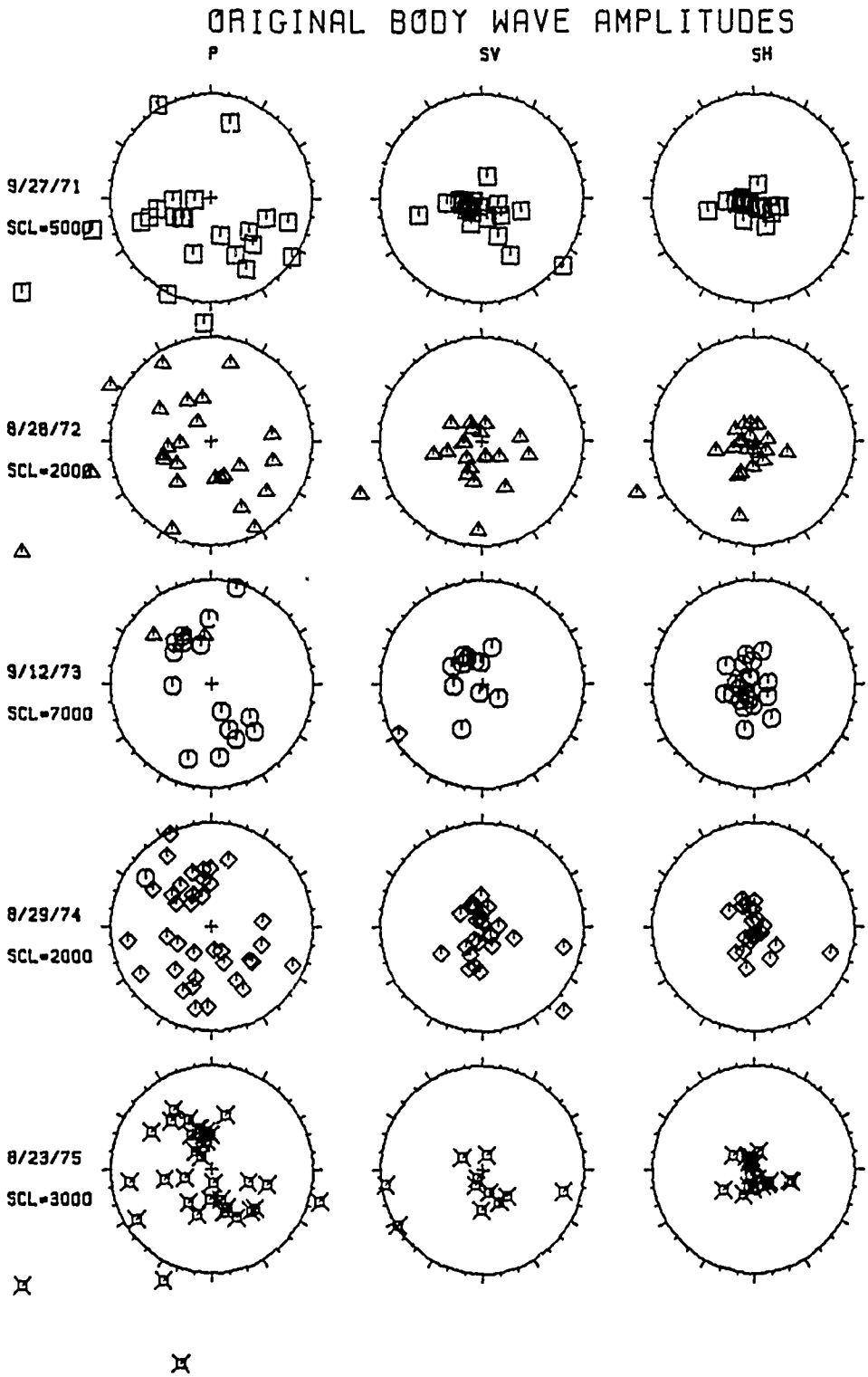

FIGURE 11a: Original body wave amplitudes for five Novaya Zemlya events plotted in polar coordinates. Azimuth is measured clockwise from North at the top and amplitude is proportional to distance from the center. The amplitude of the circle edge is shown on the right and applies to all three circles on a row.

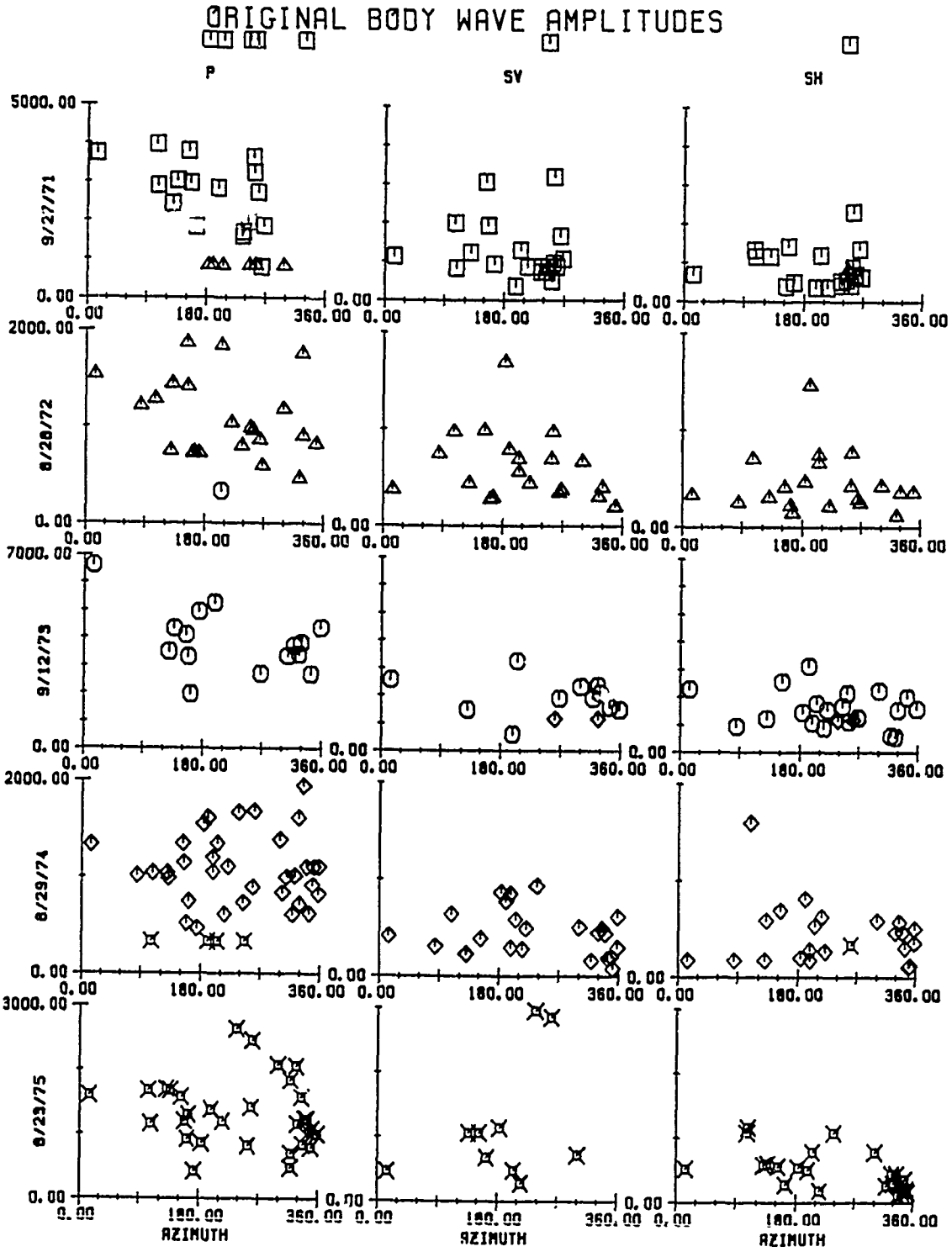

FIGURE 11b: Same as Figure 11a except plotted in rectangular coordinates.

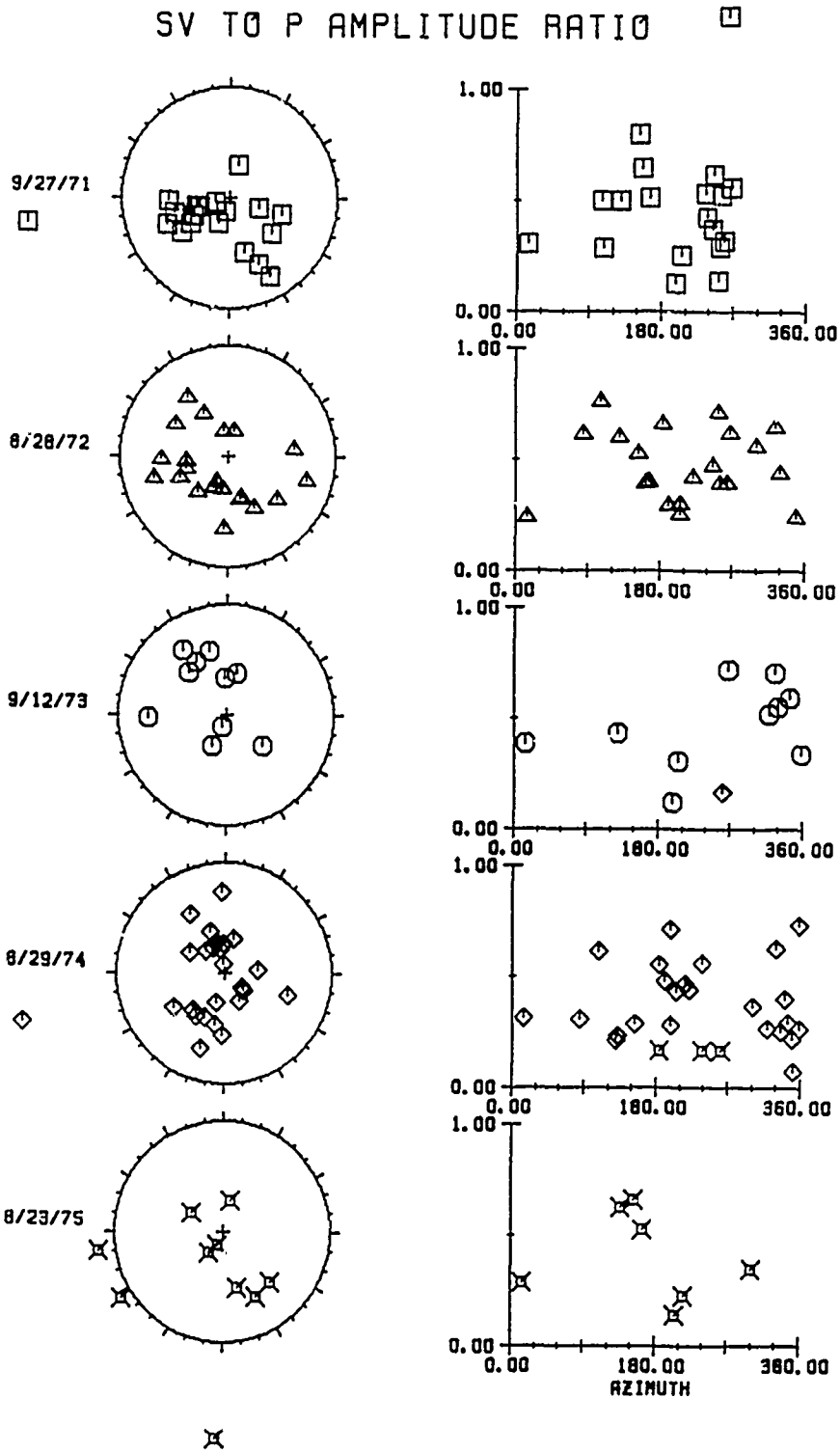

FIGURE 12: SV to P amplitude ratios for five Novaya Zemlya events plotted in both polar and rectangular coordinates.

4.2.4.2 Station Corrections

We next tried to reduce the scatter by computing and applying station corrections. The need for station corrections is clearly shown in Figure 11 by the behavior of station COP at an azimuth 246° (for the events of 9/27/71, 8/28/72, and 8/23/75). It is roughly five to ten times larger than stations within a few degrees to either side of it. It can also be seen by considering the neighboring stations QUE, SHI, NAI, and EIL located at azimuths of 165°, 183°, 199°, and 205°. For the event of 9/12/73, these stations had respective SV amplitudes of 1213, 3437, 887, and 2941 (Burger et al., 1986). Although the presence of a node could explain a large change in amplitude between two stations, it can not explain such extreme alternating amplitude behavior for stations within 40° of each other.

The station corrections shown in Figure 13 were computed by performing a least squares inversion which simultaneously solved for the event magnitudes. We started with the equation:

(5) $$\log(P_{ij}) = M_j + C_i$$

where P_{ij} is the observed amplitude at station i for event j, M_j is an unknown magnitude for event j, and C_i is the station correction for station i. From this we constructed the standard matrix equation

(6) $$Ax = b$$

where vector b contains the $\log(P_{ij})$, vector x contains the M_j and C_i, and matrix A is relatively sparse as each row is all zeros except for two ones which select the appropriate event and station.

The drawback to this method is that the resulting station corrections tend to contain not only the desired adjustment for station specific amplitude effects, but also a sinusoidal pattern due to the average tectonic release. However, when the corrections in Figure 13 are inspected, no sinusoidal pattern is apparent which suggests that the average tectonic release is small. A small average could result either from all the events having low tectonic release (as predicted by the surface wave results) or from a fortuitous cancellation of large tectonic release which varies from event to event. These two possibilities can be distinguished by examining the radiation patterns that result after the station corrections have been applied. If the tectonic release is truly small, no large residual sinusoidal pattern will be apparent. This is the case shown in Figure 14. Note that, in comparison to the original radiation patterns shown in Figure 11, the scatter has been greatly reduced. Unfortunately, however, there is still enough

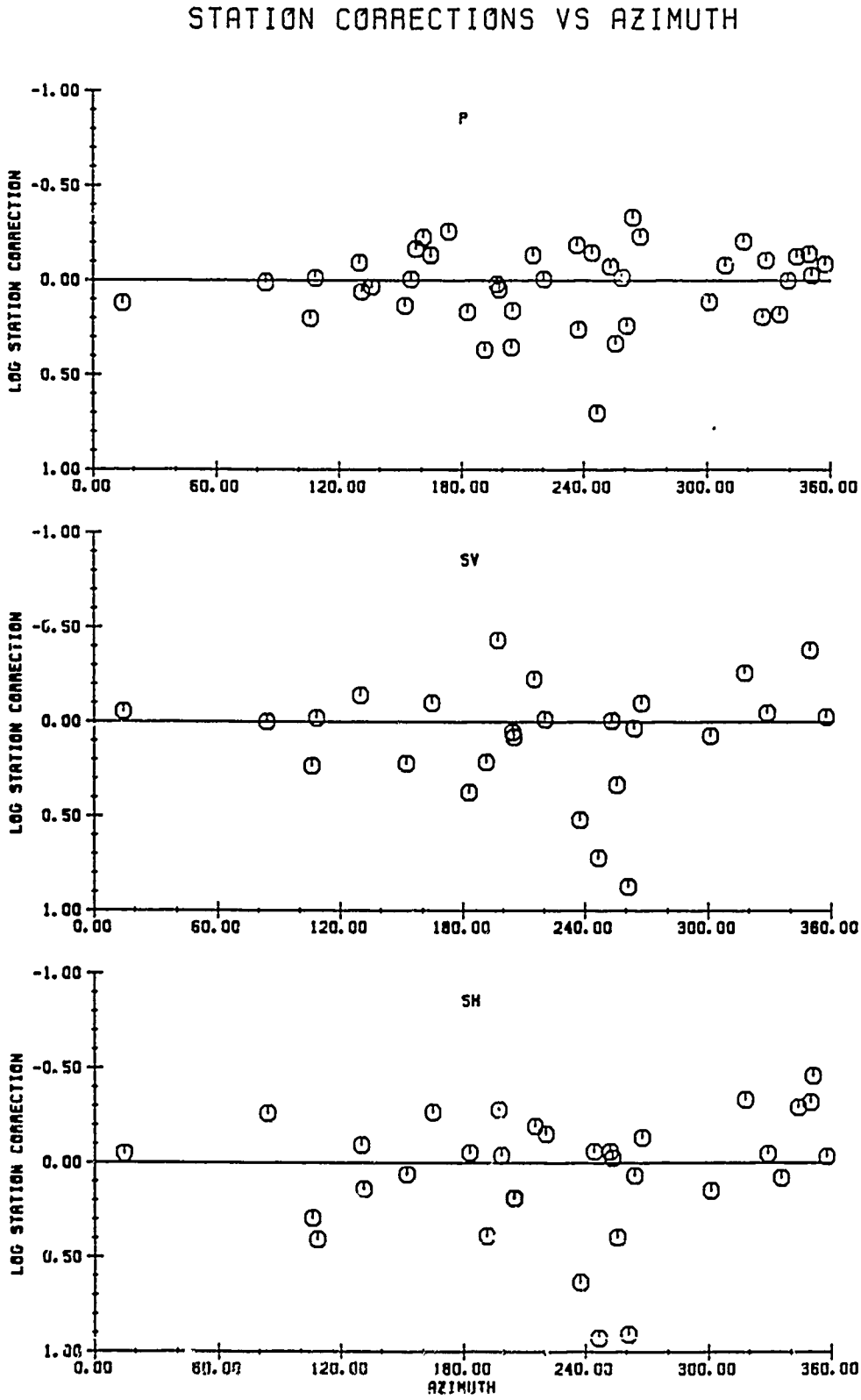

FIGURE 13: Log station corrections plotted as a function of azimuth. Note that no sinusoidal trend is apparent.

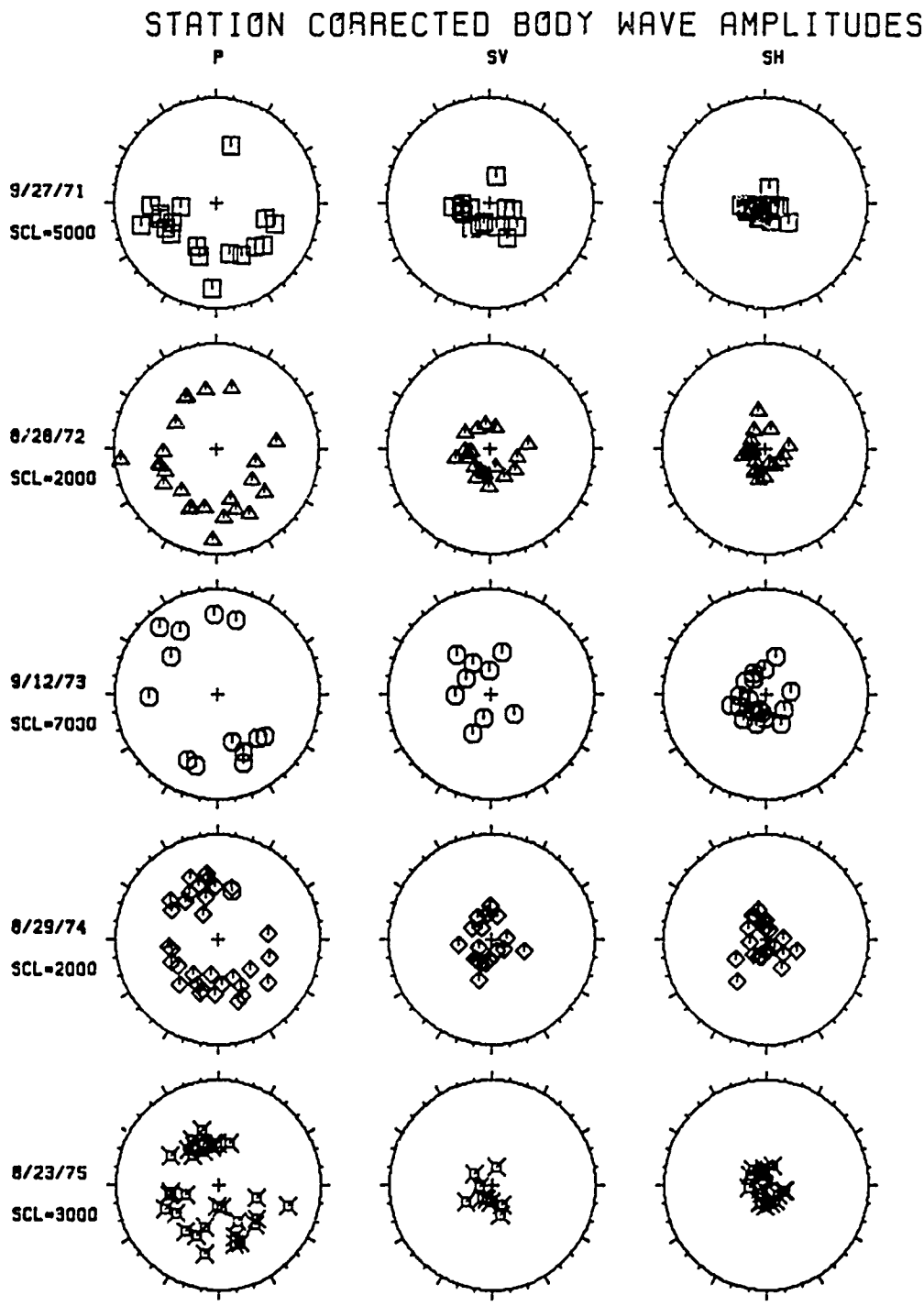

FIGURE 14a: Body wave amplitudes with station corrections applied for five Novaya Zemlya events plotted in polar coordinates. Azimuth is measured clockwise from North at the top and amplitude is proportional to distance from the center. The amplitude of the circle edge is shown on the right and applies to all three circles on a row. Compare with Figure 11 to see the improvement in scatter.

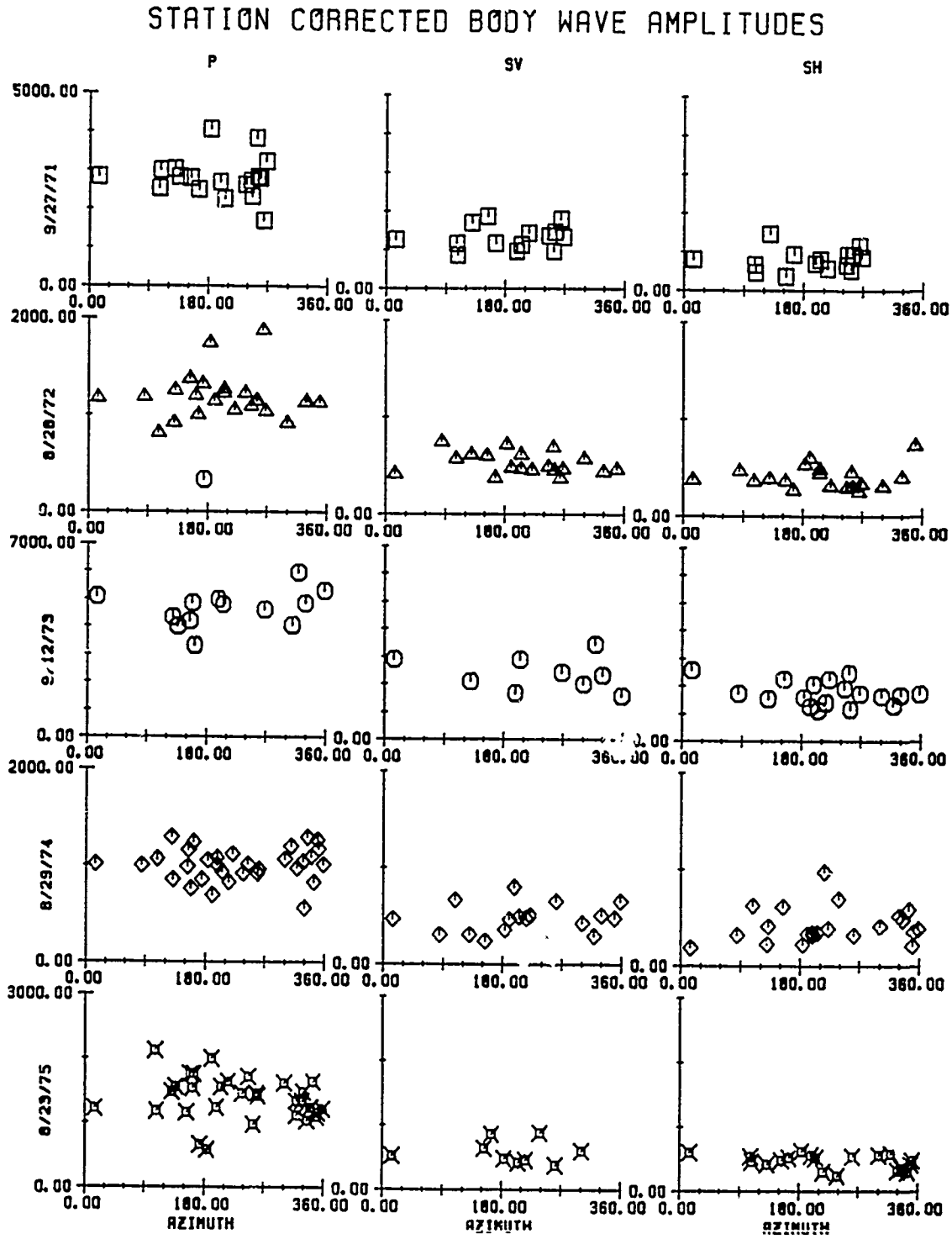

FIGURE 14b: Same as Figure 14a except plotted in rectangular coordinates.

scatter to prevent definite identification of the small sinusoidal patterns expected to be present, thereby preventing the determination of the tectonic release orientation.

4.2.4.3 Statistical Fit Criterion

Up to this point, we have been judging the amplitude results on the basis of whether or not a sinusoidal pattern was easily visible. We now wish to employ a more formal criterion with which to judge the results. To this end, we define the misfit or fit error between the data points and a fit line as:

$$(7) \qquad Err = \sqrt{\frac{\Sigma\ (X_{pt} - X_{crv})^2}{N - 1}}$$

where X_{pt} is the observed point, X_{crv} is the corresponding point on the curve, and N is the total number of points.

We considered the Northern Novaya Zemlya event of 9/12/73 since it is the largest event and was focused on by Burger et al. (1986). To remain more consistent with that earlier work, we used SV amplitudes measured from their Figure 9. These amplitudes are listed in our Table 11.

We first solved, in a least squares fashion, for the best fitting curve having the five term form described above. The resulting equation is:

(8) $A = -500.051 \sin(2\Theta) + 224.057 \cos(2\Theta) - 69.842 \sin(\Theta) - 496.310 \cos(\Theta) + 1658.243$

For comparison, we also computed the average of the data points:

(9) $A = 1745.575$

Both of these fit curves are shown in Figure 15, along with an approximation of the curve presented by Burger et al. (1986). For the five term curve, the fit error is 749 and, for the simple average curve, the fit error is 852. However, this direct comparison is misleading as it is not corrected for degrees of freedom. Although the absolute number of degrees of freedom present is somewhat uncertain, because we can not quantify the extent to which neighboring stations are influenced by similar geological conditions (and, therefore, are not

AZIMUTH	AMPLITUDE	AZIMUTH	AMPLITUDE
0.000	773.000	255.000	955.000
5.000	977.000	264.000	1318.000
15.000	1523.000	268.000	1886.000
84.000	1795.000	304.000	2068.000
87.000	1727.000	319.000	1977.000
109.000	1750.000	319.000	1386.000
131.000	1023.000	323.000	1250.000
136.000	3273.000	327.000	3159.000
153.000	2909.000	329.000	1705.000
163.000	1364.000	333.000	1682.000
165.000	1227.000	337.000	2182.000
173.000	3909.000	339.000	1364.000
183.000	3636.000	340.000	2727.000
199.000	909.000	344.000	2727.000
205.000	2955.000	345.000	2045.000
220.000	2386.000	351.000	733.000
236.000	636.000	353.000	1000.000
245.000	1273.000	355.000	1409.000
249.000	955.000	357.000	1250.000
252.000	1455.000	358.000	545.000

TABLE 11: List of SV amplitudes used for fitting event 9/12/73

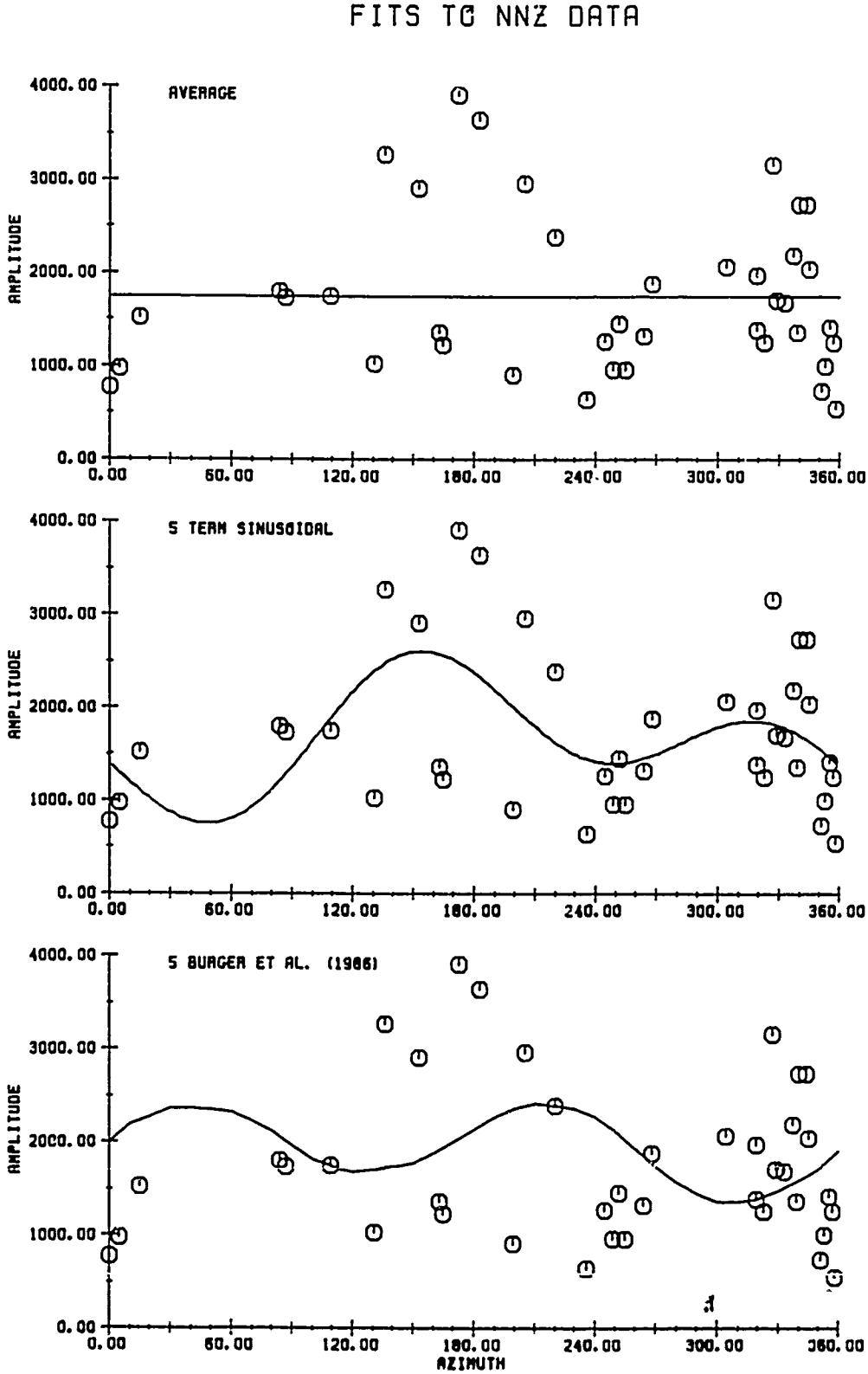

FIGURE 15: Various fits to the SV amplitudes of event 9/12/73. The top curve is a simple average, the middle curve is of the form A sin(2θ) + B cos(2θ) + C sin(tθ) + D cos(tθ) + E, and the bottom curve is an estimate of one presented by Burger et al. (1986).

independent), the five term curve clearly has four degrees of freedom less (and four free parameters more) than the average curve. To compensate for this difference we replace the N-1 term in the denominator of the misfit error computation with the term N-n-1 where n is the number of free parameters defining the curve (Gerald, 1978). Applying this modification, the fit error is 802 for the five term curve and 863 for the average curve.

Although the error for the five term curve is still smaller than the error for the average curve, it is not much smaller. In order to determine whether or not this difference in errors is meaningful, we apply an F-test for the equality of variances (Gulezian, 1979). First, we make the hypothesis (H0) that the true (population) variances are equal and that difference between the measured (sample) variances of the two fits is the result of a limited number of data points. Then we compute F, the ratio of the squared variances, and compare it with the value listed in one of the standard F-distribution tables. Assuming 35 and 39 degrees of freedom and working at the 5% significance level, we find a listed value of approximately 1.7. As this is greater than our computed value of 1.16, we can accept hypothesis H0 with 95% confidence. In other words, the five term curve does not provide a significantly better fit than the simple average curve. So, the formal, statistical results support our earlier visual judgements.

4.3 Joint Inversion Results

Our failure to find a reliable method for reducing scatter in SV amplitudes leaves us with surface wave, SH polarity, and relative P phase amplitude data. We apply our inversion methods to each of these data types successively to study the additional constraints imposed by each data type. We restrict ourselves to isotropic plus double couple solutions, as the data types available can not resolve a completely general moment tensor due to tradeoffs between the $(M_{xx} + M_{yy})$ and M_{zz} moment tensor elements.

We first consider the Novaya Zemlya event of 9/12/73. Our trial solutions use a 15° increment in strike, a 10° increment in dip, a 10° increment in slip, and a .05 increment in F#. Using a tolerance in d_{s1} of $\pm .1$ and d_{s2} of 10°, we find 2,832 possible solutions that fit the surface wave data within specified tolerance. These solutions span the complete space of slip angles from pure thrust to pure normal.

Using the SH polarities alone, we find 19,744 solutions that honor at least 8 of the 10 polarities, 272 of these honor all 10 polarities. Requiring the solutions to fit both the surface wave data and the SH polarity data (at the 8/10 level), we find 431 acceptable solutions. These are illustrated in Figure 16. Each figure represents one choice of F#. The axes indicate slip and dip angle, while strike is represented by the direction of the small line segment. For

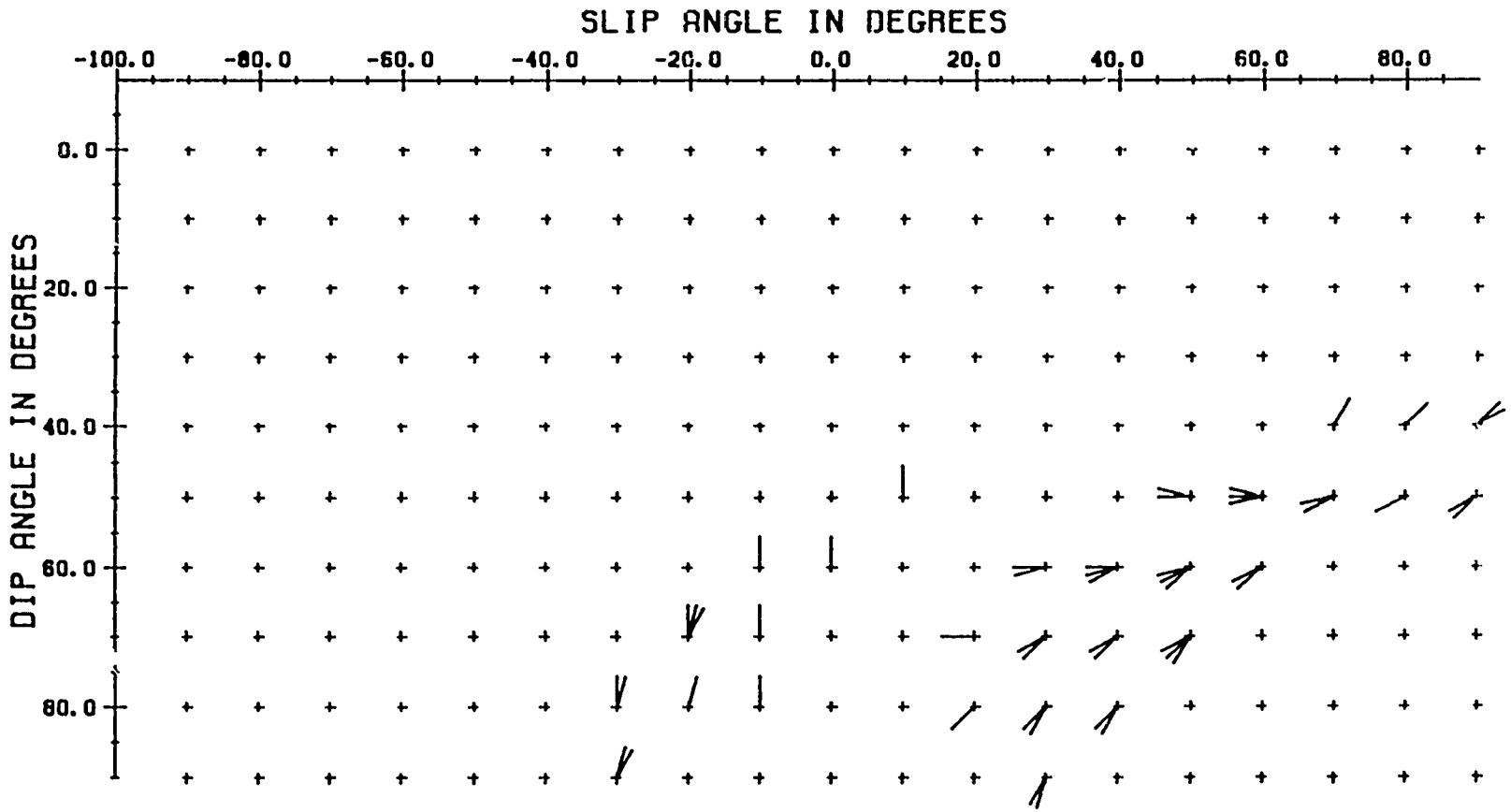

FIGURE 16a: Joint SH and surface wave inversion of Northern Novaya Zemlya event of 9/12/73. Two allowable SH inconsistencies and F# = .25.

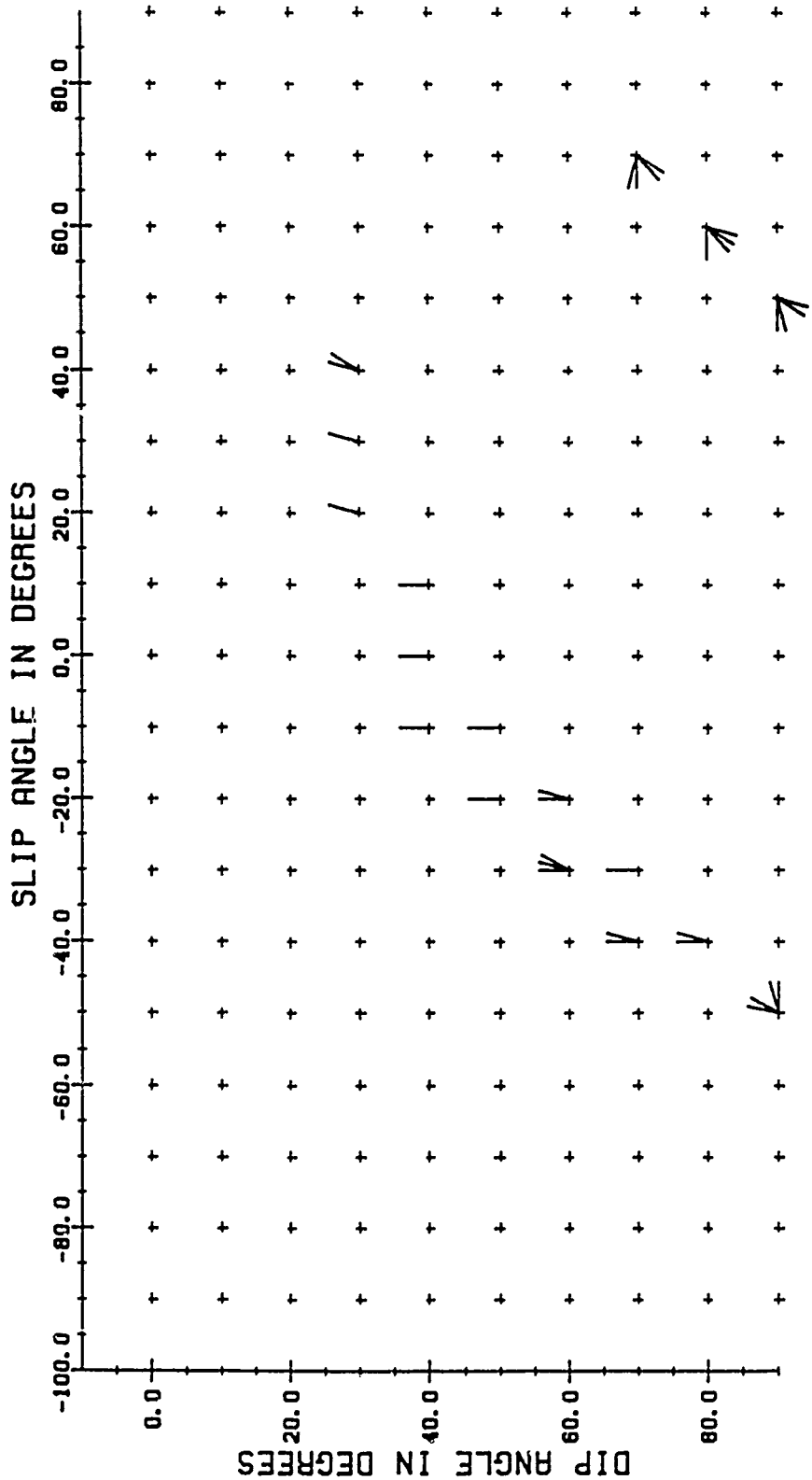

FIGURE 16b: Same as Figure 16a except with F# = .35.

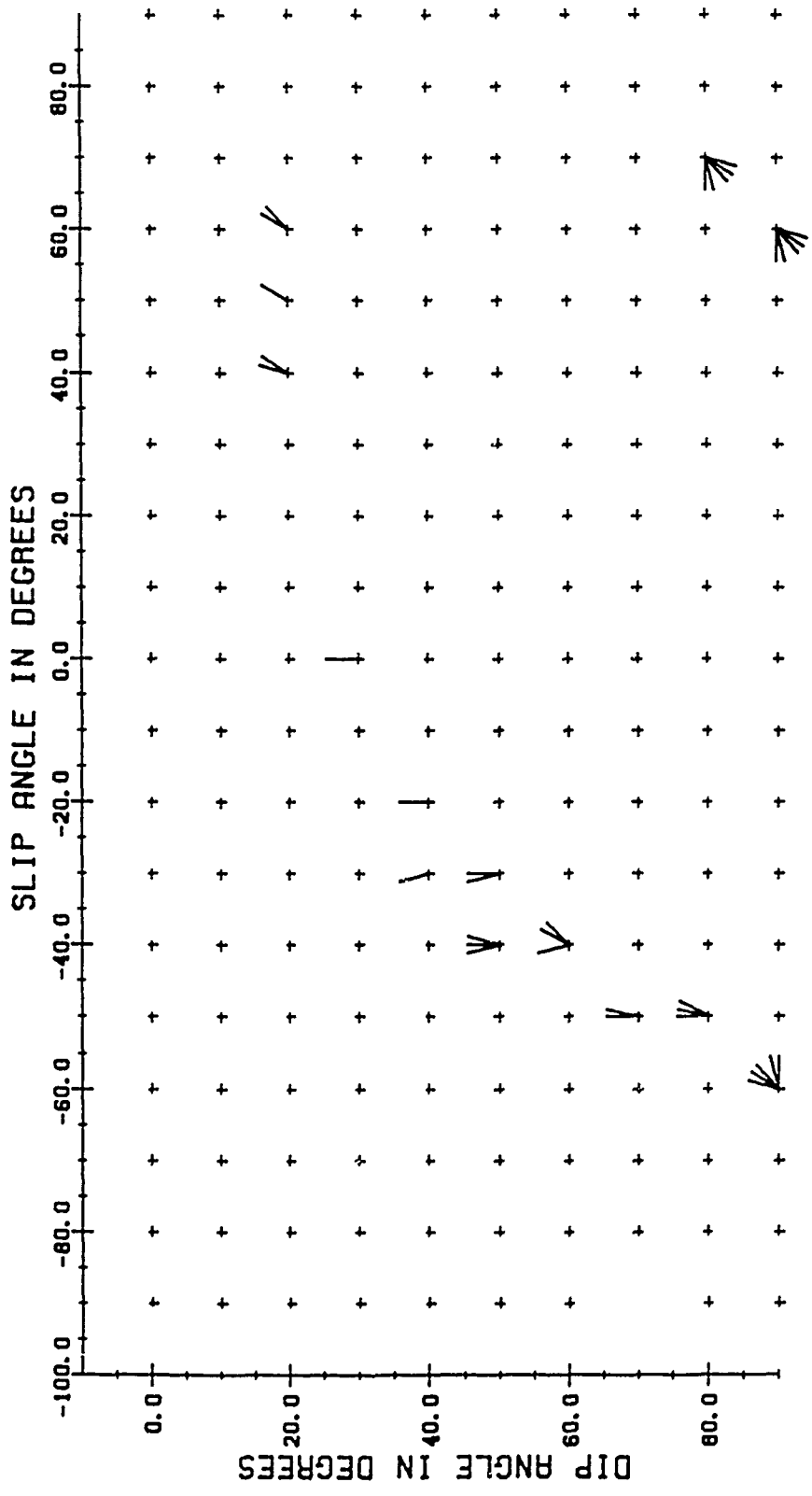

FIGURE 16c: Same as Figure 16a except with F# = .45.

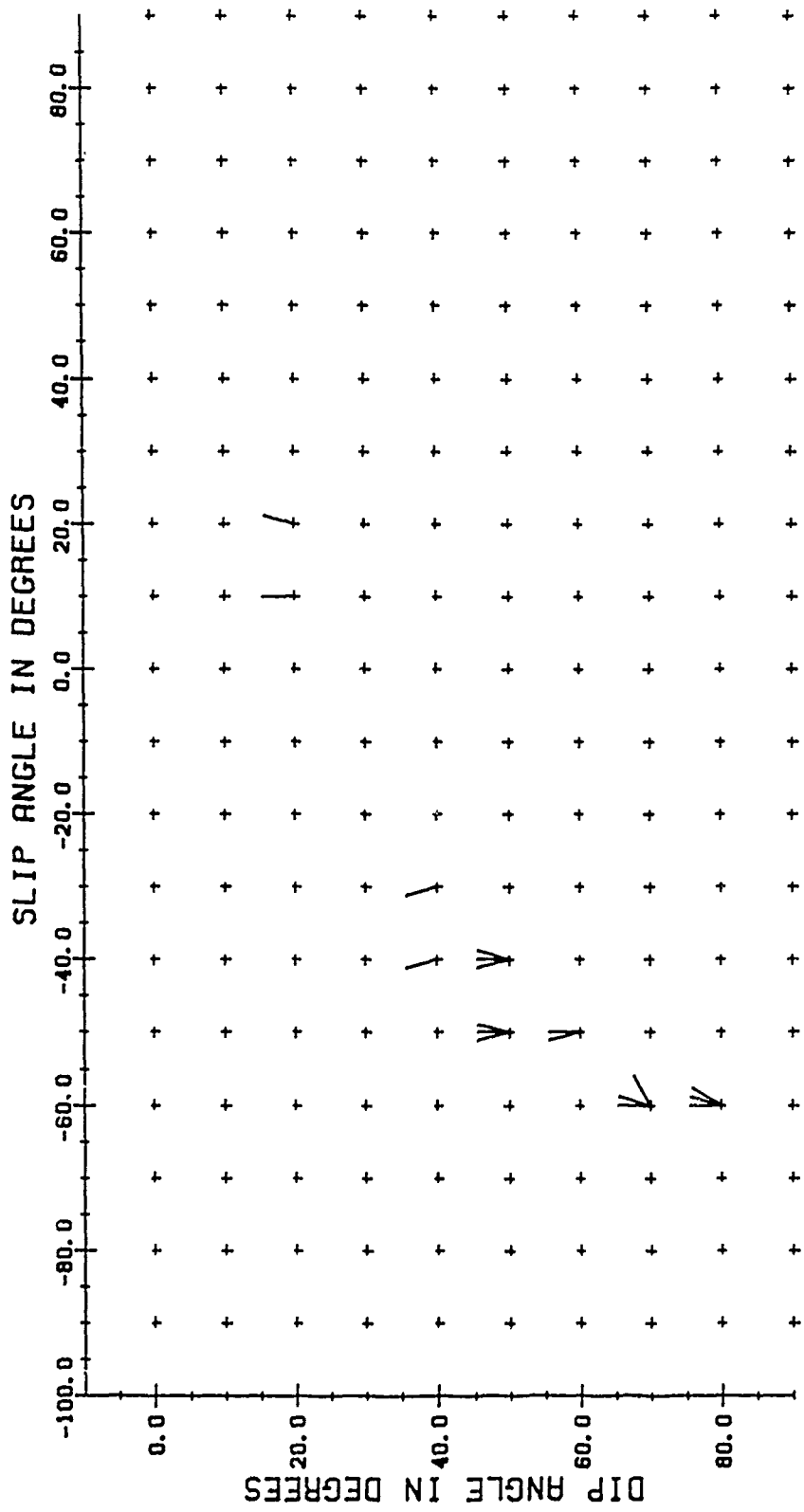

FIGURE 16d: Same as Figure 16a except with F# = .55.

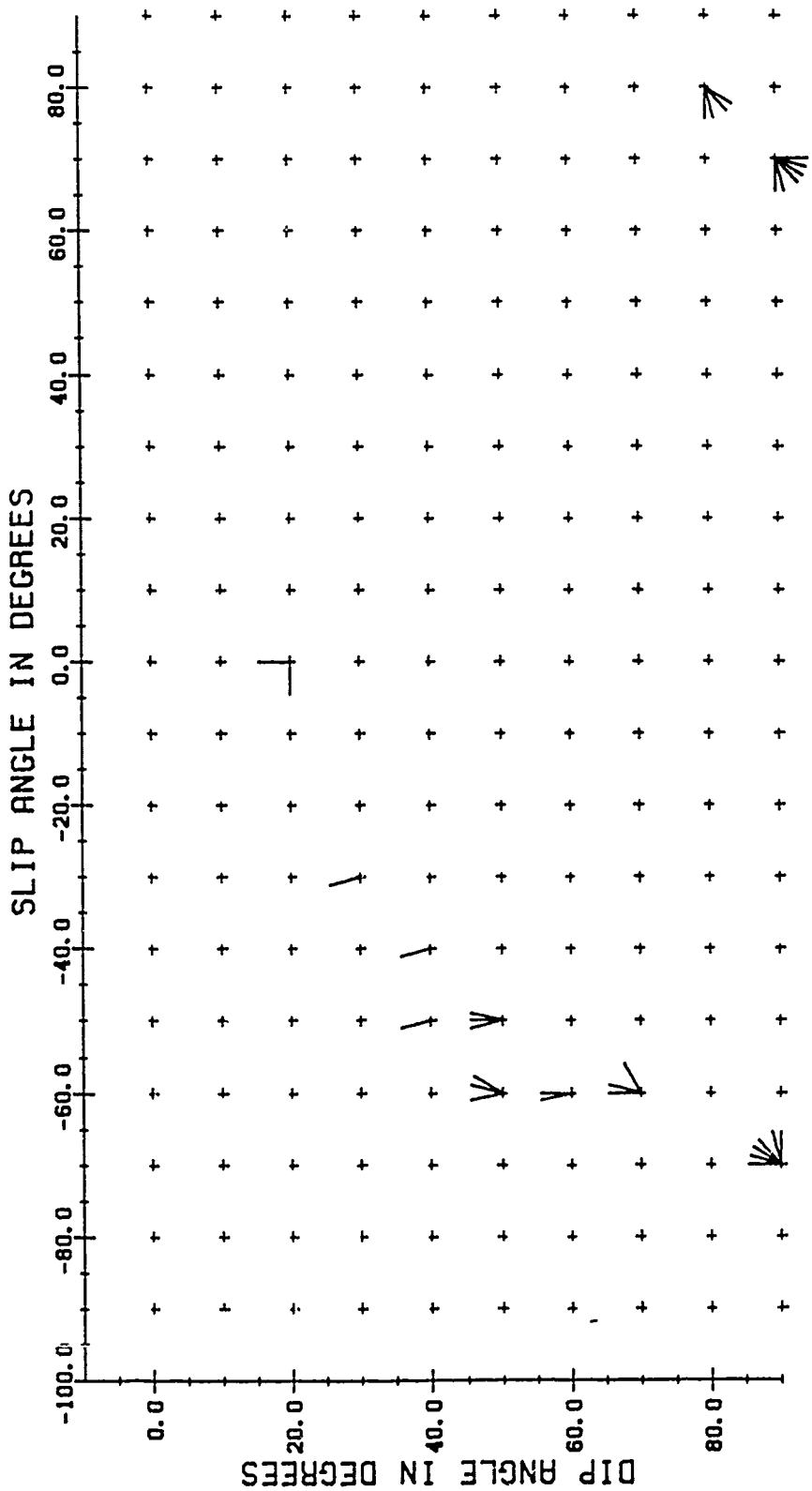

FIGURE 16c: Same as Figure 16a except with F# = .65.

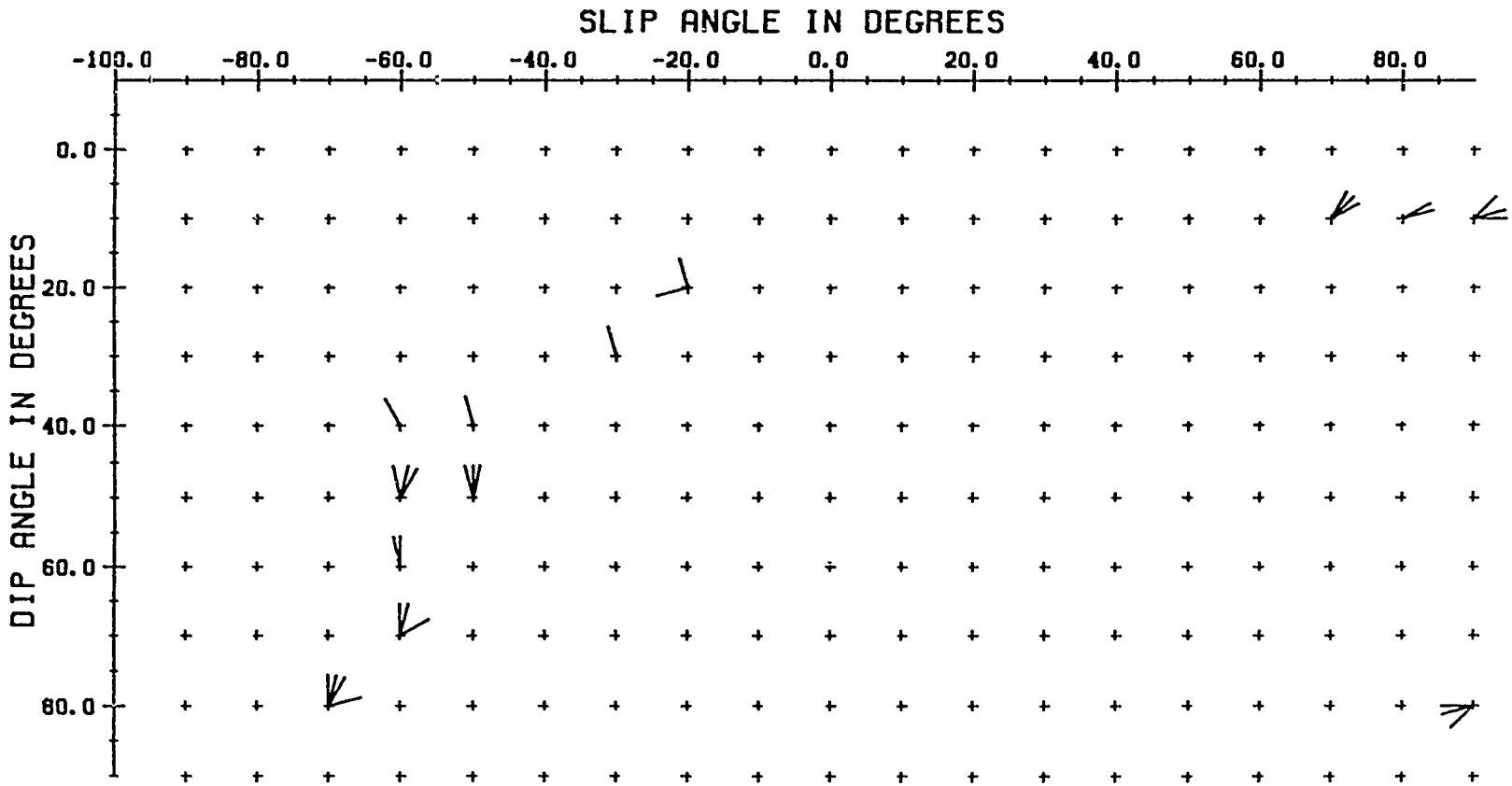

FIGURE 16f: Same as Figure 16a except with F# = .75.

brevity, we show plots of F#'s at .1 increments starting at F# = .25. Note the migration of solutions with increasing F#. This is caused by the decrease of efficiency of quadrapole radiation for dip angles near 0^0 or 90^0 and for slip angles near $\pm 90^0$. Only 4 of the solutions which fit both the surface wave data and the SH polarities actually honor all 10 SH polarities. These solutions are shown in Figure 17. Note that, despite the extremely small number of solutions, both oblique normal and pure thrust mechanisms are represented.

Adding the further requirement that solutions must fit the P wave data (pP/P and sP/P to a tolerance of .1) as well as the surface wave data and the SH polarities (at the 8/10 level), we find 38 possible solutions. These are shown in Figure 18. Although adding the P wave constraints significantly reduces the number of thrust solutions (down to 2), those solutions are not totally eliminated. Of the 38 solutions which fit all three types of data, there is only a single orientation which actually honors all 10 SH polarities. This solution, corresponding to a dip of 70^0 and a slip angle of -20^0, with F#'s of .25 and .30, is shown in Figure 19. With this orientation, tectonic release would have the effect of very slightly increasing the size of observed surface waves. Hence, M_S would produce a slight overestimate of explosion yield due to tectonic release effects.

Using the orientation from the joint inversion solutions and the surface wave source parameters (S_0, S_1, and S_2) from Tucker et al. (1989), we can compute the moment (M_I) for this event. The equation for moment, taken from Given and Mellman (1986) is

$$(10)\quad M_I = \frac{\alpha^2}{2\beta^2} S_0 + \frac{3\alpha^2}{4\beta^2} - 1 \qquad \frac{2 \sin \quad \sin 2\delta}{\sin^2 \quad \sin^2 2\delta + 4 \cos^2 \quad \sin^2 \delta}^{1/2} \quad (S_1^2+S_2^2)^{1/2}$$

where α is the P wave velocity, β is the S wave velocity, λ is the slip, and δ is the dip. The range of log moments determined using the various types of data are shown in Table 12, referenced to a strike slip solution. From this table, we can see that the existence of acceptable oblique normal and thrust solutions for the surface wave and SH cases leads to a large range of possible M_I values for each event. Only when all P phase and SH polarity constraints are met do we reject the thrust solution and place meaningful constraints on M_I. We applied the joint inversion method to the Northern Novaya Zemlya presumed underground explosions shown in Table 10. We set the error limits on pP/P and sP/P at .2, to reflect the probable reliability of these amplitude ratios and required all SH polarities to fit. The allowable solutions are summarized in Table 13. Note that for four of six events both thrust ($\delta=70^0, \lambda=90^0$) and oblique normal (about $\delta=60^0, \lambda=-30^0$) solutions are permitted. For one event, only thrust solutions are permitted, while for another, no solutions exist.

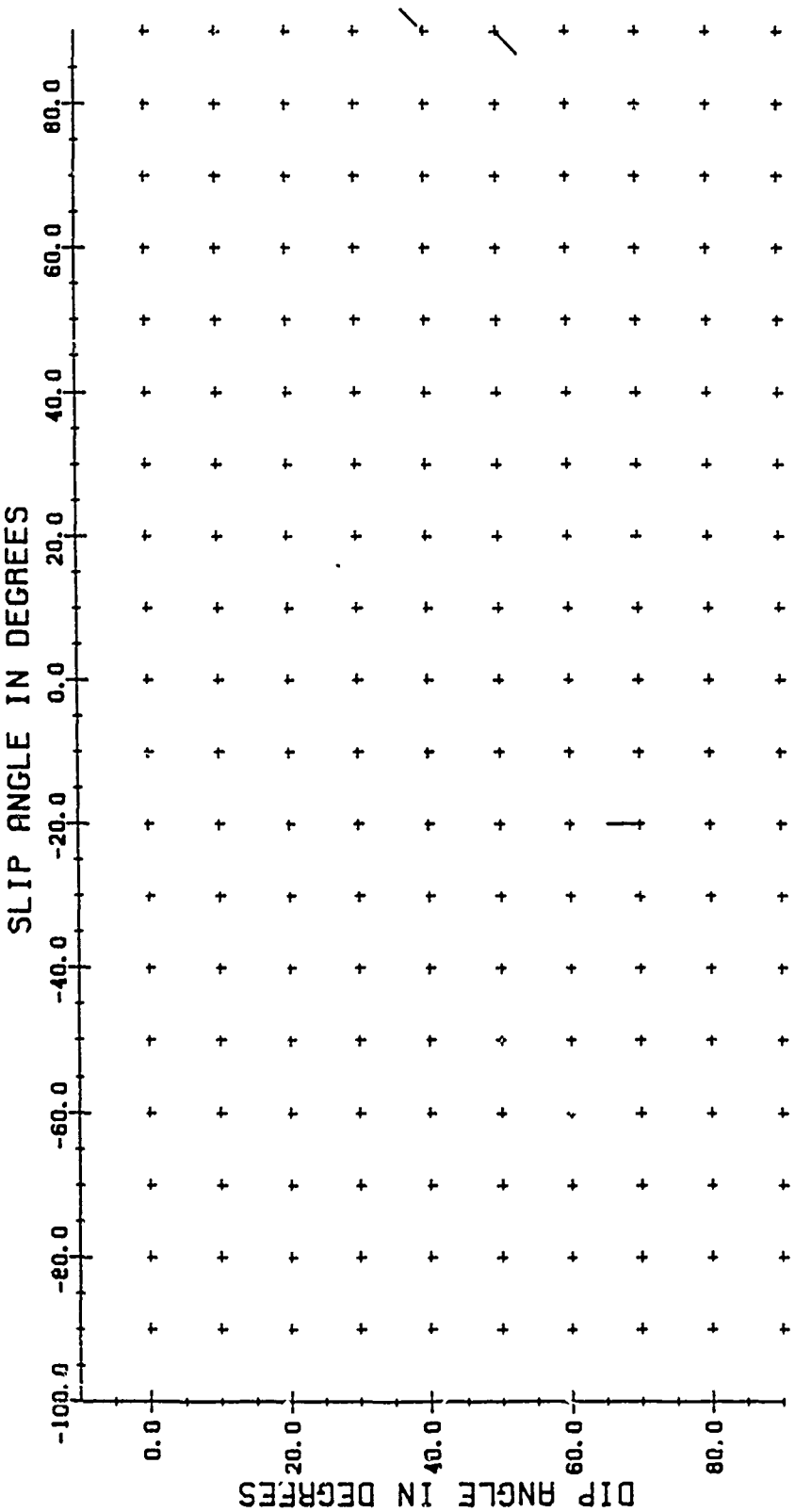

FIGURE 17a: Joint SH and surface wave inversion of Northern Novaya Zemlya event of 9/12/73. Zero allowable SH inconsistencies and F# = .25.

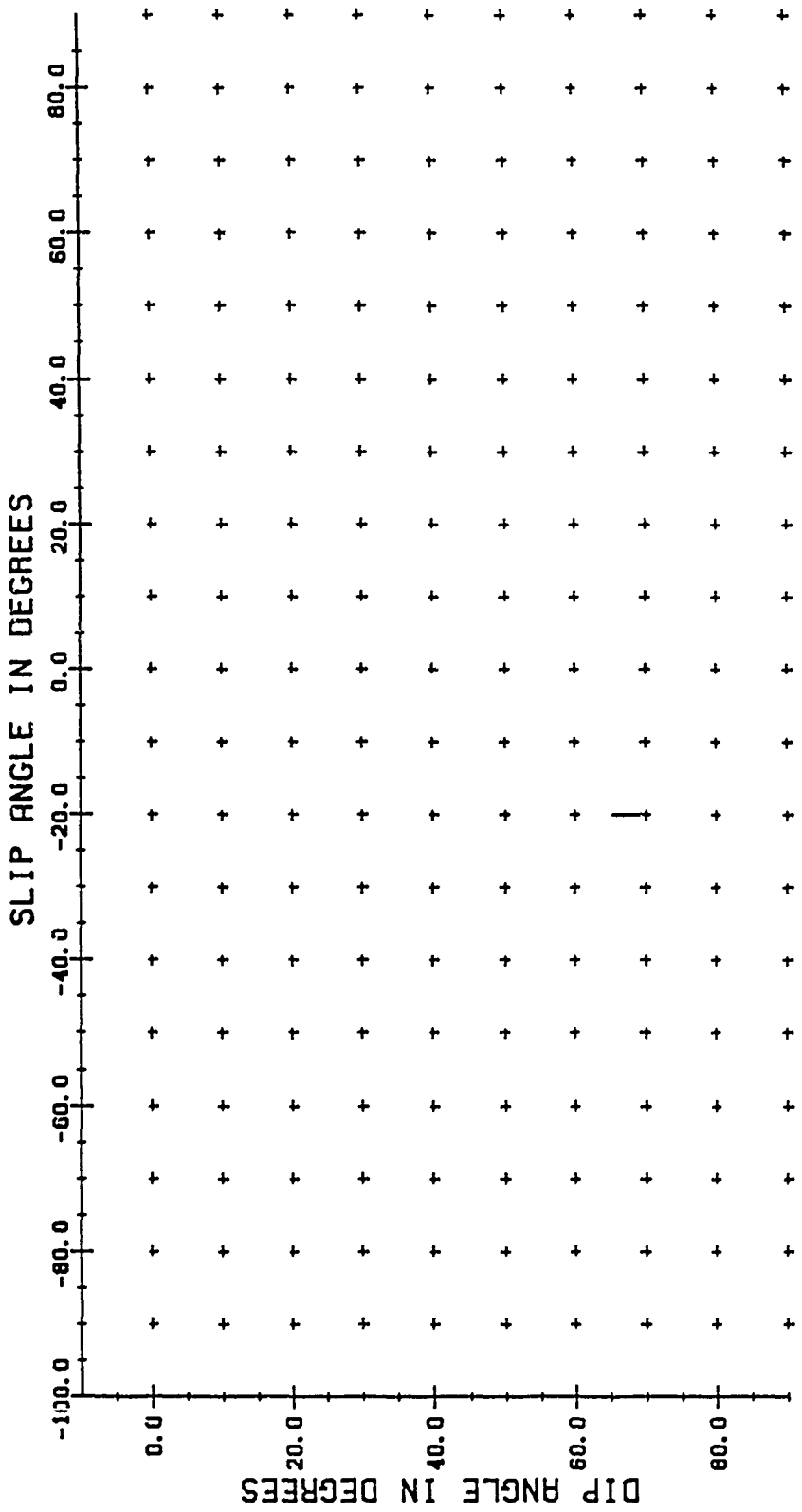

FIGURE 17b: Same as Figure 17a except with F# = .30.

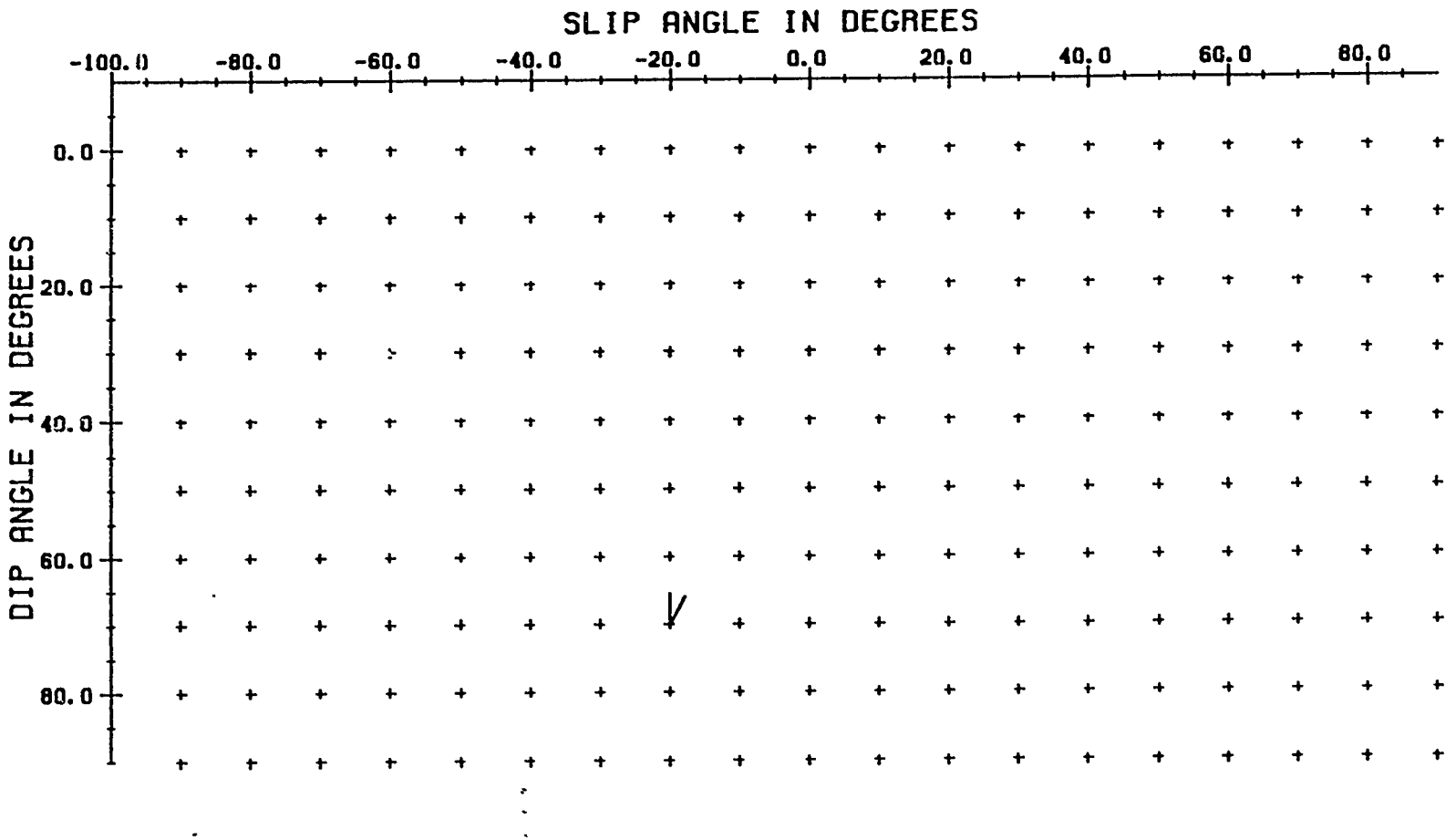

FIGURE 18a: Joint P wave, SH polarity, and surface wave inversion of Northern Novaya Zemlya event of 9/12/73. Two allowable SH inconsistencies and F# = .25.

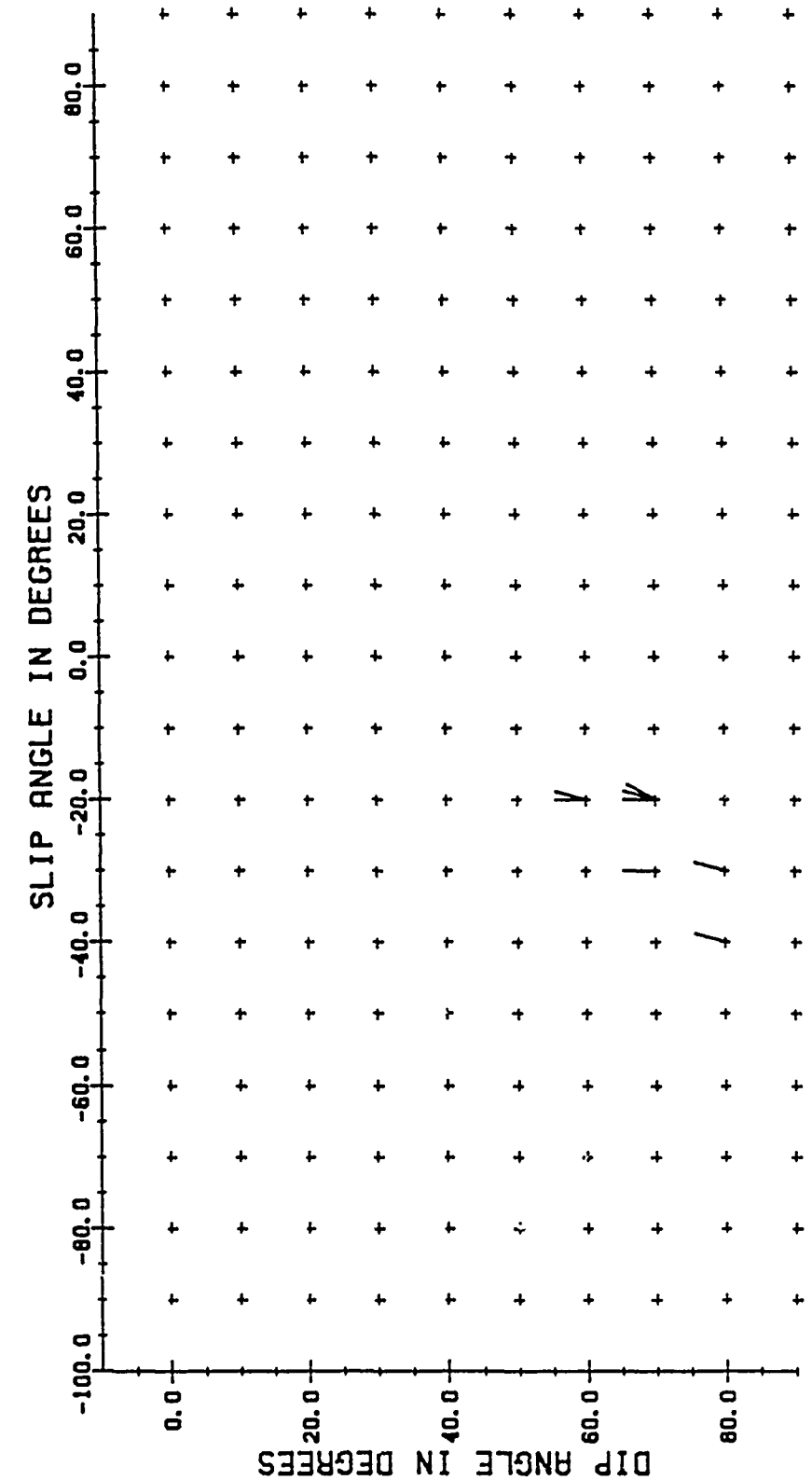

FIGURE 18b: Same as Figure 18a except with F# = .30.

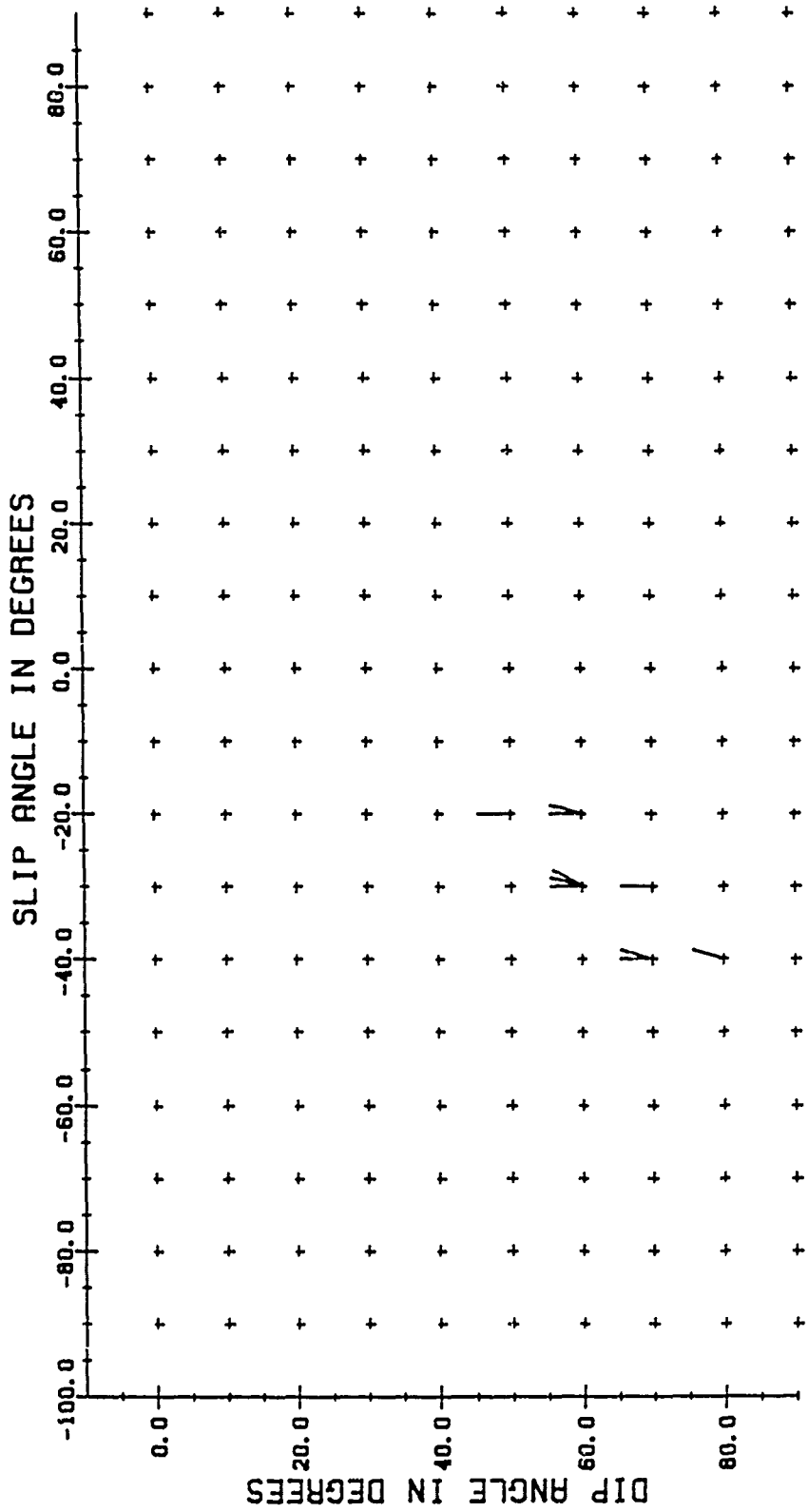

FIGURE 18c: Same as Figure 18a except with F# = .35.

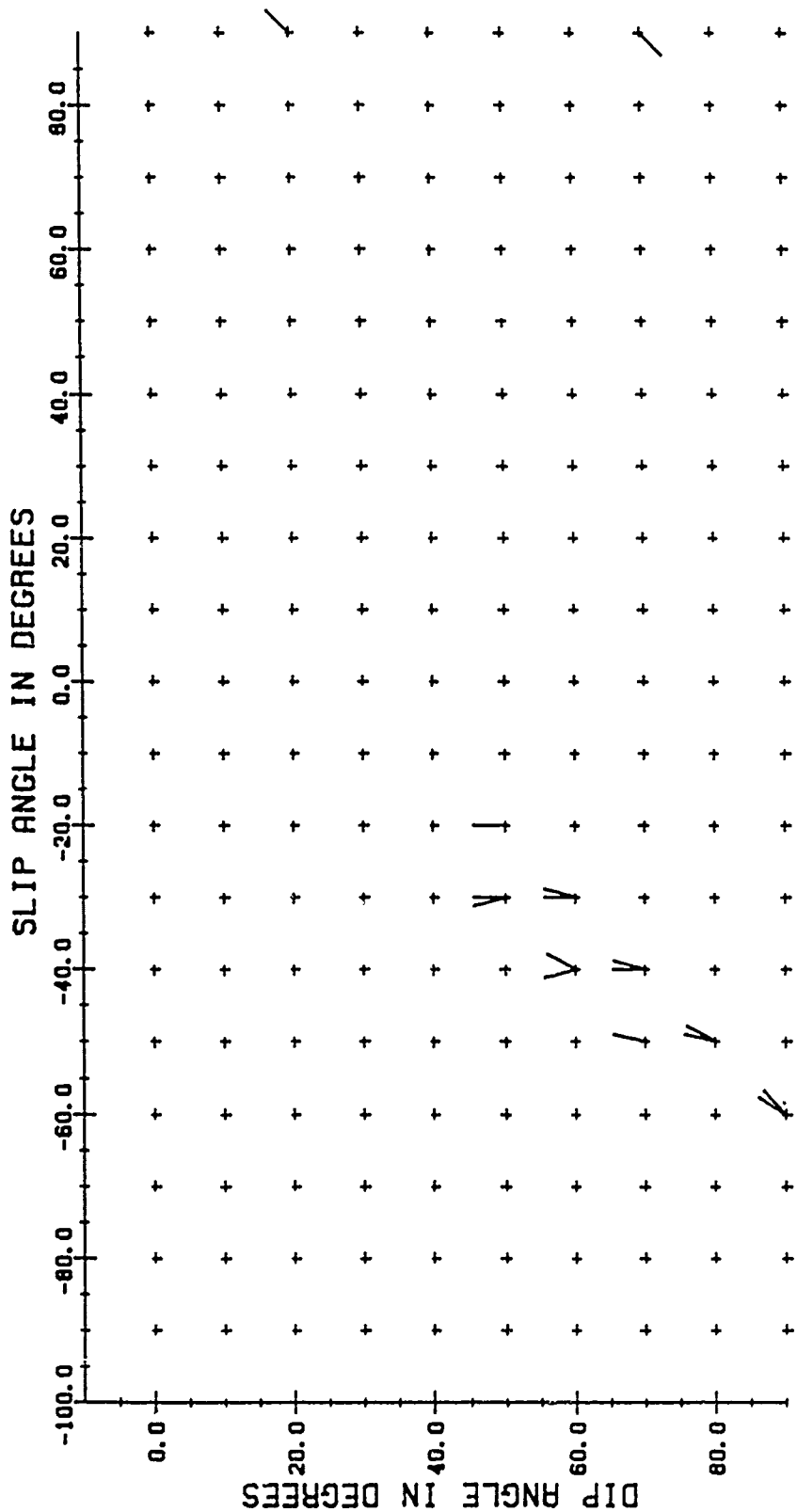

FIGURE 18d: Same as Figure 18a except with F# = .40.

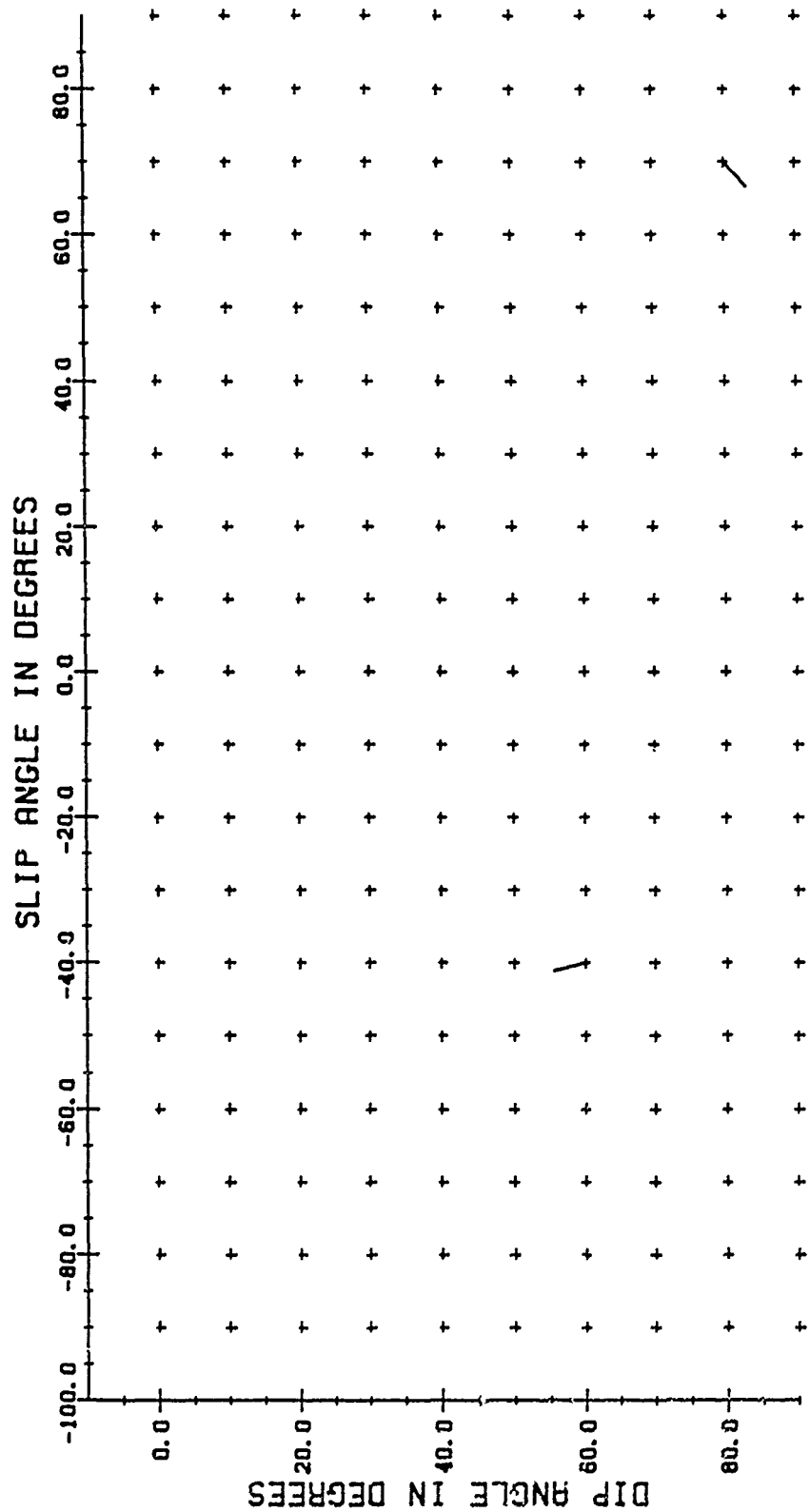

FIGURE 18c: Same as Figure 18a except with F# = .45.

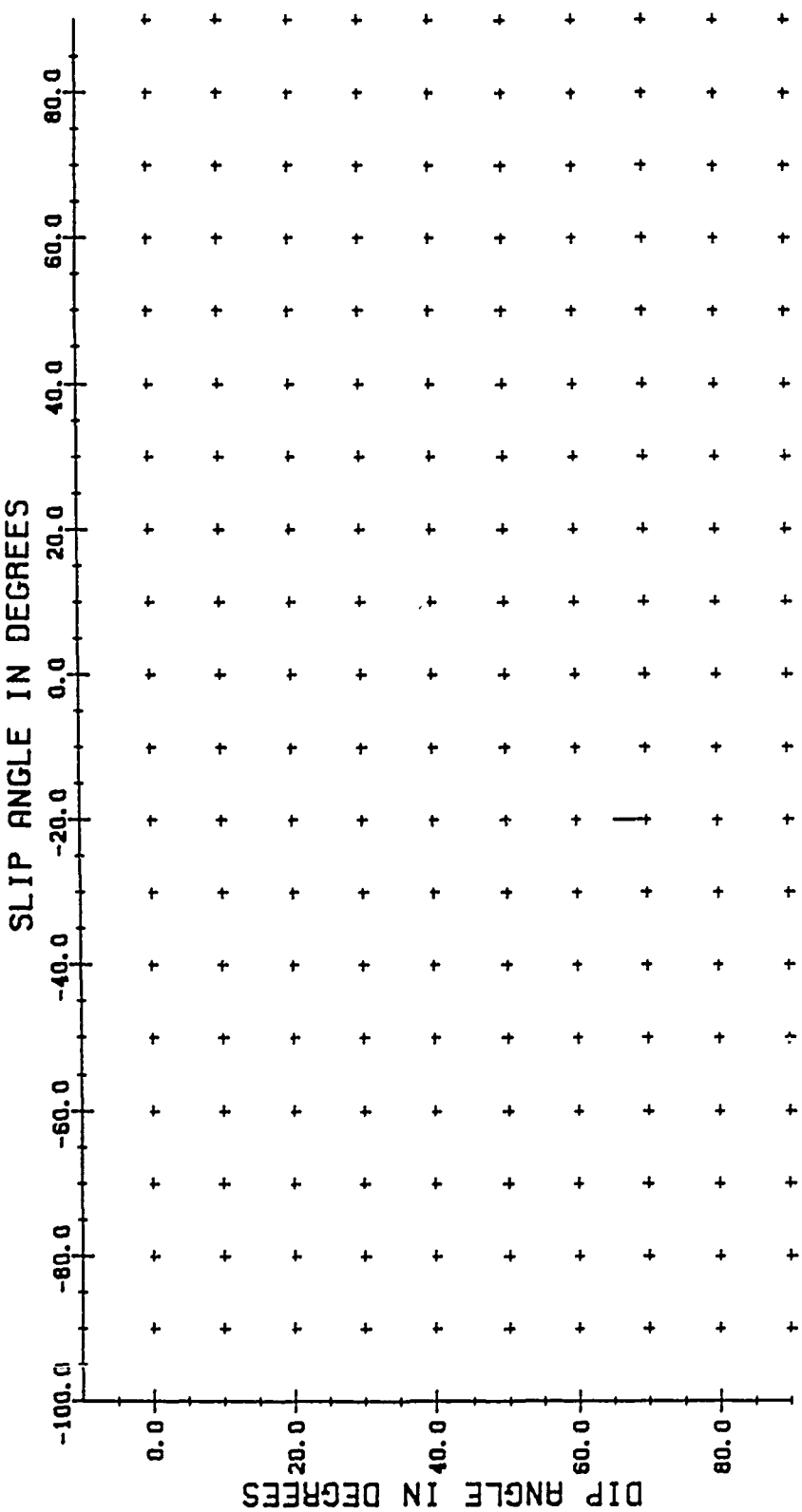

FIGURE 19a: Joint P wave, SH polarity, and surface wave inversion of Northern Novaya Zemlya event of 9/12/73. Zero allowable SH inconsistencies and F# = .25.

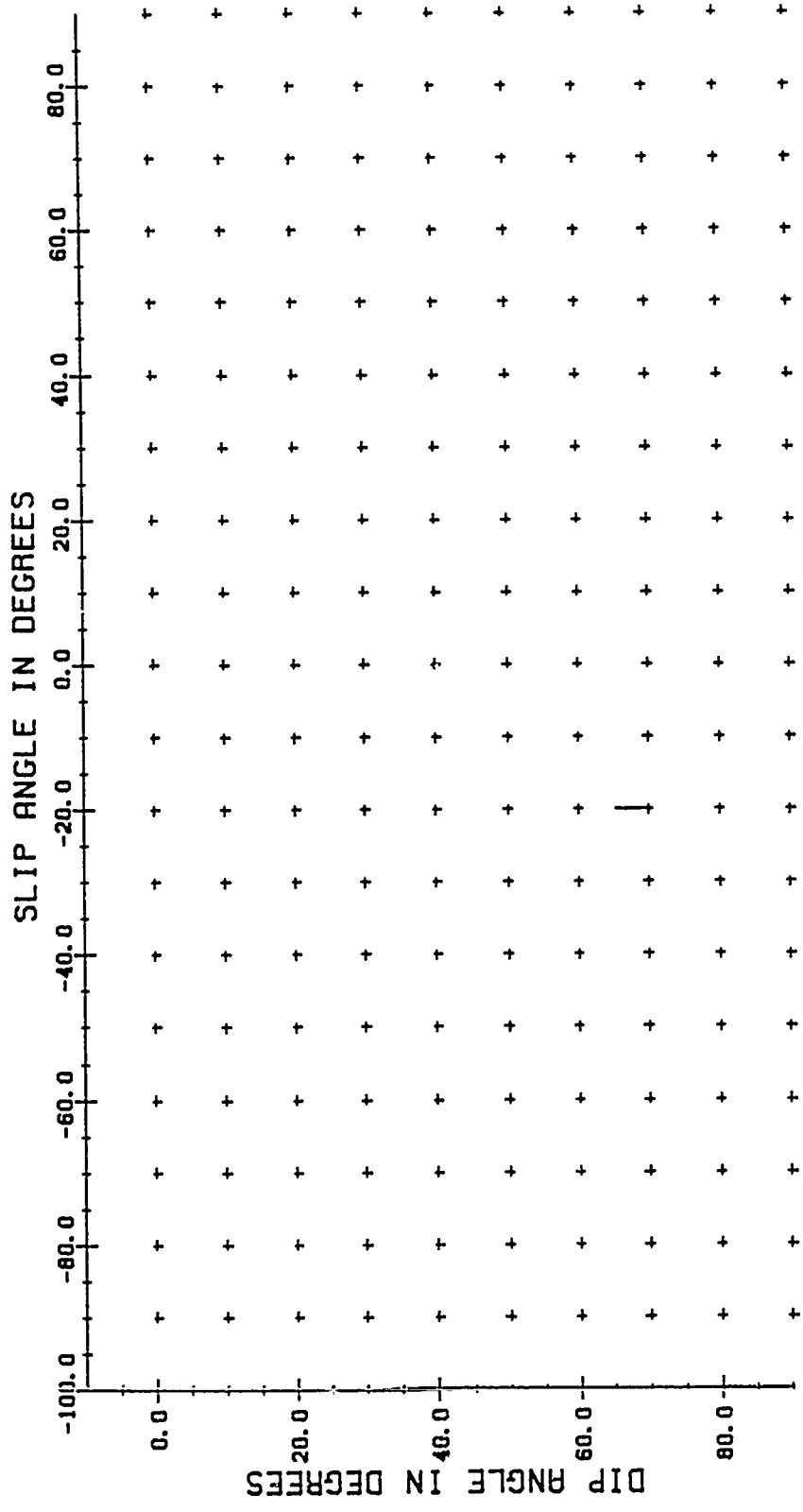

FIGURE 19b: Same as Figure 19a except with F# = .30.

DATA USED	MAX	MIN
Surface wave only	.21	-.44
Surface wave + SH 2 inconsistencies	.21	-.30
Surface wave + SH 0 inconsistencies	.21	-.04
Surface wave + P + SH 2 inconsistencies	.21	-.12
Surface wave + P + SH 0 inconsistencies	-.04	-.04

TABLE 12: Constraints on δ log M_I for 9/12/73 event.

Event Data	Strike	Slip	Dip	$\delta \log M_I$	m_b -.75logM_I
10/14/70	345	-30	60	-.09	5.22
	45	90	20	.20	5.44
	225	90	70	.20	5.44
9/27/71	No Solutions Found				
9/28/72	345	-30	60	-.09	5.03
	45	90	20	.13	5.19
	225	90	70	.13	5.19
	225	80	80	.12	5.18
9/12/73	345	-30	60	-.09	5.10
	345	-20	60	-.05	5.14
	30	80	20	.21	5.40
	45	90	20	.21	5.40
	225	90	70	.21	5.40
8/29/74	345	-30	60	-.02	5.08
	30	80	20	.10	5.20
	45	90	20	.11	5.21
	225	90	70	.11	5.21
8/29/74	45	90	20	.17	5.42
	225	90	70	.17	5.42

TABLE 13: Solutions using surface, P, and SH waves (no inconsistencies)

We repeated these inversions allowing one inconsistent SH polarity. The number of acceptable solutions increased dramatically, to about 80 per event. These solutions included both thrust and oblique normal mechanisms. Table 14 summarizes the constraints on log moment that can be inferred from these results.

4.4 Conclusions

The inclusion of P waveform and SH polarity data with surface wave data in a joint inversion yields multiple acceptable orientations when reasonable error bounds are used. For the six Northern Novaya Zemlya events studied in this report, it does not appear possible to distinguish between a thrust and an oblique normal orientation for tectonic release given the data available. The presence of multiple solutions does not appear to be a theoretical problem, but rather is caused by limitations imposed by data noise, modeling uncertainties and station distribution. Improved distribution of stations recording SH polarities, especially relatively close-in stations, may well resolve these ambiguities.

The ambiguity in orientation might theoretically be resolved through the use of P or SV wave amplitude data. Unfortunately, the high noise level in the SV amplitude data ruled out use of these data in the present study. Potentially more promising is the use of geologic data to determine the probable strike direction of the tectonic release component. Since the thrust and oblique normal mechanisms have strikes that differ by more than 45^{o}, it may be possible to distinguish between these mechanisms based on the general tectonic fabric of the source region. This study was not successful in explaining anomalous $M_I(f)$ behavior in terms of orientation changes. All events seem to share the same two basic possible solutions. Although a change between these two solution types could explain large M_I-m_b discrepancies, it seems extremely unlikely. There is far too much coincidence in changing between mechanisms that produce virtually identical SH radiation patterns for that scenario to be credible.

The presence of multiple, substantially different orientations that fit waveform, surface wave, and polarity data is rather disconcerting. It suggests that more effort than has generally been done in the past needs to be made to systematically search the model space for alternative solutions in studies involving both isotropic and double couple sources.

EVENT DATE	δ log M_I	m_b-.75logM_I
10/14/70	-.17 to .20	5.16 to 5.44
09/27/71	-.23 to .17	4.88 to 5.18
09/28/72	-.10 to .13	4.97 to 5.15
09/12/73	-.17 to .21	5.06 to 5.35
08/29/74	-.13 to .11	5.00 to 5.18
08/23/75	-.20 to .17	5.10 to 5.38

TABLE 14: Constraints on δ log M_I using surface, P, and SH waves (1 inconsistency)

5.0 REFERENCES

Aki, K. and P.G. Richards (1980). Quantitative seismology: theory and methods, W.H. Freeman and Co., San Francisco.

Burdick, L.J. and G.R. Mellman (1976). Inversion of the body waves from the Borrego Mountain earthquake to the source mechanism, Bull.Seism. Soc. Am. 66, 1485-1499.

Burger, R.W., T. Lay, T.C. Wallace, and L.J. Burdick (1986). Evidence of tectonic release in long period S waves from underground nuclear explosions at the Novaya Zemlya test sites, Bull. Seism. Soc. Am. 76, 733-755.

Gerald, C.F. (1978). Applied numerical analysis, second edition, Addison-Wesley Publishing Company, Reading, MA, 473.

Given, J.W. and G.R. Mellman (1986). Estimating explosion and tectonic release source parameters of underground nuclear explosions from Rayleigh and Love wave observations, Sierra Geophysics Report (SGI-R-86-126), Kirkland, WA.

Given, J.W. and G.R. Mellman (1986S). m_b-Yield relations for the Soviet test site at Shagan River inferred from comparison of long-period measurement of explosion source strength at NTS and Shagan River, Sierra Geophysics Report (SGI-R-86-122, SECRET), Kirkland, WA.

Gulezian, R.C. (1979). Statistics for decision making, W.B. Saunders Company, Philadelphia, 395-396.

Kanamori, H. and G.S. Stewart (1976). Mode of the strain release along the Gibbs Fracture Zone, Mid-Atlantic Ridge, Phys. Earth Planet. Int. 11, 312-332.

McLaughlin, K.L., D.W. Rivers, and M.A. Brennan (1983). Pearce focal sphere analysis of explosion and earthquake mechanisms, Teledyne Geotech Technical Report (TGAL-TR-83-4), Alexandria, VA.

Murphy, J.R. and A. O'Donnell (1987S). Comparisons of explosion test sites using network-averaged teleseismic P wave spectra, S-Cubed Technical Report (SSS-CR-87-8529, SECRET), La Jolla, CA.

Pearce, R.G. (1977). Fault plane solutions using relative amplitudes of pP and P, Geophys. J. R. Astr. Soc. 50, 381-394.

Stevens, J.L. and K.L. McLaughlin (1989). Analysis of surface waves from Novaya Zemlya, Mururoa, and Amchitka test sites, and maximum likelihood estimation of scalar moments from earthquakes and explosions, S-Cubed Technical Report (SSS-TR-89-9953), La Jolla, CA.

Tucker, W.C., G.R. Mellman, and J.W. Given (1989). Using long period surface waves to estimate the isotropic moment of underground explosions at Novaya Zemlya, Sierra Geophysics Report (SGI-R-89-141), Kirkland, WA.

DISTRIBUTION LIST
FOR UNCLASSIFIED REPORTS
DARPA-FUNDED PROJECTS
(Last Revised: 26 Sep 89)

RECIPIENT	NUMBER OF COPIES
DEPARTMENT OF DEFENSE	
DARPA/NMRO ATTN: Dr. R. Alewine and Dr. R. Blandford 1400 Wilson Boulevard Arlington, VA 22209-2308	2
Defense Intelligence Agency Directorate for Scientific and Technical Intelligence Washington, D.C. 20340-6158	1
Defense Nuclear Agency Shock Physics Directorate/SD Washington, D.C. 20305-1000	1
Defense Technical Information Center Cameron Station Alexandria, VA 22314	2
DEPARTMENT OF THE AIR FORCE	
AFOSR/NP Bldg 410, Room C222 Bolling AFB, Washington, D.C. 20332-6448	1
AFTAC/STINFO Patrick AFB, FL 32925-6001	1
AFTAC/TT Patrick AFB, FL 32925-6001	3
AFWL/NTESG Kirkland AFB, NM 87171-6008	1
GL/LWH ATTN: Mr. James Lewkowicz Terrestrial Sciences Division Hanscom AFB, MA 01731-5000	1
DEPARTMENT OF THE NAVY	
NORDA ATTN: Dr. J.A. Ballard Code 543 NSTL Station, MS 39529	1

DEPARTMENT OF ENERGY

Department of Energy — 1
ATTN: Mr. Max A. Koontz (DP-331)
International Security Affairs
1000 Independence Avenue
Washington, D.C. 20585

Lawrence Livermore National Laboratory — 3
ATTN: Dr. J. Hannon, Dr. S. Taylor, and Dr. K. Nakanishi
University of California
P.O. Box 808
Livermore, CA 94550

Los Alamos Scientific Laboratory — 2
ATTN: Dr. C. Newton
P.O. Box 1663
Los Alamos, NM 87544

Sandia National Laboratories — 1
ATTN: Mr. P. Stokes, Dept. 9110
P.O. Box 5800
Albuquerque, NM 87185

OTHER GOVERNMENT AGENCIES

Central Intelligence Agency — 1
ATTN: Dr. L. Turnbull
OSI/NED, Room 5G48
Washington, D.C. 20505

U.S. Arms Control and Disarmament Agency — 1
ATTN: Dr. M. Eimer
Verification and Intelligence Bureau, Rm 4953
Washington, D.C. 20451

U.S. Arms Control and Disarmament Agency — 1
ATTN: Mr. R.J. Morrow
Multilateral Affairs Bureau, Rm 5499
Washington, D.C. 20451

U.S. Geological Survey — 1
ATTN: Dr. T. Hanks
National Earthquake Research Center
345 Middlefield Road
Menlo Park, CA 94025

U.S. Geological Survey MS-913 — 1
ATTN: Dr. R. Masse
Global Seismology Branch
Box 25046, Stop 967
Denver Federal Center
Denver, CO 80225

UNIVERSITIES

Boston College 1
ATTN: Dr. A. Kafka
Western Observatory
381 Concord Road
Weston, MA 02193

California Institute of Technology 1
ATTN: Dr. D. Harkrider
Seismological Laboratory
Pasadena, CA 91125

Columbia University 1
ATTN: Dr. L. Sykes
Lamont-Doherty Geological Observatory
Palisades, NY 10964

Cornell University 1
ATTN: Dr. M. Barazangi
INSTOC
Snee Hall
Ithaca, NY 14853

Harvard University 1
ATTN: Dr. J. Woodhouse
Hoffman Laboratory
20 Oxford Street
Cambridge, MA 02138

Massachusetts Institute of Technology 3
ATTN: Dr. S. Soloman, Dr. N. Toksoz, and Dr. T. Jordan
Department of Earth and Planetary Sciences
Cambridge, MA 02139

Southern Methodist University 2
ATTN: Dr. E. Herrin and Dr. B. Stump
Geophysical Laboratory
Dallas, TX 75275

State University of New York at Binghamton 1
ATTN: Dr. F. Wu
Department of Geological Sciences
Vestal, NY 13901

St. Louis University 2
ATTN: Dr. B. Mitchell and Dr. R. Herrmann
Department of Earth and Atmospheric Sciences
3507 Laclede
St. Louis, MO 63156

The Pennsylvania State University 1
ATTN: Dr. S. Alexander
Geosciences Department
403 Deike Building
University Park, PA 16802

University of Arizona 1
ATTN: Dr. T. Wallace
Department of Geosciences
Tucson, AZ 85721

University of California, Berkeley 1
ATTN: Dr. T. McEvilly
Department of Geology and Geophysics
Berkeley, CA 94720

University of California, Los Angeles 1
ATTN: Dr. L. Knopoff
405 Hilgard Avenue
Los Angeles, CA 90024

University of California, San Diego 1
ATTN: Dr. J. Orcutt
Scripps Institute of Occanography
La Jolla, CA 92093

University of Colorado 1
ATTN: Dr. C. Archambeau
CIRES
Boulder, CO 80309

University of Illinois 1
Dr. S. Grand
Department of Geology
1301 West Green Street
Urbana, IL 61801

University of Michigan 1
ATTN: Dr. T. Lay
Department of Geological Sciences
Ann Arbor, MI 48109-1063

University of Nevada 1
ATTN: Dr. K. Priestly
Mackay School of Mines
Reno, NV 89557

University of Southern California 1
ATTN: Dr. K. Aki
Center for Earth Sciences
University Park
Los Angeles, CA 90089-0741

DEPARTMENT OF DEFENSE CONTRACTORS

Analytical Sciences Corporation, The 1
Dr. Richard Sailor
ATTN: Document Control
55 Walkers Brook Drive
Reading, MA 01867

Applied Theory, Inc. 1
ATTN: Dr. J. Trulio
930 South La Brea Avenue
Suite 2
Los Angeles, CA 90036

Center for Seismic Studies 2
ATTN: Dr. C. Romney and Mr. R. Perez
1300 N. 17th Street, Suite 1450
Arlington, VA 22209

ENSCO, Inc. 1
ATTN: Mr. John R. Stevenson
P.O. Box 1346
Springfield, VA 22151

ENSCO, Inc. 2
ATTN: Dr. R. Kemerait
445 Pineda Court
Melbourne, FL 32940-7508

Gould Inc. 1
ATTN: Mr. R.J. Woodard
Chesapeake Instrument Division
6711 Baymeado Drive
Glen Burnie, MD 21061

Maxwell Laboratories, Inc. 1
S-CUBED Reston Geophysics Office
Reston International Center
ATTN: Mr. J. Murphy, Suite 1112
11800 Sunrise Valley Drive
Reston, VA 22091

Pacific Sierra Research Corporation 1
ATTN: Mr. F. Thomas
12340 Santa Monica Boulevard
Los Angeles, CA 90025

Rockwell International 1
ATTN: B. Tittmann
1049 Camino Dos Rios
Thousand Oaks, CA 91360

Rondout Associates, Inc. 1
ATTN: Dr. P. Pomeroy
P.O. Box 224
Stone Ridge, NY 12484

Science Applications International Corporation 1
ATTN: Document Control (Dr. T. Bache, Jr.)
10260 Campus Point Drive
San Diego, CA 92121

Science Horizons 2
ATTN: Dr. T. Cherry and Dr. J. Minster
710 Encinitas Blvd.
Suite 101
Encinitas, CA 92024

S-CUBED, A Division of Maxwell 1
Laboratories, Inc.
ATTN: Dr. Keith L. McLaughlin
P.O. Box 1620
La Jolla, CA 92038-1620

SRI International 1
ATTN: Dr. A. Florence
333 Ravensworth Avenue
Menlo Park, CA 94025

Teledyne Industries Inc. 1
Teledyne Geotech Alexandria Laboratories
ATTN: Mr. W. Rivers
314 Montgomery Street
Alexandria, VA 22314-1581

Woodward-Clyde Consultants 1
ATTN: Dr. L. Burdick
P.O. Box 93254
Pasadena, CA 91109-3254

Blacknest Seismological Center 1
ATTN: Mr. Peter Marshall
Atomic Weapons Research Establishment
UK Ministry of Defense
Brimpton, Reading RG7-4RS
United Kingdom

National Defense Research Institute 1
ATTN: Dr. Ola Dahlman
Stockhold 80, Sweden

NTNF NORSAR 1
ATTN: Dr. Frode Ringdal
P.O. Box 51
N-2007 Kjeller
Norway

OTHER DISTRIBUTION

To be determined by the project office 9

TOTAL 81